



University  
of Glasgow

van Well, Ben Russell (2006) A portable laser system for the remote detection of methane gas. PhD thesis

<http://theses.gla.ac.uk/6145/>

Copyright and moral rights for this thesis are retained by the author

A copy can be downloaded for personal non-commercial research or study, without prior permission or charge

This thesis cannot be reproduced or quoted extensively from without first obtaining permission in writing from the Author

The content must not be changed in any way or sold commercially in any format or medium without the formal permission of the Author

When referring to this work, full bibliographic details including the author, title, awarding institution and date of the thesis must be given.

# A Portable Laser System For The Remote Detection Of Methane Gas

by

Ben Russell van Well

DOCTOR OF PHILOSOPHY

in

The Faculty of Physical Science

Department of Physics and Astronomy

THE UNIVERSITY OF GLASGOW

4th January 2006

© Ben Russell van Well, 2006

# Abstract

We have developed an open-path hand-held gas detector incorporating a distributed feedback InGaAs laser diode at  $1.65\mu\text{m}$ . Incorporated into a hand-held transceiver unit, the emitted laser beam is backscattered from nearby surfaces, collected and focussed onto an amplified InGaAs detector using a 150mm diameter plastic Fresnel lens. At ranges of 4-5metres, a typical backscattered signal is tens of nanowatts of laser light. Applying second derivative wavelength modulation spectroscopy (WMS) gives a sensitivity to methane of better than 10 parts per million over a one metre path length.

Chapter 1 gives background information on existing detection methods, and explains why we chose to implement WMS. Chapter 2 discusses the various models created to justify the decision to use WMS. It also describes techniques used to help visualise escaping gas. Chapter 3 discusses the various stages of design and build of the actual prototypes, starting with a laboratory based prototype and finishing with a fully portable technology demonstrator. Chapter 4 give details of the laboratory testing undertaken in order to characterise and benchmark the system performance. Chapter 5 is concerned with the design and construction of an additional add-on scanning platform which scans the pointer instrument in order to build a 2-dimensional image of the gas escape. Chapter 6 mirrors chapter 3 in format, and discusses the various field-trials where the instruments were tested in representative conditions. Finally Chapter 7 highlights the work performed in developing a pre-production prototype and advertising the instrument to a wider market.

## Acknowledgements

Firstly I'd like to thank Professor Miles Padgett for his excellent guidance during the course of this study, and also for his undying enthusiasm and motivation. A big thank you to everyone else in the optics group at Glasgow University who has contributed in their own way to my education! A particular mention to Graham Gibson for help with the project, Martin O'Dwyer for letting me beat him at squash, and Graeme Whyte for being a drinking buddy. Also worthy of a mention is Johannes Courtial for sharing his office during my time writing up.

A huge thank you to all the project partners for making the project as enjoyable as it was, in particular Jane Hodgkinson, Stuart Murray and Rainer Strzoda who have proved to be invaluable during the project.

Finally a massive thanks to Stephanie Evers for putting up with me for so long, and for her unwavering support throughout.

## Preface

Chapter 1 of this thesis is background information and was produced with reference to several periodicals and books. Chapter 2 concerns the computer modelling performed by myself. Chapter 3 relates to the design and construction of the laser pointer instrument which was done by myself, with occasional input from Graham Gibson. Chapter 4 involves the laboratory based evaluation of the instrument which was done solely by myself. Chapter 5 discusses the design and construction of the scanning platform which I did together with Graham Gibson. The field trials discussed in Chapter 6 were performed by myself, with some input coming from Miles Padgett and Jane Hodgkinson. The development of a pre-production prototype discussed in Chapter 7 was performed by Rainer Strzoda based on my design information.

## Declaration

I, Ben van Well, hereby certify that this thesis, which is approximately 20,000 words in length, has been written by me and has not been submitted in any previous application for a higher degree.

Date..... Signature of candidate.....

I was admitted as a candidate for the degree of Ph.D. in September of 2001; the higher study for which this is a record was carried out in the University of Glasgow between 2001 and 2004.

Date..... Signature of candidate.....

I hereby certify that the candidate has fulfilled the conditions of the resolution and regulations appropriate for the degree of Ph.D. in the University of Glasgow and that the candidate is qualified to submit this thesis in application for that degree.

Date..... Signature of supervisor.....

---

# Contents

Contents . . . . .	6
List of Figures . . . . .	10
<b>1 Trace Gas Detection Methods . . . . .</b>	<b>16</b>
1.1 Industrial Gas Detection . . . . .	16
1.2 Optical Gas Detection . . . . .	19
1.2.1 Fourier Transform Spectroscopy . . . . .	19
1.2.2 Cavity Leak Out Spectroscopy - CALOS . . . . .	20
1.2.3 Faraday Rotation Spectroscopy . . . . .	21
1.2.4 Photo-acoustic Spectroscopy . . . . .	22
1.2.5 Raman Spectroscopy . . . . .	23
1.2.6 Light Detection And Ranging, LIDAR . . . . .	24
1.2.7 Wavelength Modulation Spectroscopy . . . . .	25
1.3 Comparison of Optical Techniques . . . . .	27
<b>2 Modelling . . . . .</b>	<b>31</b>
2.1 Wavelength Modulation Spectroscopy . . . . .	32
2.1.1 Mathematical explanation of WMS . . . . .	36
2.1.2 Graphical explanation of WMS . . . . .	36

---

2.1.3	Phase Sensitive Detector . . . . .	39
2.2	Gas Dispersion . . . . .	40
2.2.1	Gas Concentration At A Point Down Wind Of The Source . . . . .	41
2.2.2	Integrated Concentration Over Optical Path . . . . .	42
2.3	Collection Optics . . . . .	45
2.4	Processing of Gas Cloud Images . . . . .	46
2.4.1	Colour Enhancement of Monochrome Video Clips . . . . .	49
2.4.2	Smoothing . . . . .	54
<b>3</b>	<b>Instrument Development . . . . .</b>	<b>56</b>
3.1	Bench Top Demonstrator . . . . .	57
3.1.1	Ramp Generation and Data Acquisition . . . . .	60
3.2	Proof of Concept System . . . . .	62
3.3	Portable System . . . . .	66
3.3.1	Waveform Generation . . . . .	69
3.3.2	Combining Ramp and Modulation . . . . .	70
3.4	Functional Cost Efficient Prototype . . . . .	71
3.4.1	Phase Sensitive Detector Design . . . . .	75
3.4.2	Line Locking . . . . .	77
3.4.3	Transimpedance Amplifier . . . . .	77
3.5	Technology Demonstrator . . . . .	79
3.5.1	Self Executing Program . . . . .	83
<b>4</b>	<b>Laboratory Characterisation . . . . .</b>	<b>87</b>
4.1	Parallax Optimisation . . . . .	88
4.1.1	Laser On/Off . . . . .	92

---

4.2	Detector Sensitivity . . . . .	92
4.2.1	Backscatter From Surface . . . . .	95
<b>5</b>	<b>Scanning . . . . .</b>	<b>101</b>
5.1	Imaging Requirements . . . . .	102
5.2	Optical Scanner . . . . .	106
5.3	Real Time Gas Imaging . . . . .	111
5.3.1	Acquiring Gas Data . . . . .	111
5.3.2	Processing Gas Data Into An Image . . . . .	112
<b>6</b>	<b>Field Trials . . . . .</b>	<b>114</b>
6.1	Proof of Concept System . . . . .	115
6.2	Portable System . . . . .	118
6.2.1	User Methods . . . . .	118
6.2.2	Real World Reflectivity . . . . .	122
6.2.3	Scanning Through A Gas Cloud . . . . .	122
6.3	Functional Cost Efficient Prototype . . . . .	125
6.3.1	Reflectivity Update . . . . .	126
6.3.2	Comparison with Flame Ionisation Detector . . . . .	126
6.4	Technology Demonstrator . . . . .	130
6.4.1	Bar Hole Examination . . . . .	130
6.4.2	Blind Leak Search . . . . .	131
6.4.3	Saturation Test . . . . .	132
6.4.4	Real World Verification . . . . .	137
6.5	Scanning The Pointer . . . . .	137

---

<b>7 Commercialisation</b> . . . . .	141
7.1 Pre-production Prototype . . . . .	142
7.2 Advertising . . . . .	144
7.3 Marketing . . . . .	146
<b>Bibliography</b> . . . . .	147
<b>A Brochure</b> . . . . .	153
<b>B Published Paper</b> . . . . .	160

---

## List of Figures

1.1	Early FID design with the jet as one of the electrodes, and filtered air [1]	17
1.2	Optical layout of the static Fourier-transform ultra-violet spectrometer	20
1.3	Typical cavity leak out spectrometer system	21
1.4	Schematic apparatus for technique used to measure time-resolved Faraday rotations	22
1.5	Typical photo-acoustic spectroscopy system	23
1.6	Lidar system using light reflected from gases in the atmosphere	25
1.7	Wavelength modulation spectroscopy parameters	26
2.1	Theoretical transmission spectrum for 10ppm methane over a 20m path length [2]	33
2.2	Theoretical first order spectrum based on absorption curve as in figure 2.1	34
2.3	Theoretical second order spectrum based on absorption curve as in figure 2.1	35
2.4	Theoretical third order spectrum based on absorption curve as in figure 2.1	35
2.5	Theoretical transmission spectrum for a 1mm (1000ppm.m) gas cloud of pure methane	37
2.6	Laser output and methane absorption combined	37
2.7	WMS returns the derivative of the transmission signal	38
2.8	LabVIEW program which mimics the action of a phase sensitive detector	39

---

2.9	An idealised gas leak and dispersion . . . . .	41
2.10	The leaking gas concentration at a point decreases with the square of the distance from the leak. Note: $\text{Log}(\text{Fractional Concentration})=0$ corresponds to pure gas . . . . .	42
2.11	The concentration x path length is inversely proportional to the distance from the leak. Note: $\text{Log}(\text{Fractional Concentration})=0$ corresponds to pure gas . . . . .	43
2.12	Comparing theoretical responses from point measurement and line of sight measurement techniques. The cross over point is arbitrary, and related to leak conditions . . . . .	44
2.13	Light is scattered back into the collection optics . . . . .	46
2.14	Predicted photocurrent varies with the square of the distance (reflectivity taken as 3%) . . . . .	47
2.15	Test site in Sweden with radiators to create an artificial background temperature . . . . .	48
2.16	Functionality of video image processing . . . . .	49
2.17	LabVIEW code to open background image . . . . .	50
2.18	LabVIEW code to open gas leak images . . . . .	50
2.19	LabVIEW code to resample image . . . . .	51
2.20	LabVIEW code to replace the colour plane of the gas cloud image . . . . .	52
2.21	LabVIEW code to save the images which can then be viewed as a movie . . . . .	53
2.22	Gas image resampled at lower resolution . . . . .	54
2.23	Gas image blurred, by passing through a low-pass filter, before being superimposed onto background image . . . . .	55
3.1	Theoretical methane spectrum obtained using HITRAN [2] . . . . .	58

---

3.2	left: DFB laser diode mounted onto a TEC, right: close up showing laser diode mounted onto a metal carrier, with copper connection wires . . . . .	58
3.3	The temperature control was hard-wired to the TEC element, the diode current controller is under computer control via an IEEE interface . . . . .	59
3.4	100mm diameter Fresnel lens (50mm focal length) mounted in front of the InGaAs detector . . . . .	60
3.5	Schematic showing signal path through the setup . . . . .	61
3.6	Left: 1st derivative spectrum, Right: 2nd derivative spectrum (both with 1.5kHz modulation and 100ms time constant). The additional structure evident in these spectra is due to the gas cell; when not aligned exactly collinear with the laser light, extra fringes are visible. . . . .	62
3.7	LabVIEW code to ramp output voltage and acquire data . . . . .	63
3.8	Left: Internal view of laser pointer, Right: The laser pointer technology demonstrator capable of detecting methane from the back scattered light (note in this case, the reference/calibration cell is also mounted) . . . . .	65
3.9	Bench-top electronics arranged to fit into a large flight case . . . . .	66
3.10	Left: Rear half of the unit which contains a combined laser and temperature controller, two PSD's and the electronics which generate the $1\omega$ and $2\omega$ reference frequencies, Right: Front half of the unit which houses the laser, detector, electronic filter and unity gain buffer amplifier . . . . .	68
3.11	Left: Complete system rehoused into a cylinder (note that the front section is detachable and can be hand-held), Right: Internal view of the rehoused signal processing electronics (rear section) . . . . .	69
3.12	The in-house designed waveform generator . . . . .	70
3.13	Circuit designed to combine the ramp and modulation signals . . . . .	71

---

3.14	1F and 2F in-house designed and constructed PSD's . . . . .	72
3.15	Left: laser diode module with top section removed, Right: Schematic diagram showing connection points of internal components . . . . .	73
3.16	Left: Temperature controller from AOS, Right: Laser driver board from Thorlabs, both mounted inside a 120mm die-cast housing . . . . .	74
3.17	Modulator and digital phase shifter . . . . .	74
3.18	Left: 6" diameter optical head unit, Right: Shoulder mounted box containing signal processing electronics and batteries . . . . .	76
3.19	Circuit diagram of PSD designed to detect the 2nd harmonic . . . . .	76
3.20	LabVIEW code which frequency locks the laser diode onto the methane absorption line . . . . .	78
3.21	The in-house designed transimpedance amplifier using a TL071 operational amplifier . . . . .	79
3.22	Left: connection panel of control box, Middle: inside of the control box showing the embedded computer and control electronics, Right: the digital readout on the rear of the hand-held optical head . . . . .	80
3.23	Flow diagram showing pathways through control software . . . . .	82
3.24	Left: system components, Right: all the component packaged into an aluminium flight case . . . . .	83
3.25	Obtaining PSD outputs before laser is switched on . . . . .	84
3.26	Main data acquisition loop . . . . .	85
3.27	Calculating fault code to display to user . . . . .	86
4.1	Trade off between operating distance and parallax to achieve a suitable dynamic range . . . . .	91
4.2	User interface of software designed to switch laser on and off . . . . .	93

---

4.3	Methane transmission in the $1.65\mu\text{m}$ region . . . . .	94
4.4	Comparing real-world reflectivities with an early prototype pointer (1mm gas cloud thickness is equivalent to 1000ppm.m) . . . . .	98
4.5	Theoretical sensitivity based on quoted detector performance compared with sensitivity achieved . . . . .	100
5.1	Snapshots at one second intervals of a gas leak, taken with a thermal camera, with colour enhancement as described in subsection 2.4 . . . . .	103
5.2	Comparing original image quality with resampled, and then smoothed image. On the left are the original images, on the right are the images which have been reduced to $10\times 10$ and then processed . . . . .	105
5.3	Scanning options. The instrument will be acquiring data while scanning horizontally (as shown); otherwise it is moving on-the-fly to reach a data acquisition start point . . . . .	106
5.4	Tripod mounted scanning mechanism . . . . .	107
5.5	Schematic of scanning mechanism . . . . .	108
5.6	Routine which defines scan parameters . . . . .	109
5.7	Schematic signal path through scanner software . . . . .	110
5.8	Trigger from scanning mechanism defines scan pattern . . . . .	111
5.9	Building a $10\times 10$ array . . . . .	112
5.10	Adding gas information to the red colour plane from the web-cam . . . . .	113
5.11	Displaying resulting image . . . . .	113
6.1	Signal flare released to show turbulent nature of wind conditions . . . . .	116
6.2	Second harmonic trace from 4m looking at 1l/min leak . . . . .	117
6.3	Various surfaces at Malmö test site . . . . .	119

---

6.4	Aiming the pointer around the leak location . . . . .	120
6.5	Signal levels varying with pointer direction . . . . .	121
6.6	(Left) Scanning parallel and then (right) perpendicular to the wind direction	123
6.7	Results when positioned parallel to the wind direction (1mm gas cloud is equivalent to 1000ppm.m) . . . . .	124
6.8	Results when positioned perpendicular to the wind direction . . . . .	125
6.9	Carbon coated storage tank used to test the sensitivity of the instrument under low backscattered-light conditions . . . . .	127
6.10	Aiming the pointer instrument at the flame ionisation detector . . . . .	128
6.11	Comparing the FID output with the results from the pointer instrument (note similar performance but the pointer is operating remotely) . . . . .	129
6.12	Detecting gas escaping from bar-holes . . . . .	131
6.13	Layout of Leicester depot training area . . . . .	133
6.14	Signal saturated by large amounts of methane . . . . .	135
6.15	Trying to saturate the pointer . . . . .	136
6.16	Locating a real leak location in Brussels . . . . .	138
6.17	Narrow opening in metal pit lid . . . . .	139
6.18	Pit lid completely open allowing gas to escape freely . . . . .	140
7.1	Instrument developed by Siemens, based on the Glasgow design . . . . .	144
7.2	Website hosted at Glasgow University . . . . .	145

---

# 1. Trace Gas Detection Methods

The low-cost, sensitive detection of methane gas has wide use amongst the gas utility companies for both routine pipeline inspection and leak-report response applications [3]. This chapter firstly outlines the instrument techniques currently employed by the industrial gas utility companies for leak detection and location. These instruments measure the concentration of gas at a point, and are used to survey the area in question by systematically displaying gas concentration data as the operator progresses over the suspected leak location.

Secondly, this chapter discusses some of the optical techniques that have been applied to trace gas detection. One advantage that some optical techniques bring to the field of trace gas detection is that it is possible to use remote techniques. This enables the user not to enter potentially explosive situations, but monitor from a safe distance. It also allows for surveying above-ground pipe-work which may be difficult to access.

Finally this chapter will discuss the advantages and disadvantages of current optical techniques and give an overview of current detection limits achieved by other groups.

## 1.1 Industrial Gas Detection

Flame ionisation detectors (FID's) (see figure 1.1) are the predominant natural-gas detection tool utilised by gas utility engineers today, and have been developed from a gas

chromatography detection system. Early gas chromatographers for detecting natural-gas were based around a hydrogen flame, and were initially developed in 1954 [4]. In the hydrogen flame detector, the carrier gas contained hydrogen, which was burned at the column end, and the temperature of the flame was continually monitored. Without sample, the carrier gas produced a constant signal; however, when a combustible organic vapour appeared at the column, the temperature of the flame increased, resulting in a response which was proportional to the amount of the compound present. Investigations

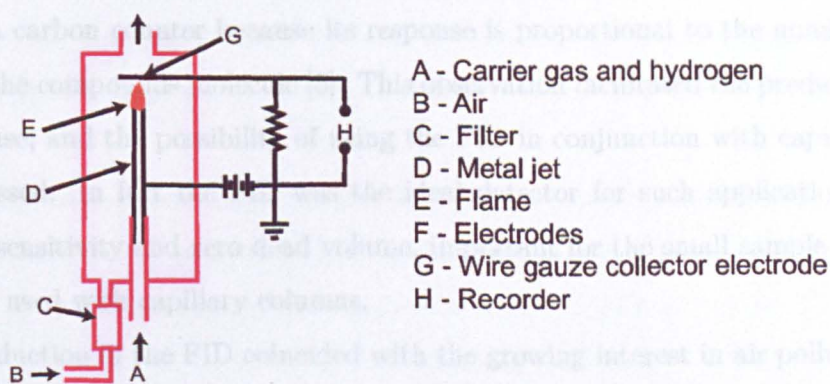


Figure 1.1: Early FID design with the jet as one of the electrodes, and filtered air [1]

in early 1957 by McWilliam and Dewar showed that the continually burning hydrogen results in a high background, while the burning of small concentrations of sample components causes only small temperature changes. They decided to modify the system by measuring the ion current in the flame and not its temperature. A filter was added to remove the dust from the air which was used for combustion, as the dust increased the noise within the system.

Original designs used a hypodermic needle as a jet, with two metal electrodes placed on opposite sides of the flame. The ion current produced by placing a battery in series with the electrodes could be measured, and fluctuations in this current could be attributed to

the presence of volatile compounds. Changes to the electrical system saw the metal jet nozzle become used as one electrode, and a wire gauze used as the collector electrode.

A further modification was to use two FID's, one at the end of the analytical column and the second at the end of a reference column, and measuring the difference between the outputs of the two detectors. In this way, background current disturbances could be offset.

Further research into his early design led McWilliams to comment that the FID is essentially a carbon counter because its response is proportional to the number of carbon atoms in the compounds molecule [5]. This observation facilitated the prediction of detector response; and the possibility of using the FID in conjunction with capillary columns was discussed. In fact the FID was the ideal detector for such applications because it had high sensitivity and zero dead volume, important for the small sample sizes and low flow-rates used with capillary columns.

The introduction of the FID coincided with the growing interest in air pollution research and control. Because of this, an easy and accurate way to measure the total organic content of the atmosphere and automobile exhaust was much sought after. Because the FID was essentially a carbon counter (for gaseous hydrocarbons), it was proposed almost immediately after its introduction that it should be adapted for this purpose. Such portable instruments were developed in 1959; in these instruments no column was used, and the sample gas (e.g. atmospheric air or automobile exhaust) was pumped at a constant flow-rate through the detector in lieu of the carrier gas. The detector's response was proportional to the total concentration of gaseous hydrocarbon compounds present in the sample gas.

## 1.2 Optical Gas Detection

### 1.2.1 Fourier Transform Spectroscopy

There are many designs of Fourier transform (FT) spectrometer, including the Michelson interferometer. One particular spectrometer design [6] [7] is based on two Wollaston prisms which when placed between polarisers aligned at 45 degrees to the optic axis of the prisms, form an interferogram in the spatial domain that can be recorded with a detector array. This interference pattern encodes the spectrum of the broadband light source. Applying an inverse transform to this interference pattern yields the transmission spectra.

The two Wollaston prisms utilised in this instrument are manufactured from quartz wedges and are aligned at 6 degrees and 11.8 degrees respectively. The resulting maximum path difference gives this instrument an effective resolution of  $200\text{cm}^{-1}$  in the UV. An example instrument is shown in figure 1.2. The advantage of using a FT spectrometer stems from its high optical efficiency. "For the same resolving power, a FT spectrometer has an étendue (optical efficiency) approximately 190 times greater than that of a dispersive instrument" [8] [9]. In this application, the use of a FT spectrometer, removes the need for collimating and focusing optics which would be required to couple the light into the input slit of a dispersive spectrometer. Consequently, any small-angle scattering of the light by the sample does not influence either the collection efficiency of the FT spectrometer or the recorded spectrum. It is possible to use a FT spectrometer as a passive gas imaging tool [10], although the detection capabilities of this technique are heavily influenced by prevailing weather conditions.

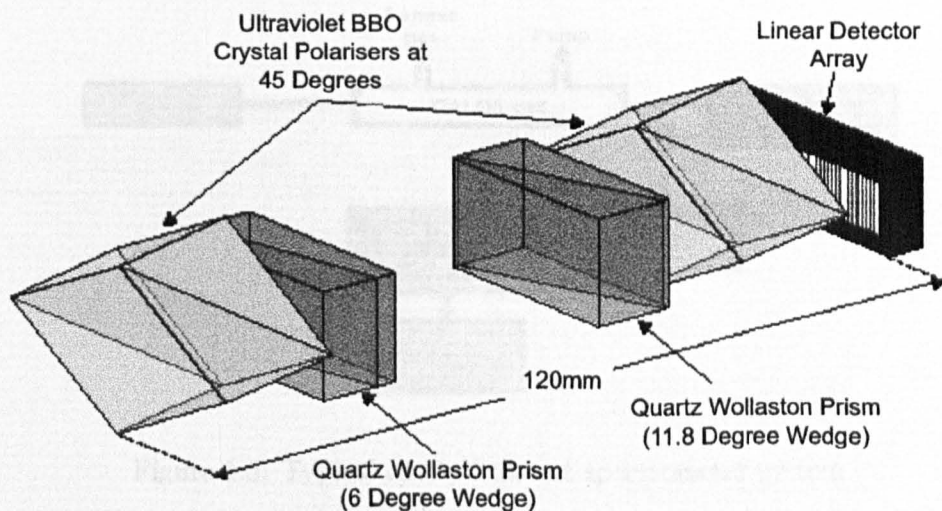


Figure 1.2: Optical layout of the static Fourier-transform ultra-violet spectrometer

## 1.2.2 Cavity Leak Out Spectroscopy - CALOS

The cavity leak out spectroscopy technique, utilizing CW lasers, is ideal for trace gas detection as it combines high sensitivity and a fast response. CALOS relies on optical excitation of the cavity followed by turning off the laser power and observing the subsequent power decay of the radiation. The gas sample to be analysed is sent through the absorption cell and after determination of the power decay rate of the cavity field, the mixing ratio of the trace constituent of interest is calculated from the absorption coefficient achieved [11]. A typical CALOS system is shown in Fig 1.3 which is a simplified version of the system used by Dahnke et al [12]. A close relation of CALOS is cavity ring down spectroscopy (CRDS) which is described in [13], [14] or [15].

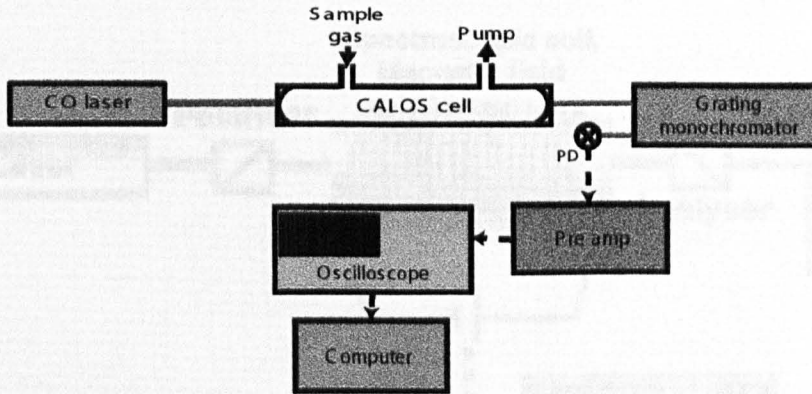


Figure 1.3: Typical cavity leak out spectrometer system

### 1.2.3 Faraday Rotation Spectroscopy

Faraday rotation spectroscopy (FRS) is a sensitive detection method for many radicals and ions. The method utilises the fact that the absorption frequency of radicals is tunable with an external magnetic field, enabling a user to gain a factor in sensitivity compared to standard approaches. A diagram of a Faraday rotation optical set up is shown in figure 1.4. A linearly polarised laser beam is sent through the spectroscopic cell, and a magnetic field is applied. When any of the target gas is in the cell, the polarisation axis shifts slightly. The analyser then transmits only the rotated part of the light to the detector, with a lock-in amplifier utilised to increase sensitivity. An example of a Faraday rotation system is described in [16]. Faraday rotation spectroscopy has been used in many diverse applications such as the study of magnetic two-dimensional electron gases [17].

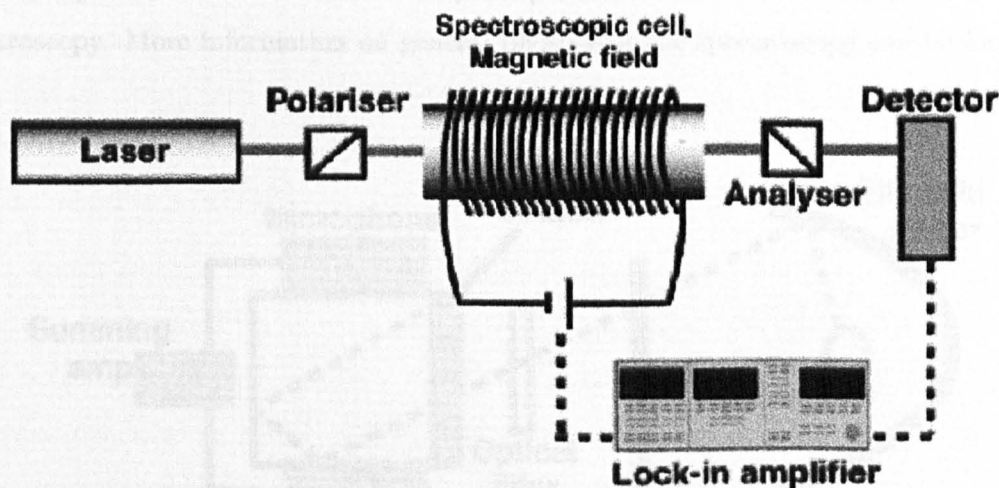


Figure 1.4: Schematic apparatus for technique used to measure time-resolved Faraday rotations

### 1.2.4 Photo-acoustic Spectroscopy

In photo-acoustic spectroscopy (PAS), the gas is irradiated by intermittent light of preselected wavelength. The gas molecules absorb some of the light energy and convert it into an acoustic signal, detected by a microphone. Figure 1.5 depicts an example of such a system. A mirror focuses the light through the light chopper and the optical filter, onto the window of the PAS cell. If the wavelength of the light coincides with the absorption wavelength of the gas, the gas absorbs some of the energy. As this happens, the gas heats up, expands and therefore causes a pressure rise. The light is being chopped at a particular chopping frequency and so the pressure increases and decreases at this same frequency, producing an acoustic signal which is picked up by the microphones. The main advantage of PAS over conventional techniques is that no gas means no signal. Herpen et al [18]

recently reported a detection limit of 10 parts per trillion for ethane using photo-acoustic spectroscopy. More information on general photo-acoustic spectroscopy can be found in [19].

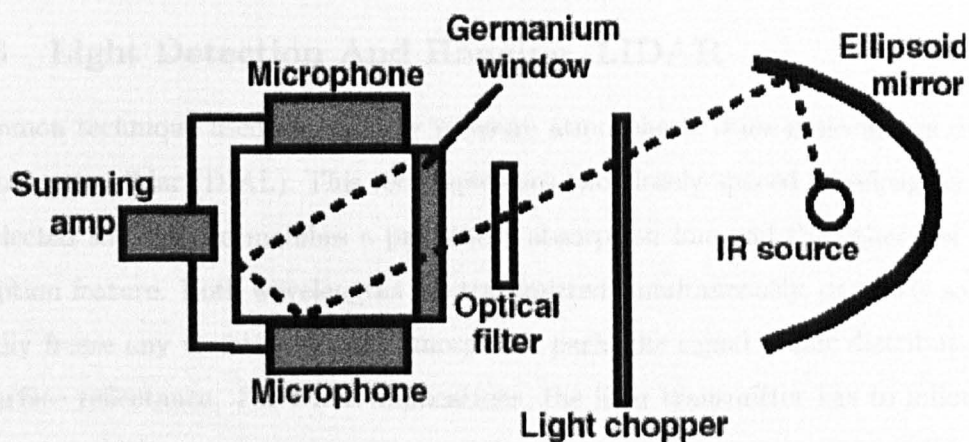


Figure 1.5: Typical photo-acoustic spectroscopy system

### 1.2.5 Raman Spectroscopy

If a beam of light is passed through a transparent substance, some of the light is scattered, even if all external materials are excluded. If a very narrow frequency band of radiation is used, the scattered energy will consist almost entirely of radiation of the incident frequency (Rayleigh scattering), but will also contain small amounts of other discrete frequencies above and below the incident. This is referred to as Raman scattering. A detector is placed at 90 degrees to the incident beam. If the collision is elastic this detector will collect light of energy  $h\nu$ . However, if the collision is inelastic the detector will collect light of a different energy (i.e. frequency), therefore energy transfer to and from the molecule has taken place [20]. This technique, while offering the potential to identify the

presence of a gas, is not at all practical for gas detection outside of the confinements of a laboratory; the signal levels involved with this technique are too small for real-world gas detection.

### 1.2.6 Light Detection And Ranging, LIDAR

A common technique used to remotely measure atmospheric trace molecules is differential absorption lidar (DIAL). This technique uses two closely spaced wavelengths, which are selected so that one matches a prominent absorption line and the other lies off the absorption feature. Both wavelengths are transmitted simultaneously, or nearly so, to essentially freeze any variation in the atmospheric path, the signal plume distribution and the surface reflectance. For DIAL applications, the lidar transmitter has to follow some requirements [21]:

1. the wavelength must be tunable to match appropriate absorption lines of the investigated molecule
2. the bandwidth and the spectral stability should be considerably smaller than the linewidth of the absorption line
3. a high spectral purity (>99%) has to be guaranteed
4. a sufficient pulse energy and average power is required
5. a high repetition rate is desirable

The DIAL technique involves the transmission of a laser pulse and the detection of the backscattered radiation by using a telescope. The time of flight of the laser pulse allows range information to be gathered; the ratio of the intensities of the backscattered signals gives information about the concentration of the species under study. Many DIAL

systems need to detect more than one species [22], and hence require a laser radiation source that is tunable over a large spectral range, often as much as  $1\mu\text{m}$ . These systems often employ optical parametric oscillators (OPO's) and amplifiers (OPA's) as their light source [23], [24].

Lidar techniques have been applied to the detection of methane, chiefly for pipeline surveillance [25]. These systems are often designed to be aircraft mounted to reduce survey time. Many fixed LIDAR systems use a retro-reflector to improve returned signal levels, and hence operational range, but this is not always practical. Some rely entirely on topographic reflection [26]. Yet more LIDAR systems rely on the light backscattered from the atmosphere (see figure 1.6). Lidar systems can also be developed which use various other detection principles such as a Raman lidar system [27], or a gas correlation lidar system [28].

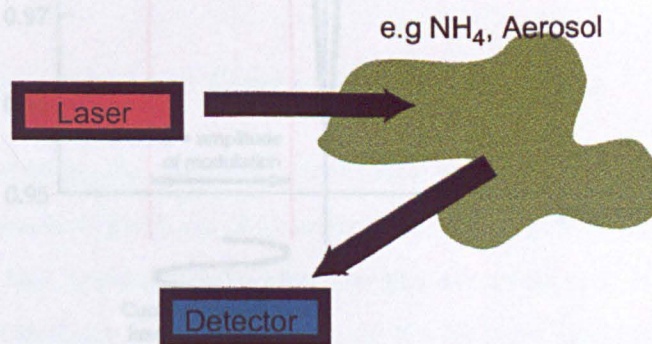


Figure 1.6: Lidar system using light reflected from gases in the atmosphere

### 1.2.7 Wavelength Modulation Spectroscopy

Wavelength modulation spectroscopy (WMS) is a widely used technique for trace-gas detection. It can be implemented by use of semiconductor lasers in the mid-infrared and

near infrared. WMS is based on the rapid wavelength modulation of the light emitted by a laser as it is slowly tuned through an absorption feature of the species to be detected. The interaction of the wavelength modulated light with the absorption line leads to the generation of signals at different harmonics of the modulation frequency. The signal at a given harmonic can be measured with lock-in detection and is proportional to the absorption [29].

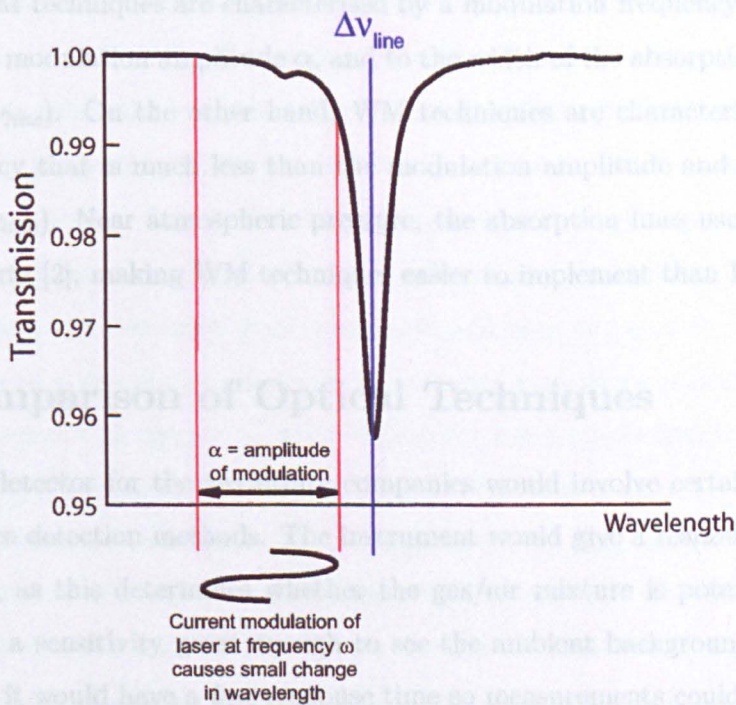


Figure 1.7: Wavelength modulation spectroscopy parameters

In a semiconductor laser, a frequency/wavelength modulation can be easily performed by modulation of the injected current. This produces a combined frequency modulation (FM) and intensity (amplitude) modulation (AM) of the emitted light, with a phase dif-

ference between the two modulations. In WMS the detected signals are mainly due to the FM of the laser emission, whereas AM, often referred to as residual amplitude modulation [30], is an unwanted effect that distorts the signals.

Although they are basically identical, the trace-gas detection methods that use current-modulated semiconductor lasers are generally separated into two categories, wavelength modulation (WM) and frequency modulation (FM) techniques; this is simply a naming convention. FM techniques are characterised by a modulation frequency,  $\omega$ , that is comparable to the modulation amplitude  $\alpha$ , and to the width of the absorption feature  $\Delta\nu_{line}$  ( $\omega \approx \alpha \approx \Delta\nu_{line}$ ). On the other hand, WM techniques are characterised by a modulation frequency that is much less than the modulation amplitude and width of feature ( $\omega \ll \alpha \approx \Delta\nu_{line}$ ). Near atmospheric pressure, the absorption lines usually extend over several gigahertz [2], making WM techniques easier to implement than FM techniques.

### 1.3 Comparison of Optical Techniques

An ideal gas detector for the gas utility companies would involve certain characteristics of various trace detection methods. The instrument would give a readout in terms of gas concentration, as this determines whether the gas/air mixture is potentially explosive; it would have a sensitivity great enough to see the ambient background levels (1.6ppm for methane); it would have a fast response time so measurements could be made in real time; it would be substance specific so the user know which gases were being detected; it would detect remotely in order to provide a safe distance between the substance being detected and the user, and the detector would be robust enough to be used daily in harsh environments by the operator. Unfortunately, an instrument of this nature would greatly exceed the cost of, and be less portable than, existing tools, and therefore not be an

economic solution.

To find a compromise it is important to satisfy as many of these criteria as possible, but specifically the remote sensing criteria as this is the main advantage over a FID or other existing point measurement device.

To get a readout in terms of gas concentration requires knowing the distribution of gas throughout the sampled volume. For a small enough sample it is a sufficiently good approximation to assume that the gas concentration is homogeneous. For a remote line of sight measurement, the returned signal gives units of concentration times path length. Knowing the sampled distance can reduce the units simply to concentration, but that assumes the gas is equally distributed, which may not be the case. A longer path length increases the possibility that there will be gas present in the line of sight, but reduces the positional information content. Longer path length instruments will require highly collimated beams and retro-reflectors, which will add bulk and cost to the instrument.

The sensitivity of a line of sight instrument depends on receiving enough returned light, that has interacted with the gas. A retro-reflector is not a viable option as its movement would need to be synchronised with that of the transceiver unit, reducing the portability of the instrument. This means that a large diameter, high efficiency collection lens which could collect as much of the returning light as possible would be an advantage. An instrument of this nature which will rely on light backscattered from a diffuse target (brick wall, ground, paving etc) will ultimately have its sensitivity limited by the amount of collected light.

One way to make an optical instrument substance-specific is to have control over which wavelength of light is used. This enables the design to choose a wavelength which corresponds to an absorption line of the required substance, and not to any commonly found other substance. The response time of an instrument depends on which signal processing

Persons	Sensitivity	Method
Jackson et al [31]	32.2ppt	Static mass spectroscopy
Kleine et al [32]	290ppt	Cavity leak-out spectroscopy
Zahniser et al [33]	precision 1.8ppb	Direct spectroscopy with tunable diode laser
Werle et al [34]	2ppb	FMS with an antimonide semiconductor laser
Blaha et al [35]	5ppb	Direct spectroscopy with He-Ne laser
Petrov et al [36]	12ppb mHz <sup>5</sup>	WMS with 3.2 $\mu$ m diode laser
Liang et al [37]	20-30ppb	Photoacoustic trace detection
Uehara et al [38]	400ppb	WMS with He-Ne at 3.392 $\mu$ m
Prasad et al [26]	0.05 ppm	OPO based DIAL over 1 mile range
Werle et al [39]	2ppm	FMS using 7.8 $\mu$ m lead-salt diode
Minato et al [28]	4.4ppm	Gas correlation lidar over 20m range
Tai et al [40]	5ppm	Direct spectroscopy using 1.66 $\mu$ m diode laser
Fowler et al [41]	40 $\mu$ mol m <sup>2</sup>	Static chamber measurements
Ikuta et al [25]	1000ppm.m	Compact DIAL system at 130m range

Table 1.1: The work done by other groups in methane detection

method is used, but many techniques could easily be implemented with a response time less than 1 second.

The ideal instrument concept now appears to be a lightweight transceiver unit which illuminates a diffuse topographical target and collects the backscattered light, of a known wavelength. The signal from the returned light can then be processed to determine whether the gas is present. There are various signal processing techniques which can be used to increase the detection sensitivity of the instrument. Table 1.1 gives a comparison of the current situation in methane detection. Some techniques from this table

---

can be ruled out because of their cost or the bulk of the necessary equipment. The sensitivity of the chosen method not only depends on the technique used, but also on the relative absorption depth of the gas line which is used, and hence the wavelength. Hydrocarbon gases have strong absorption bands in the mid infrared ( $\sim 3\mu\text{m}$ ) but low cost laser light sources do not currently operate in this region at room temperature. Detecting at  $\sim 1.6\mu\text{m}$  gives a reduction in sensitivity because these wavelengths correspond to an overtone of the  $\sim 3\mu\text{m}$  absorption, but is considerably cheaper. The resulting conclusions mean that wavelength modulation spectroscopy appears to give the required sensitivity, and it can be implemented in a cost-effective manner and within suitable size and weight considerations.

## 2. Modelling

This chapter describes various models that have been used in the development of a remote gas detector. The models help to estimate the theoretical limits of detection, against which our instrument can be compared.

Firstly the modelling covers a theoretical view of wavelength modulation spectroscopy (WMS), which is a commonly employed signal recovery method. Here the computer simulation uses a known direct absorption result, and produces the expected harmonic spectra. This reveals which absorption lines are preferential to use and hence which wavelength of diode laser should be sourced.

Secondly a model has been created to estimate the dispersal of the gas cloud and simulate the readings that a line of sight instrument would return. The effectiveness of the remote pointer relies heavily on knowledge of the dispersion of the leaking gas.

Thirdly, a method of directly viewing simulated gas leaks was desirable to further understanding of their often turbulent nature, and to assist in training an end user on how best to search for leaks. An artificially high background temperature was created, against which the cooler escaping gas was made visible using a thermal imaging camera. The processing of these black and white thermal video clips enabled the gas cloud to be colour enhanced, improving the effectiveness of the training videos. These video clips have been included in a compact disc based training aid.

## 2.1 Wavelength Modulation Spectroscopy

Wavelength modulation spectroscopy (WMS) and frequency modulation spectroscopy (FMS) are commonly employed methods for improving the detection sensitivity of spectroscopic instruments. The difference between WMS and FMS is that WMS employs modulation frequencies much lower than the absorption linewidth whereas FMS uses frequencies comparable to or much larger than the absorption bandwidth.

If one were to measure the direct transmission signal, the change due to levels of gas being present would be insignificant compared to fluctuations in the light level due to other mechanisms acting on a similar timescale. Even over a path length of  $20m$  a concentration of  $10ppm$  would only result in an intensity change of  $0.8\%$  as shown in figure 2.1. WMS essentially delivers the derivative of the direct transmission signal; in our case specifically the 1st, 2nd and 3rd order derivatives as shown in figures, 2.2, 2.3 and 2.4. The 2nd order spectrum is the most important processed signal for our application since for a given absorption line, the peak of the 2nd derivative is directly proportional to the amount of gas in the optical path, as shown in equation 2.3. This means that zero gas should give zero signal. As can be seen from figure 2.3 there is actually a small offset. This discrepancy arises because the optical output of the laser is not quite linear with the current. The  $2f$  offset is small and constant for a given laser and detected power level and so, once the laser has been characterised, can be directly subtracted from each value of the  $2f$  spectrum to allow "zero gas equals zero reading" to hold. As figure 2.3 clearly shows there are two distinct advantages for using the second order derivative over direct absorption for detecting the presence of a gas:

- If there is no gas present there is no signal, so WMS is better suited to accurately determining when no gas is present

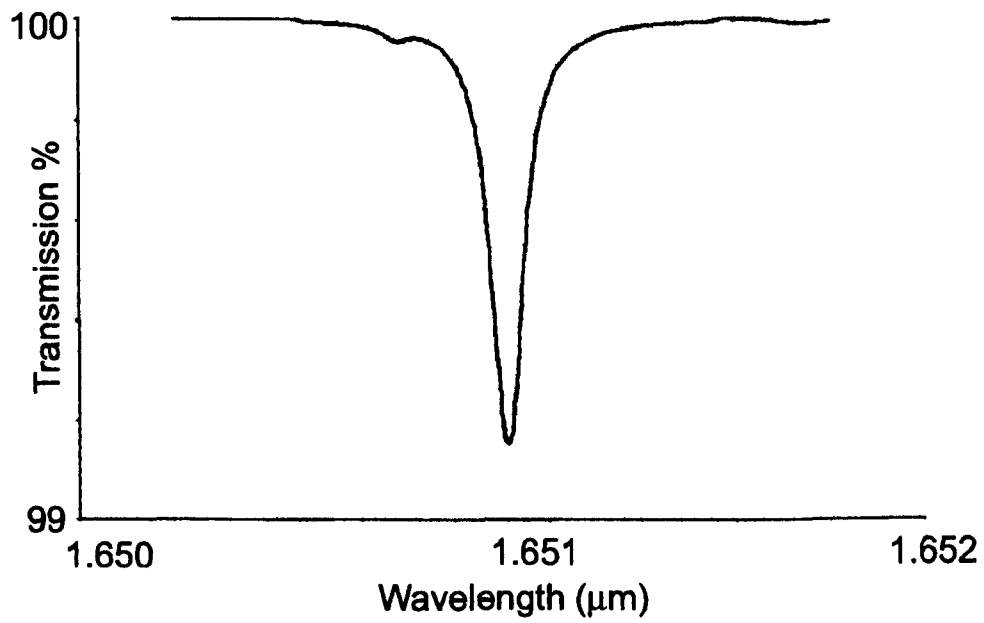


Figure 2.1: Theoretical transmission spectrum for 10ppm methane over a 20m path length

[2]

- The first and third harmonics of WMS precisely indicate the centre of the absorption band as there is a zero crossing at line centre.

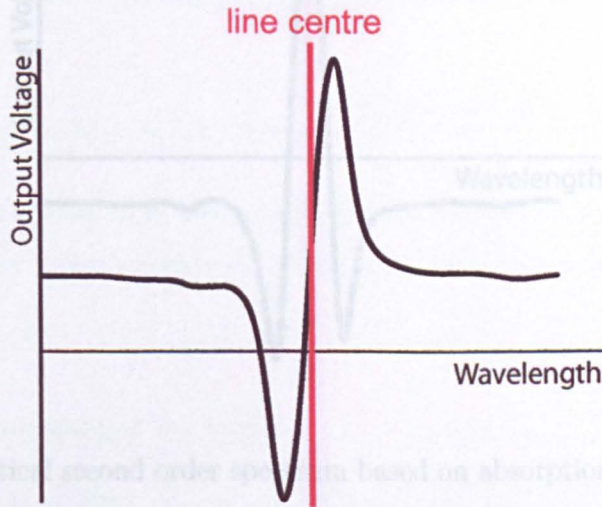


Figure 2.2: Theoretical first order spectrum based on absorption curve as in figure 2.1

In wavelength modulation spectroscopy, a modulation of frequency  $\omega$  (with an amplitude  $\alpha$ ), is added to the laser output. If the detector signal is multiplied by a phase shifted reference oscillator of frequency  $\omega$  (or its rectified equivalent) and the result averaged, the first order differential is produced. This averaging is important as it removes the local oscillator beats. If the  $n^{\text{th}}$  order is sought then the reference oscillator will have a frequency of  $n\omega$  and the output will be the  $n^{\text{th}}$  order differential. The first three orders are as shown in figures 2.2, 2.3 and 2.4. The theory behind wavelength modulation spectroscopy can be explained mathematically (section 2.1.1, and further examined graphically (section 2.1.2).

Figure 2.4: Theoretical third order spectrum based on absorption curve as in figure 2.1

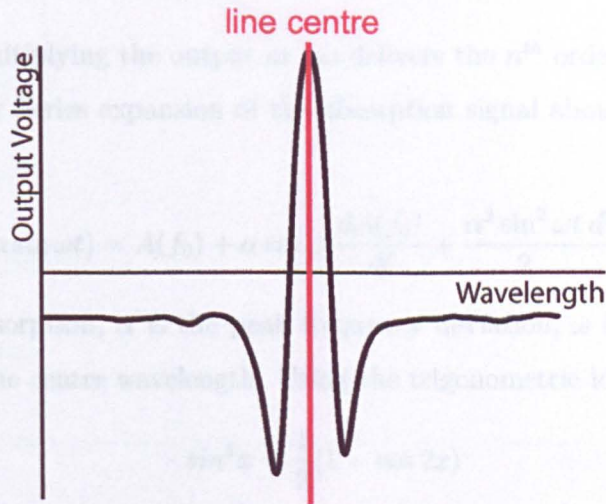


Figure 2.3: Theoretical second order spectrum based on absorption curve as in figure 2.1

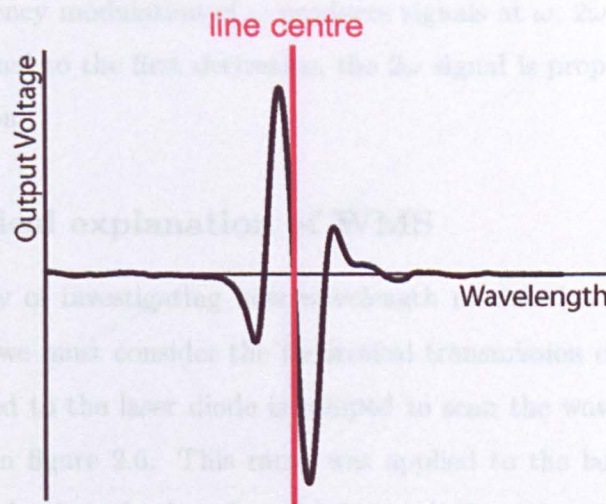


Figure 2.4: Theoretical third order spectrum based on absorption curve as in figure 2.1

### 2.1.1 Mathematical explanation of WMS

To explain why multiplying the output at  $n\omega$  delivers the  $n^{\text{th}}$  order harmonic we should consider the Taylor Series expansion of the absorption signal about the laser centre frequency:

$$A(f_0 + \alpha \sin \omega t) = A(f_0) + \alpha \sin \omega t \frac{dA(f_0)}{df} + \frac{\alpha^2 \sin^2 \omega t}{2} \frac{d^2 A(f_0)}{df^2} + \dots \quad (2.1)$$

where  $A$  is the absorption,  $\alpha$  is the peak frequency deviation,  $\omega$  is the modulation frequency and  $f_0$  is the centre wavelength. Using the trigonometric identity:

$$\sin^2 x = \frac{1}{2}(1 - \cos 2x) \quad (2.2)$$

and substituting into equation 2.1 we get:

$$A(f_0 + \alpha \sin \omega t) = A(f_0) + \alpha \sin \omega t \frac{dA(f_0)}{df} + \frac{\alpha^2 (1 - \cos 2\omega t)}{4} \frac{d^2 A(f_0)}{df^2} + \dots \quad (2.3)$$

Hence, a frequency modulation of  $\omega$  produces signals at  $\omega$ ,  $2\omega$ ,  $3\omega$  etc. where the  $\omega$  signal is proportional to the first derivative, the  $2\omega$  signal is proportional to the second derivative and so on.

### 2.1.2 Graphical explanation of WMS

An alternative way of investigating how wavelength modulation spectroscopy works is graphically. First we must consider the theoretical transmission curve as in figure 2.5. The current applied to the laser diode is ramped to scan the wavelength, producing an output as shown in figure 2.6. This ramp was applied to the laser diode as a current ramp; the laser had a transfer function of 0.005nm/mA, with a threshold of 26mA and an upper limit of 150mA. The ramp width of 0.3nm corresponded to a current ramp from 60-120mA.

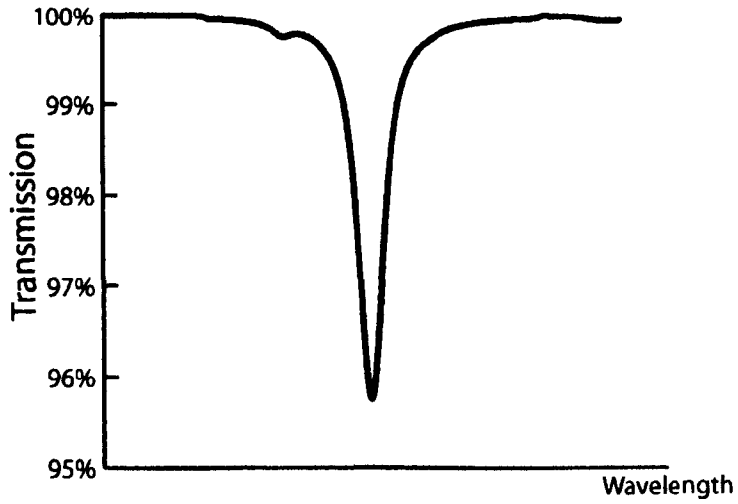


Figure 2.5: Theoretical transmission spectrum for a 1mm (1000ppm.m) gas cloud of pure methane

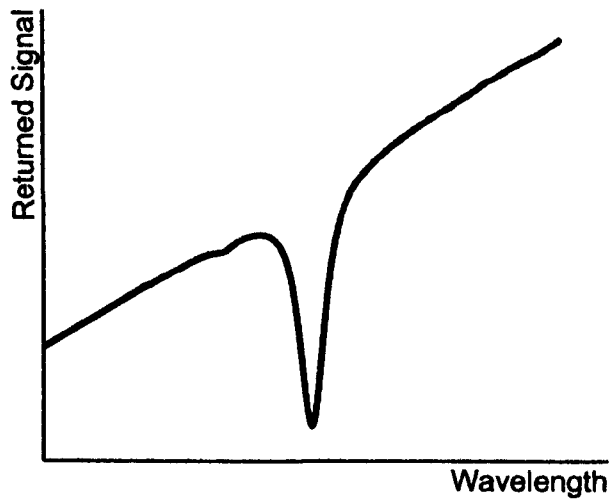


Figure 2.6: Laser output and methane absorption combined

On top of this ramp a sinusoidal modulation of frequency  $\omega$  is added. This wavelength modulation gives rise to a small variation in the recorded transmission. This change in transmission is dependent on the shape of the transmission at that wavelength, with an amplitude depending on the ratio of transmission change to wavelength change, i.e.  $\frac{\delta T}{\delta \lambda}$ , which is the gradient of the transmission curve at that point. Hence, the signal recovered by the detector has an amplitude proportional to the local gradient of the transmission trace, as shown in figure 2.7. The action of multiplying the direct transmission trace by a

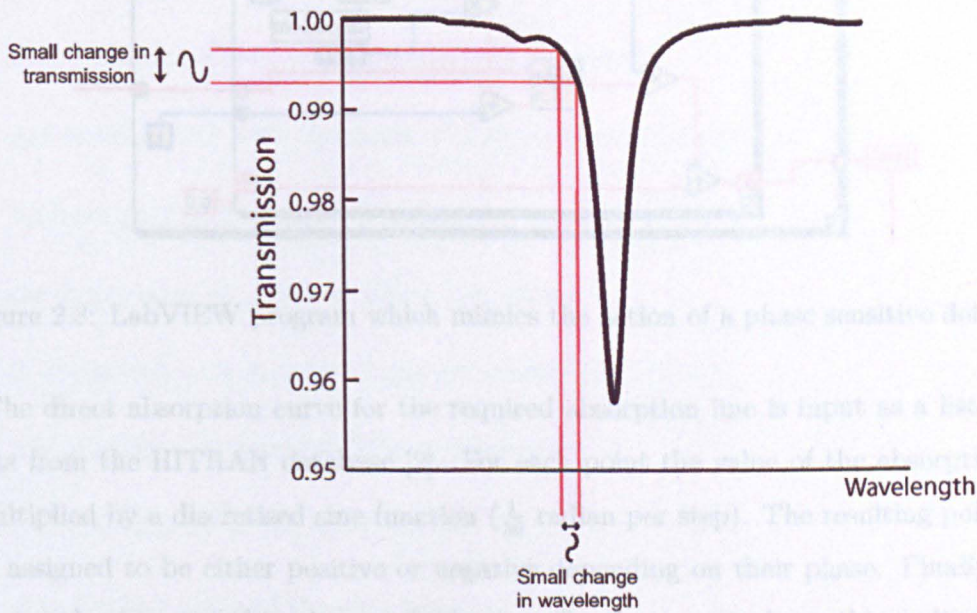


Figure 2.7: WMS returns the derivative of the transmission signal

local oscillator can be mimicked by a computer program written in LabVIEW as discussed in subsection 2.1.3. This generates the various derivatives, given the original transmission spectrum.

### 2.1.3 Phase Sensitive Detector

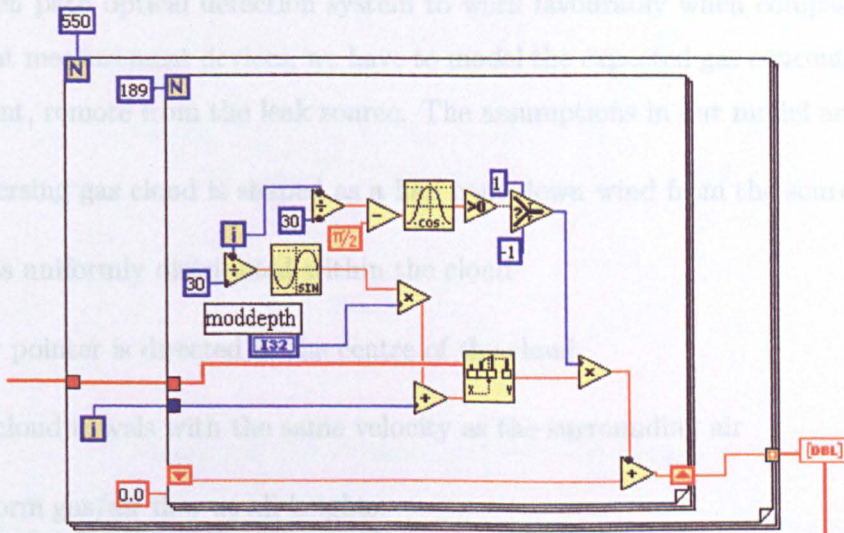


Figure 2.8: LabVIEW program which mimics the action of a phase sensitive detector

The direct absorption curve for the required absorption line is input as a list of 550 points from the HITRAN database [2]. For each point the value of the absorption line is multiplied by a discretised sine function ( $\frac{1}{30}$  radian per step). The resulting points are then assigned to be either positive or negative depending on their phase. Finally every discrete value is summed to give one final value. For the correct phase, this multiplication with a sine wave of the same frequency makes every value positive. When summed the result is always a large positive number. For other frequencies, the resulting sum will be approximately zero. The program then moves on to the next point on the absorption curve. The output from this program is a list of 550 points which corresponds to the theoretical output from a phase sensitive detector.

## 2.2 Gas Dispersion

For an open path optical detection system to work favourably when compared to traditional point measurement devices, we have to model the expected gas concentration levels at any point, remote from the leak source. The assumptions in our model are:

- dispersing gas cloud is shaped as a half cone down wind from the source
- gas is uniformly distributed within the cloud
- laser pointer is directed at the centre of the cloud
- gas cloud travels with the same velocity as the surrounding air
- uniform gas/air flow at all heights.

This gas dispersal is as shown in figure 2.9, where:

- $L$  is the leak rate in litres of gas per minute (litre/min)
- $z$  is the distance from the leaking source (m)
- $v$  is the velocity of the wind (m/s)
- $\phi$  is the half angle of the gas cloud
- $r$  is the radius of cross section through the gas cloud (m)
- $C$  is the fractional concentration of gas (i.e. range 0 to 1)

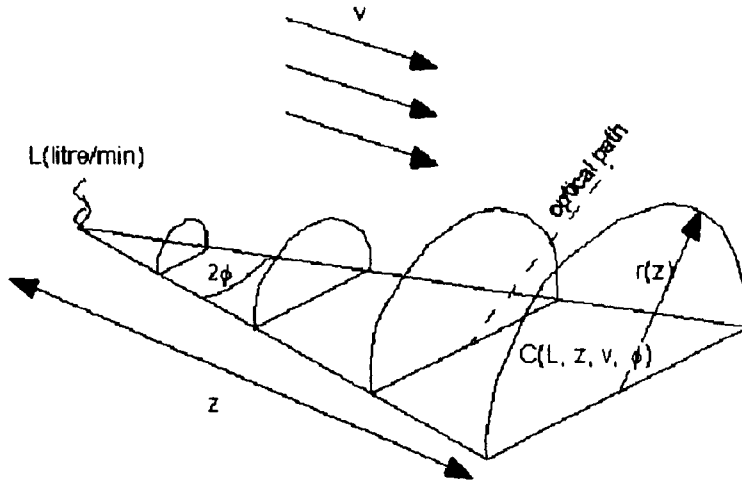


Figure 2.9: An idealised gas leak and dispersion

### 2.2.1 Gas Concentration At A Point Down Wind Of The Source

To calculate the concentration of gas at a point at a distance  $z$  first we consider the volume of gas/air mixture passing past this point per second. Consider the half-circle moving at velocity  $v$ :

$$Vol(z)/second = \frac{\pi r^2}{2} v. \quad (2.4)$$

Substituting for  $r$  into equation 2.4 gives us

$$Vol(z)/second \approx \frac{\pi(\phi z)^2}{2} v, \quad (2.5)$$

for small  $\phi$ . Dividing the volume of gas released per second, by this flowing volume gives us the fractional concentration

$$C(L, z, v, \phi) = \frac{L}{60000} \frac{2}{\pi(\phi z)^2} \frac{1}{v}. \quad (2.6)$$

Within equation 2.6 the wind velocity,  $v$ , and the half cone angle,  $\phi$ , of the gas cloud are independent variables, the values of which depend upon the wind characteristics. Values of 1 litre/min for the leak rate, a wind speed of 1 m/s and a gas cloud half-cone angle of 0.1 radians are not unreasonable and give a concentration distribution as shown in figure 2.10. Note that concentration is proportional to  $1/z^2$ .

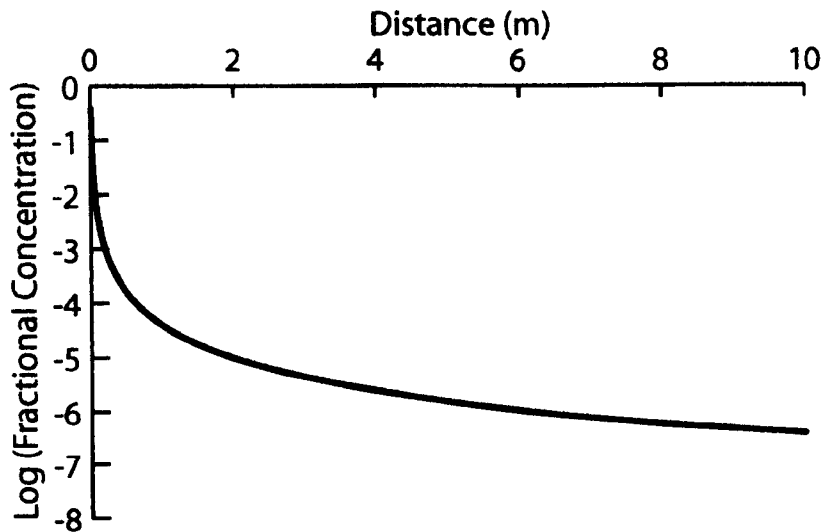


Figure 2.10: The leaking gas concentration at a point decreases with the square of the distance from the leak. Note:  $\text{Log}(\text{Fractional Concentration})=0$  corresponds to pure gas

### 2.2.2 Integrated Concentration Over Optical Path

Line of sight optical detectors measure not concentration, but the product of concentration and thickness of gas cloud. Assuming that the instrument detects the backscattered light, that the laser pointer is directed at the centreline of the gas cloud, and that the

point of view is perpendicular to the gas cloud, the optical thickness is  $2r$ . This gives a concentration x path length product of

$$C(L, z, v, \phi) \times 2r = \frac{L}{60000} \frac{4}{\pi(\phi z)} \frac{1}{v}. \quad (2.7)$$

This shows that the measured signal is inversely proportional to the distance from the leak, seen in figure 2.11. This difference in scaling with distance means that a line of sight

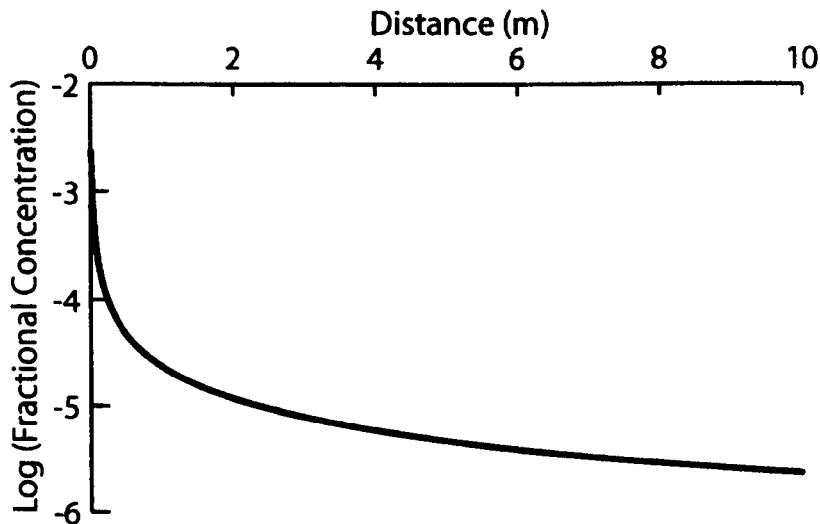


Figure 2.11: The concentration x path length is inversely proportional to the distance from the leak. Note:  $\text{Log}(\text{Fractional Concentration})=0$  corresponds to pure gas

instrument will perform better than a point sensor when operating away from the leak source. As expected, comparison between the two approaches shows a cross over point, see figure 2.12. Near the leak the point measurement system is most sensitive whereas further from the leak the line of sight system become more effective. The absolute distance at which this cross over occurs depends upon a number of factors which influence

the sensitivity of each instrument type. The distance at which both systems show the

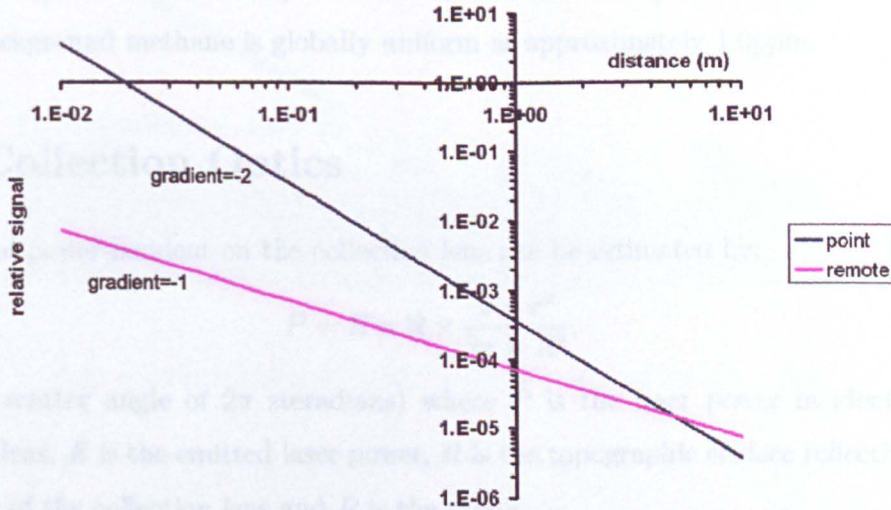


Figure 2.12: Comparing theoretical responses from point measurement and line of sight measurement techniques. The cross over point is arbitrary, and related to leak conditions

same sensitivity is not relevant since the two systems use different units and can not be compared. However, it is always the case that at a large enough distance, the line of sight instrument will be preferential over the point measurement system. The same reading could be found at a position given by  $z = \frac{1}{2\phi}$ , which for this leak is 5m, which is independent of the leak rate but not of the cone angle. A more diffuse leak (larger cone angle) will allow the line of sight instrument to dominate at a closer range. Clearly an exact comparison requires a precise definition as to the gas dispersal which itself will depend greatly upon the conditions under which the leak is found.

It is possible that two “ideal” instruments have the same maximum distance limitation

since a fundamental limitation is reached when the increase in concentration due to the leak is not significant when compared with that of the atmospheric background. Atmospheric background methane is globally uniform at approximately 1.6ppm.

## 2.3 Collection Optics

The optical power incident on the collection lens can be estimated by:

$$P = E \times \mathfrak{R} \times \frac{\pi \times r^2}{2\pi \times R^2}, \quad (2.8)$$

(for a scatter angle of  $2\pi$  steradians) where  $P$  is the laser power incident on the collection lens,  $E$  is the emitted laser power,  $\mathfrak{R}$  is the topographic surface reflectivity,  $r$  is the radius of the collection lens and  $R$  is the range.

The distributed feedback laser diodes in use emit approximately 5mW of light, surface reflectivity is discussed later (table 4.1) but is taken here as 3%, the collection lens has a 7.5cm diameter and the working range is taken as 5m. This gives:  $P = 0.005 \times 0.03 \times \frac{1}{2} \times (\frac{0.075}{5})^2$ . Thus an estimate to the received power is:  $P = 17nW$ .

This collected fraction of light is the fractional area of the sphere into which light is scattered as shown in figure 2.13.

This is the light power incident on the front of the collection lens; in our case we use a thin, plastic Fresnel lens. The important consideration is the photocurrent developed in the detector. The lens has a transmissivity of approximately 90% at 1651nm, the narrow band optical filter in front of the detector transmits approximately 50% of the light and the detector has a quoted efficiency of 0.85A/W at 1651nm. This means that the generated photocurrent in the detector will be  $\sim 6.5nA$ .

Given this information and the specification of the InGaAs detector (Thorlabs PDA400), based on the theoretical data presented in figure 4.5 (see section 4.2), the instrument

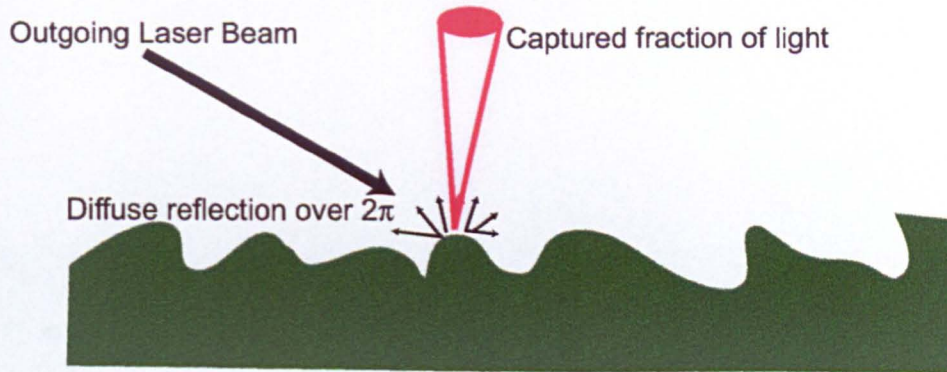


Figure 2.13: Light is scattered back into the collection optics

should have a detection limit of  $\sim 100$ ppm.metre. More generally, the predicted detector photocurrent derived from equation 2.8 varies with range as shown in figure 2.14.

## 2.4 Processing of Gas Cloud Images

To improve understanding of gas leak dispersion, it is desirable to be able to visualise this dispersion to aid the development of an active laser detection system. This was easiest to achieve by using a thermal imaging camera to survey a known leak against a heated background. Collaborators in Malmö, Sweden, developed a gas leak test site (see figure 2.15) for the purpose of studying gas leak dispersion. Water filled radiators were used to control the background temperature in order that the leaking gas would be at a different temperature, and hence detectable by the thermal imaging camera. The recorded video footage of gas dispersion is high resolution (300x300 pixels), but monochrome. This has the effect of significantly reducing the contrast of the gas movement over the background image. Our aim was to develop an automated process to boost the contrast of this video footage. A computer program (see subsection 2.4.1), written in LabVIEW, uses the first

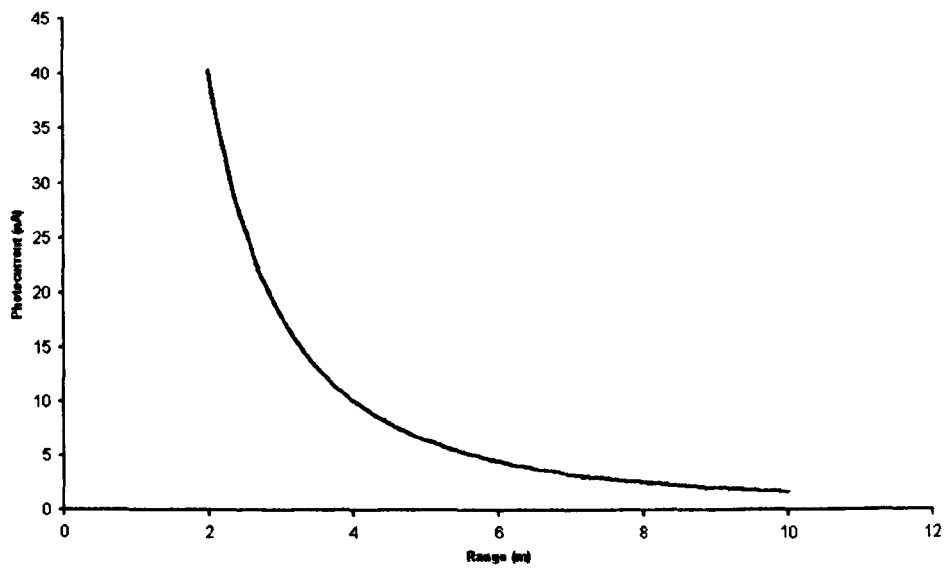
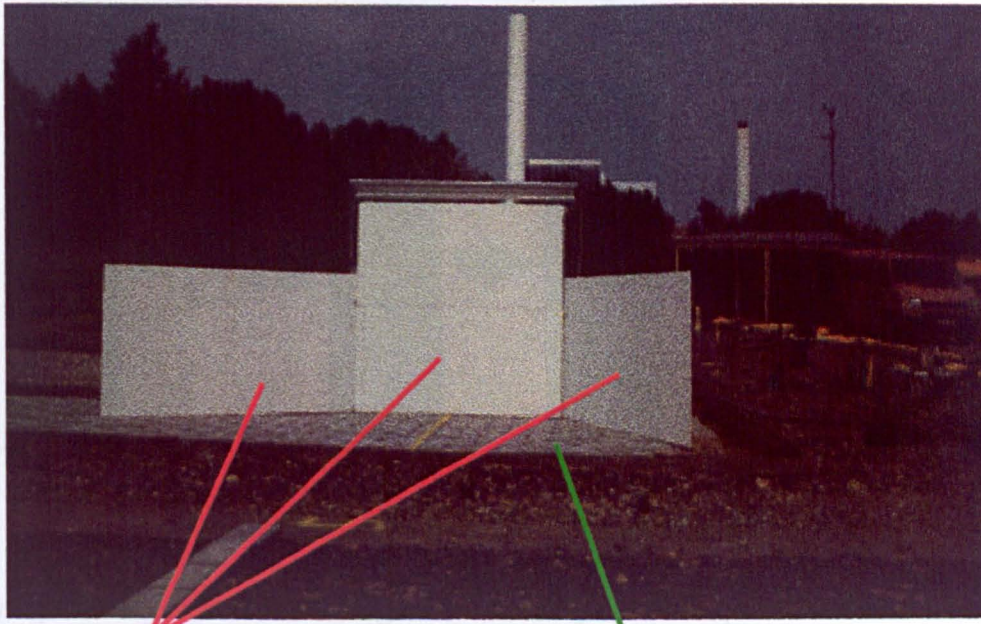


Figure 2.14: Predicted photocurrent varies with the square of the distance (reflectivity taken as 3%)

few frames of the video footage (before the artificial leak is turned on) to create a gas free background image. This saved background image can then be subtracted from all subsequent frames of the captured video leaving a raw image of the gas cloud. This is then coloured and superimposed on the original background. The functionality of these stages is shown in figure 2.16. The processed images can be further manipulated by



Water-filled radiators to create artificial temperature difference

Leaking pipes buried 80cm under paving slabs to mimic gas escape

Figure 2.15: Test site in Sweden with radiators to create an artificial background temperature

This LabVIEW program starts by loading a predetermined background image (figure 2.17). This image was created by averaging the first five frames from the monochrome video footage, before the gas leak was activated. The program then loads the first in a sequence of images that have been created from the gas leak video, as shown in figure 2.18. The background image is then subtracted from this video frame to leave an image

few frames of the video footage (before the artificial leak is turned on) to determine a gas free background image. This saved background frame can then be subtracted from all subsequent frames of the captured video leaving a raw image of the gas cloud. This is then coloured and superimposed on the original background. The functionality of these stages is shown in figure 2.16. The processed images can be further manipulated by

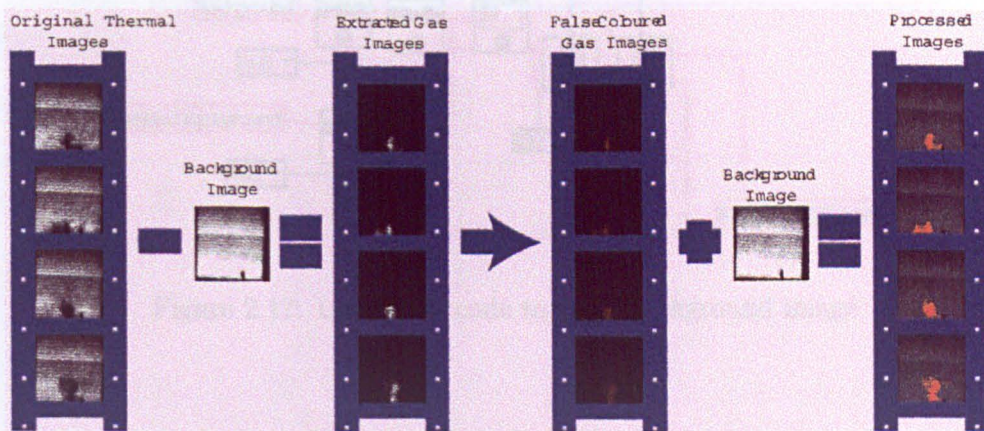


Figure 2.16: Functionality of video image processing

applying various levels of smoothing to simulate capture footage of lower resolution. This is discussed in more detail in subsection 2.4.2.

### 2.4.1 Colour Enhancement of Monochrome Video Clips

This LabVIEW program starts by loading a predetermined background image (figure 2.17). This image was created by averaging the first five frames from the monochrome video footage, before the gas leak was activated. The program then loads the first in a sequence of images that have been created from the gas leak video, as shown in figure 2.18. The background image is then subtracted from this video frame to leave an image

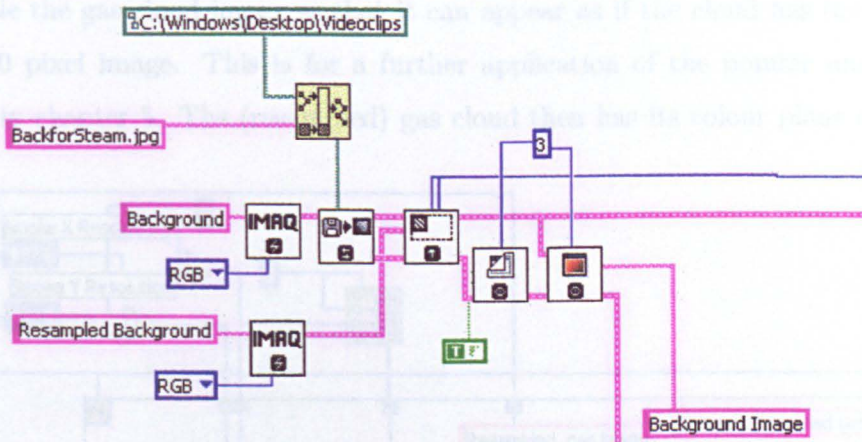


Figure 2.17: LabVIEW code to open background image

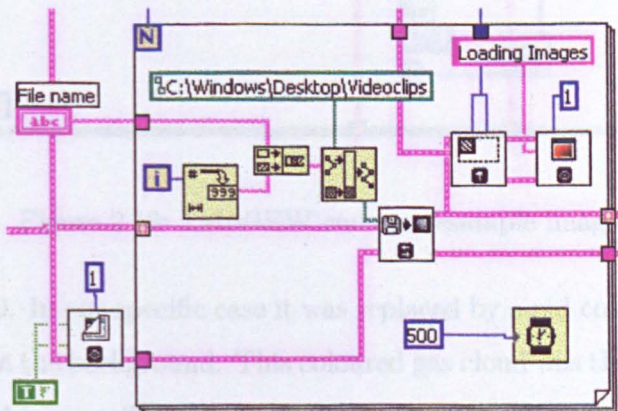


Figure 2.18: LabVIEW code to open gas leak images

solely of a gas cloud. A section has been added to the program which gives the option to resample the gas cloud image so that it can appear as if the cloud has been sampled as a 10x10 pixel image. This is for a further application of the pointer unit which is discussed in chapter 5. The (resampled) gas cloud then has its colour plane changed as

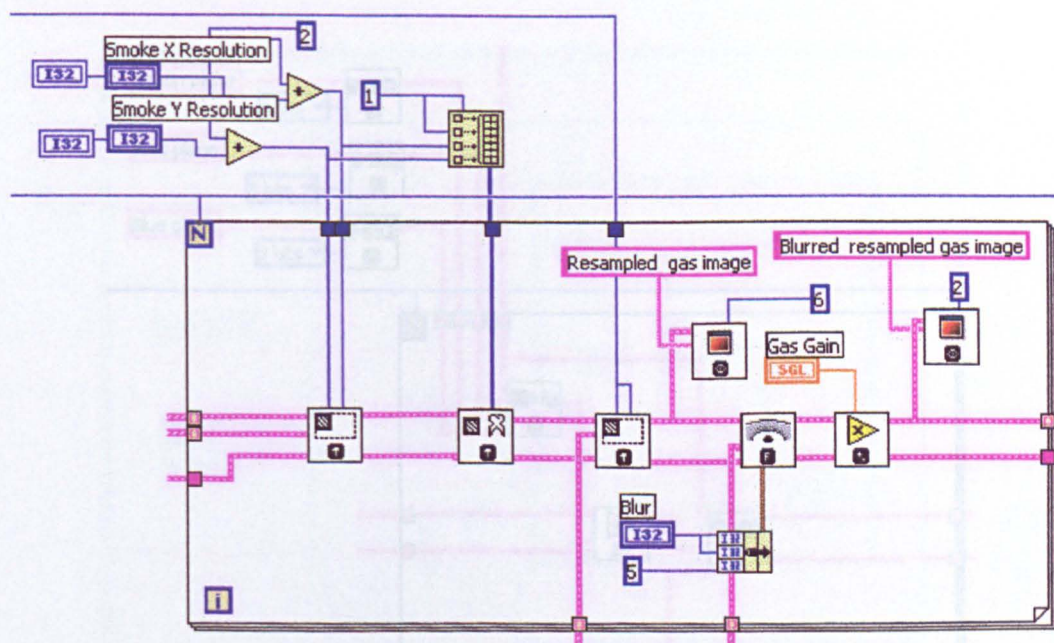


Figure 2.19: LabVIEW code to resample image

shown in figure 2.20. In our specific case it was replaced by a red colour as this was easily distinguishable from the background. This coloured gas cloud was then overlayed onto the original background image. This process repeats itself for every image in the sequence, to colour enhance the gas cloud in every frame of the video. Finally the program saves every frame it has created and gives the option to view them all sequentially, giving the effect of a flicker-book animation (see figure 2.21).





## 2.4.2 Smoothing

There is the potential to scan the methane detector over an area, building up an image of any methane leak. The fewer pixels in this image, the more time can be spent collecting data at each pixel, and so the more sensitive the instrument could be. Clearly then there is a trade-off between high methane sensitivity, and high pixel resolution of a generated image. Work was performed to simulate low pixel resolution data, and try to enhance the image such that it looked similar to a higher pixel resolution image.

This LabVIEW program starts by creating space for the processing of images. Two images are loaded into the program. Firstly, a background image of the scene. The program then loads an image which contains only the gas cloud. This image is available since the gas image is extracted when it is false coloured (see subsection 2.4.1). The gas video clip is resampled at a set resolution, lower than the background image, as shown in figure 2.22.

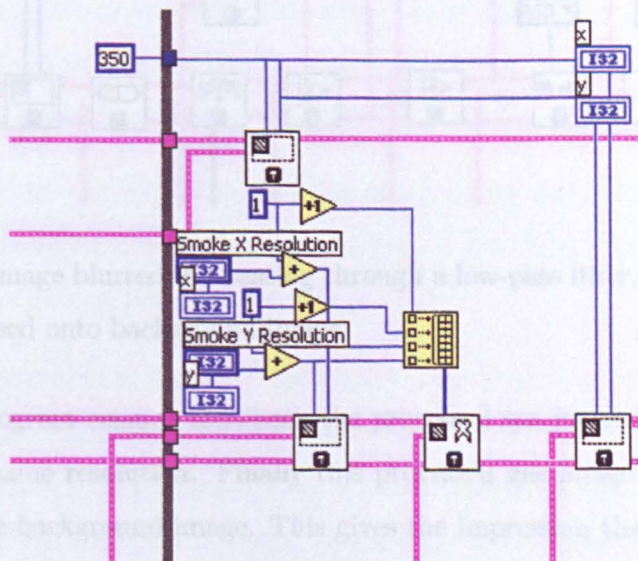


Figure 2.22: Gas image resampled at lower resolution

The sampled gas image (called smoke in the LabVIEW diagram) is then extracted and sampled again, this time at the same resolution as the background image ( $350 \times 350$  pixels here). This gas image looks identical to the lowest resolution image, but consists of more pixels. The program then low-pass filters this  $350 \times 350$  resolution gas image (figure 2.23). This has the effect of smoothing the gas cloud, so it looks like an image taken with a higher resolution gas detector.

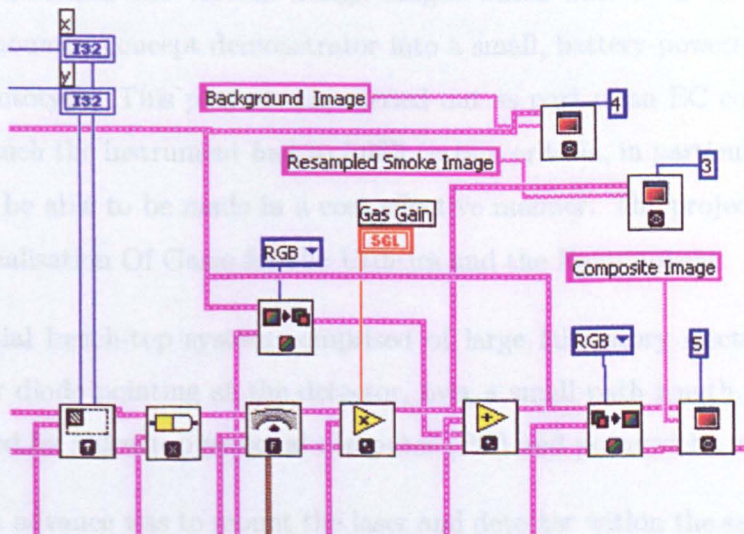


Figure 2.23: Gas image blurred, by passing through a low-pass filter, before being superimposed onto background image

The LabVIEW program ensures that both the processed gas image and the background image are of the same resolution. Finally this processed gas image is added to the red colour plane of the background image. This gives the impression that the captured data is high resolution, and looks more representative of a gas cloud.

## 3. Instrument Development

This chapter describes the various design stages which have seen the evolution of a large, bench mounted concept demonstrator into a small, battery-powered, portable pre-production prototype. This project was carried out as part of an EC co-funded consortium, and as such the instrument had to fulfill certain criteria, in particular the resulting design should be able to be made in a cost effective manner. The project was known as VOGUE; Visualisation Of Gases for the Utilities and the Environment.

1. The initial bench-top system comprised of large laboratory electronics, and had the laser diode pointing at the detector, over a small path length. All of this was controlled by a desktop personal computer (PC) and powered by mains electricity.
2. The first advance was to mount the laser and detector within the same housing and use backscattered light to detect the presence of gas. This proof of concept system still used bench-top control electronics.
3. To improve portability, the large bench-top control electronics were then replaced with smaller commercially available units. A housing was designed which made the entire instrument self contained except for a controlling laptop PC. This allowed the instrument to be more easily tested at outdoor sites. The battery power enabled testing at more remote locations.
4. The cost of reproducing the instrument was next addressed. All signal processing

electronics were designed to the necessary specification, and prototypes were made. For example, the cost of the required four phase sensitive detectors (PSD's) fell to about 5% of their commercial predecessors.

5. The final stage of development involved replacing the laptop by an automated system that required minimal training to operate. An embedded computer system was integrated into the system to automatically launch the system software, and undertake diagnostic tests on startup. A digital readout and audible tone were implemented to give feedback to the user. The final instrument was a fully portable technology demonstrator.

### 3.1 Bench Top Demonstrator

The modelling of light absorption by a 10 cm cell of 100% methane predicted that it should be possible to directly see the change in returned light levels when scanning through the absorption band as shown in figure 3.1. The initial concept demonstrator was designed to show this result.

An InGaAs distributed feedback (DFB) laser diode (supplied by Siemens) operating in the region of 1651nm was mounted onto a thermo-electric cooler (TEC) and temperature stabilised at 18°C (specific to this diode) as shown in figure 3.2. The operating wavelength of a laser diode is temperature dependant and so is required to be carefully controlled. The information about this diode, gained from Siemens, was that when operated at 18°C it would have a threshold current of 26mA, a tuning slope of 0.005nm/mA, and should not be operated above 150mA. The laser diode was placed under computer control (see figure 3.3) using LabVIEW as the interfacing software. The current applied to the laser diode was slowly varied from 80mA to 100mA (as described in subsection 3.1.1), causing

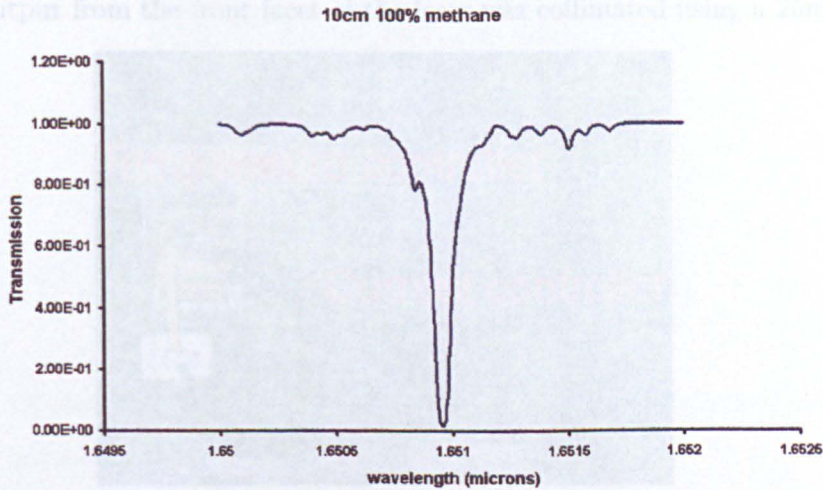


Figure 3.1: Theoretical methane spectrum obtained using HITRAN [2]



Figure 3.2: left: DFB laser diode mounted onto a TEC, right: close up showing laser diode mounted onto a metal carrier, with copper connection wires

a change in output wavelength known to include the 1651nm methane absorption band. The light output from the front facet of the laser was collimated using a 25mm diameter



Figure 3.3: The temperature control was hard-wired to the TEC element, the diode current controller is under computer control via an IEEE interface

### 3.1.1 Ramp Generation and Data Acquisition

40mm focal length lens, and directed through the gas sample cell (at room temperature and atmospheric pressure). Collimated light exiting the sample cell was collected with a 100mm diameter plastic Fresnel lens and focussed onto an InGaAs detector as shown in figure 3.4. A schematic diagram showing the entire setup can be seen in figure 3.5. In this concept demonstrator the output from the laser diode was directed at the Fresnel lens (rather than both the laser and detector aimed at a common target) and optimised to ensure maximum laser light was incident on the detector. The Fresnel lens had a larger diameter than necessary, but would be necessary with planned future changes. A 100cm sample cell was filled with 1% methane (balance of nitrogen) and placed between the laser collimating lens and the Fresnel lens. Using wavelength modulation spectroscopy (WMS) with a laser diode modulation frequency of 1.5kHz (modulation depth corresponding to half the line-width) and with a time constant of 100ms, the first and second derivative

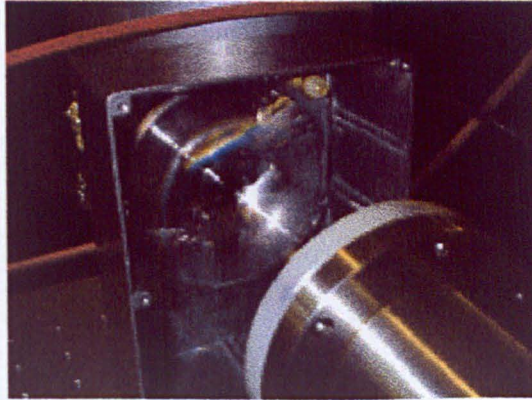


Figure 3.4: 100mm diameter Fresnel lens (50mm focal length) mounted in front of the InGaAs detector

spectra were acquired by the computer, as shown in figure 3.6.

### 3.1.1 Ramp Generation and Data Acquisition

The computer takes the (input) scan centre together with the scan width and works out the start and end points of the scan. At the first point, the computer writes the specified voltage to the configured data acquisition card output channel, and reads the voltage given at the input channels. These input voltages are stored by the computer. The output voltage is then increased by the designated step size, and the process is repeated. Once the scan end value is reached, and all channels have been communicated with, the computer then displays the stored arrays on individual graphs. This entire program is shown in figure 3.7. This program is the basis for all data acquisition, and is used with a scan width of zero to record data at a single point. The program is used as subroutine in future programs, and is labelled "Ramp 2.1".

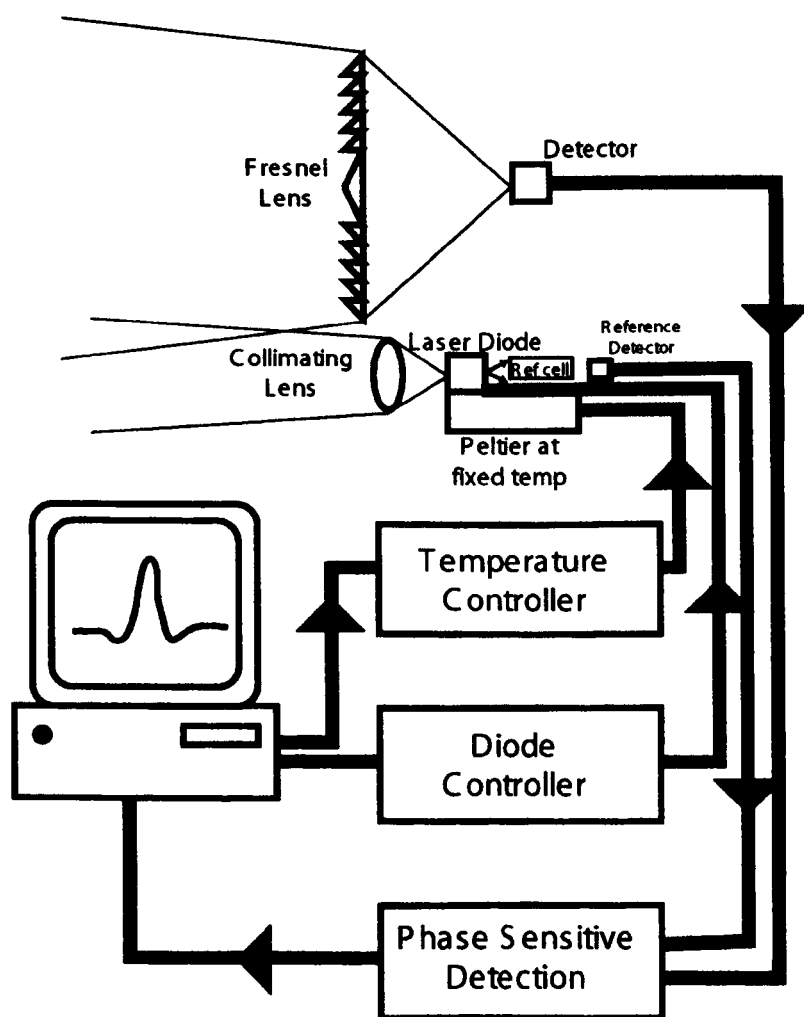


Figure 3.5: Schematic showing signal path through the setup

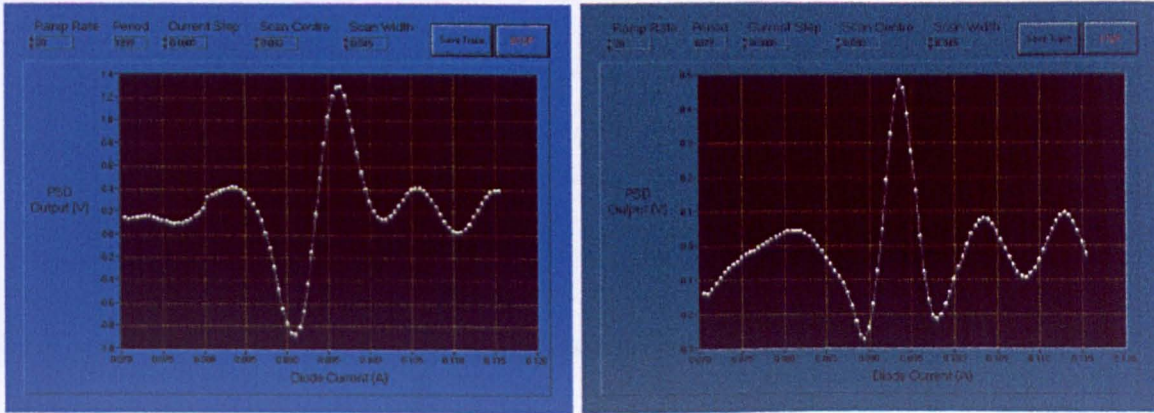


Figure 3.6: Left: 1st derivative spectrum, Right: 2nd derivative spectrum (both with 1.5kHz modulation and 100ms time constant). The additional structure evident in these spectra is due to the gas cell; when not aligned exactly collinear with the laser light, extra fringes are visible.

## 3.2 Proof of Concept System

The next developments transformed the bench top system into an open path demonstrator which could be used to assess the practical performance levels of the proposed instrument. Two main changes were proposed:

**Optical layout** The laser diode and the InGaAs detector would be placed in close proximity (approximately the radius of the Fresnel lens) with both aimed at a common distant target.

**WMS frequency** The specific WMS frequency in use would be optimised to ensure maximum signal recovery.

The lateral displacement of the outgoing beam from the collection lens reduces the potential for transmitter breakthrough but does in principle produce a parallax issue. This



would reduce the amount of collected laser light at very long or short ranges.

The primary issue was to ensure that enough returned light was collected by the Fresnel lens to ensure sufficiently noise-free signal processing could be performed. Because the amount of light incident on the detector is proportional to the area of the collection optics, it was decided to increase the diameter of the Fresnel lens to 150mm (with 80mm focal length). Both the laser diode and detector were mounted onto x-y-z translation stages to enable fine adjustment of their position, to maximise the returned light level as shown in figure 3.8. The value chosen for WMS of 1.5kHz was suggested, based on prior experience with this technique. This frequency lies comfortably within the audio band, making common integrated circuits such as operational amplifiers readily available and very cheap. However, this frequency may not be optimal. The modulation signal is derived from the phase sensitive detector, and is added to the computer generated ramp signal via a purpose built circuit board, as shown in figure 3.13. The modulation signal from the phase sensitive detector was changed in 100Hz intervals from 300Hz up to 15kHz to investigate the effect this had on the returned signal to noise ratio. There was very little deviation throughout the entire range, but some improvement could be gained toward the middle of the range, at 6kHz modulation. This was not due to lower noise from interference, but an electronics issue. By choosing a modulation frequency such that the first three harmonics lie within the audio band, a supply of low-noise and low-cost electronic integrated circuits is guaranteed.

The control electronics were all identical to the initial concept demonstrator, and were arranged so that they could be housed within a large flight case as shown in figure 3.9. This enabled the laser pointer to be tripod mounted and connected via a multi-way cable to the instruments within the flight case. For the first time outdoor tests could be carried out with the instrument.

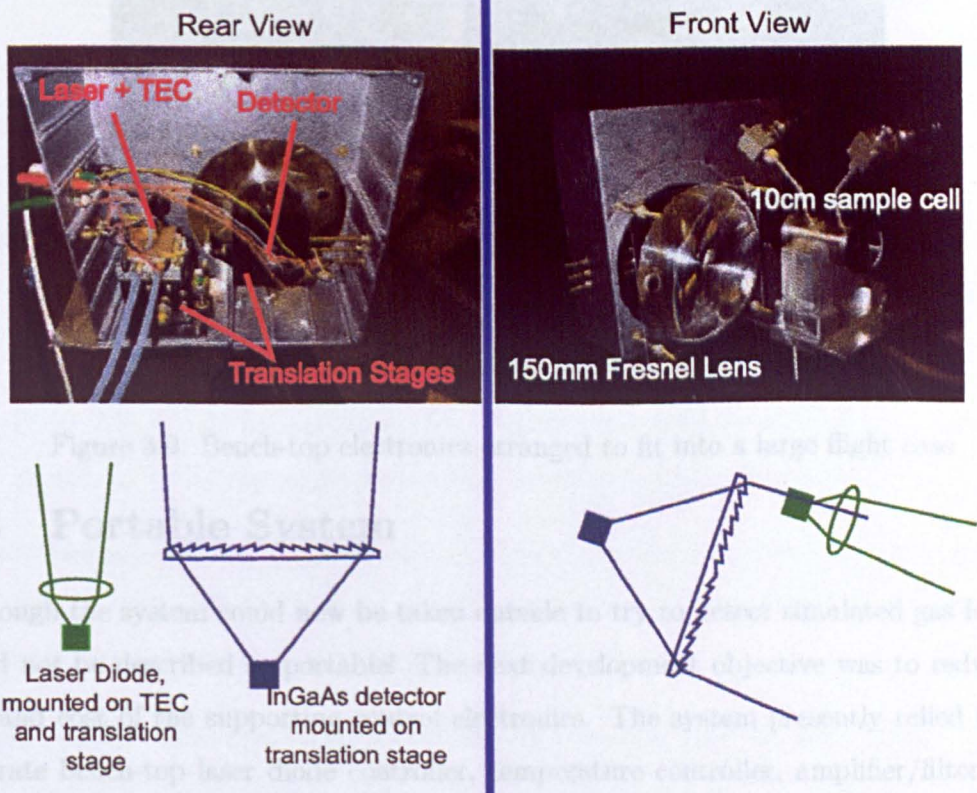


Figure 3.8: Left: Internal view of laser pointer, Right: The laser pointer technology demonstrator capable of detecting methane from the back scattered light (note in this case, the reference/calibration cell is also mounted)

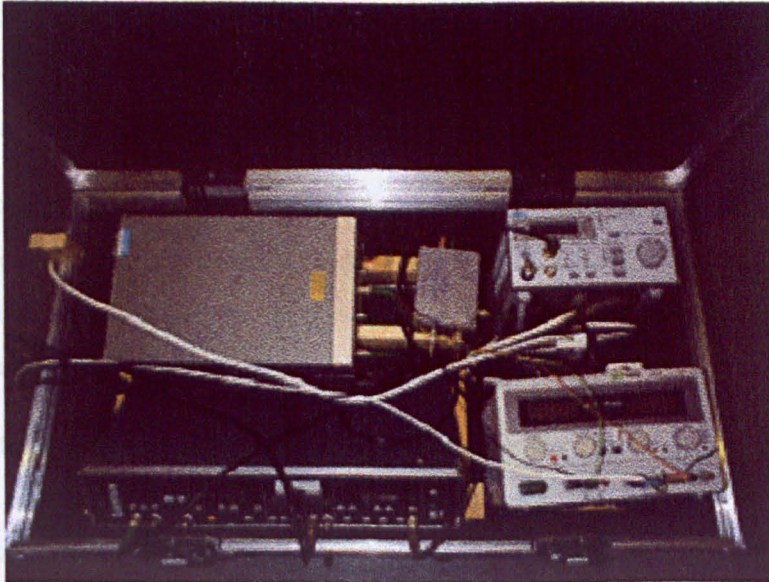


Figure 3.9: Bench-top electronics arranged to fit into a large flight case

### 3.3 Portable System

Although the system could now be taken outside to try to detect simulated gas leaks, it could not be described as portable! The next development objective was to reduce the size and cost of the supporting control electronics. The system presently relied upon a separate bench-top laser diode controller, temperature controller, amplifier/filter stage, power supply and a single phase sensitive detector which is capable of generating either of the first two harmonics.

The resulting changes replaced all of the electronics which had been housed within the flight case with either smaller commercially available units, or were designed and built in-house. Specifically:

**PC control** Using suitable PC interface cards (National Instruments Data Acquisition

– NI-DAQ), the whole system has been placed under laptop control. The modified software is "turn-key", handling all aspects of the system operation from laser diode switch-on, wavelength tuning, signal processing and provides a user-friendly display.

**Control software** The control software has been rewritten so that all data input and system control is via a single NI-DAQ card (DAQCard 6024E). The on-card oscillator is also used to generate the modulation frequency and reference frequencies for the phase sensitive detectors.

**Phase sensitive detector** The phase sensitive detector has been replaced by 2 high-quality miniature units (LIA-MV-150 units from Femto) allowing simultaneous recording of both first derivative and second derivative spectra.

**Amplifier/filter** The high-performance amplifier has been replaced by an in-house designed and constructed amplifier/filter as discussed in section 3.4.3.

**Waveform generation** Further in-house designed and constructed circuitry generates the reference waveform from the DAQ card for obtaining both first and second derivative spectrum as discussed in subsection 3.3.1.

**Power supply** Lead-acid rechargeable batteries are now used for portability.

In addition to these changes, field tests had revealed a problem when operating the instrument in strong sunlight. Wavelength modulation spectroscopy (WMS) maximises the recovered signal, but if the detector (and therefore the detector amplifier) receives too large a signal, it will become saturated and the WMS technique will fail. To counteract this, a narrow band interference filter was placed in front of the detector. Ideally the filter pass-band would be very narrow, and only allow the 1651nm laser light through. However, the angle tuning which arises because of the high numerical aperture of the

collection optics shifts the allowed wavelengths. For incident angles up to  $45^\circ$  the transmission wavelength of the filter is reduced by up to 40nm.

A bandpass filter centered at 1700nm with a 100nm bandwidth was tested and, while reducing the laser light by 50%, ensured that the detector amplifier was not saturated, even if aiming the collection optics at the Sun.

Figure 3.10 shows the entire modified system (without power supply/batteries). The system was designed to be fully enclosed within two metal cases (250x250x130 mm) which were hinged to allow access. After discussion with several potential end users (Euro-

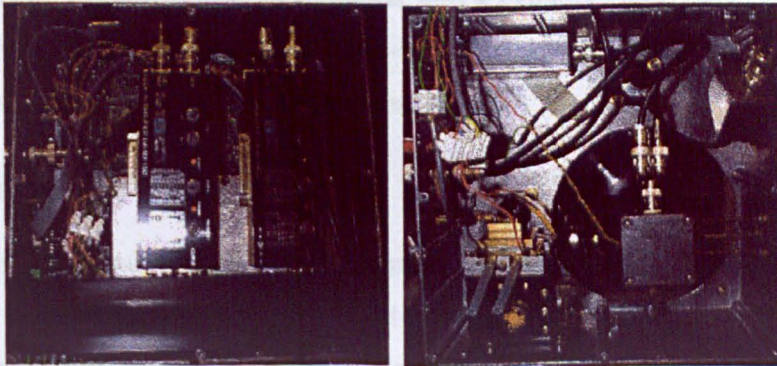


Figure 3.10: Left: Rear half of the unit which contains a combined laser and temperature controller, two PSD's and the electronics which generate the  $1\omega$  and  $2\omega$  reference frequencies, Right: Front half of the unit which houses the laser, detector, electronic filter and unity gain buffer amplifier

pean gas utility engineers) of the remote methane detector, it became clear that the ergonomics of the system would have to be improved in order that the aesthetic appeal of the instrument increased. The system was then rewired so that it could be housed within a cylindrical container, the front (optical head) of which was detachable and could be hand-held, as shown in figure 3.11.

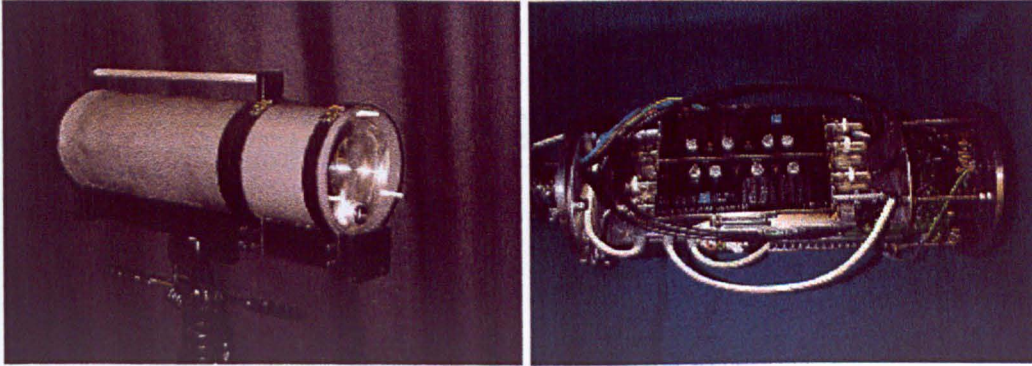


Figure 3.11: Left: Complete system rehoused into a cylinder (note that the front section is detachable and can be hand-held), Right: Internal view of the rehoused signal processing electronics (rear section)

### 3.3.1 Waveform Generation

The waveform generator was required to replace the functionality which had previously been present in the laboratory phase sensitive detector. It was also necessary to simultaneously demodulate the first and second harmonic waveforms, with two phase sensitive detectors; this requires both the  $\omega$  and  $2\omega$  frequencies to be generated.

The data acquisition card (NI-DAQCard 6024E) was capable of generating a square waveform of the desired frequency, 12kHz. This was fed into the custom designed electronics (figure 3.12). The first chip is commonly referred to as a “flip-flop” chip. The input is required to be a TTL compatible waveform. Every time it detects a rise at the input, the output changes state. This has the effect of perfectly halving the given signal. The 6kHz square output from this chip is low passed with a Sallen and Key filter to approximate a 6kHz sine wave. This is further low passed to improve the symmetry of the sine wave. This is an important stage; the sine wave will ultimately be used to drive the laser diode,

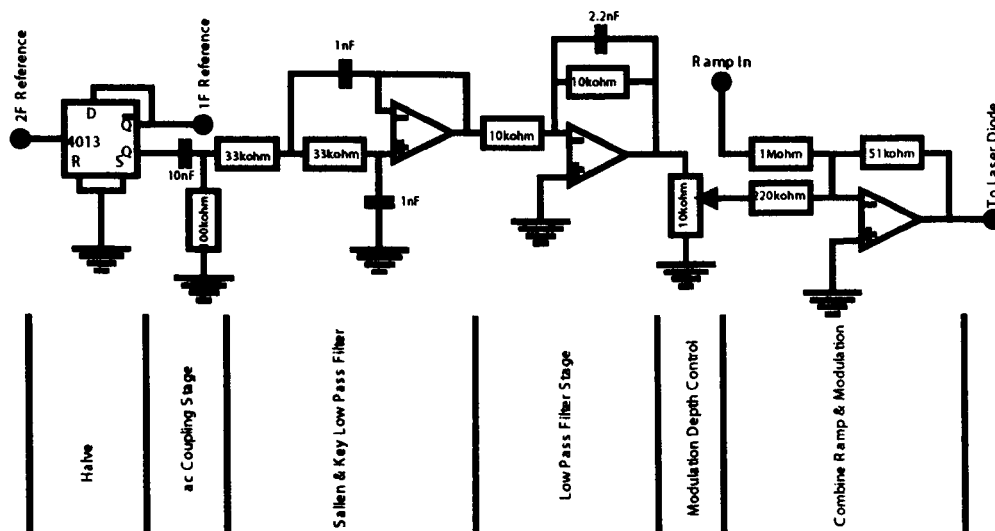


Figure 3.12: The in-house designed waveform generator

and as such must be as smooth as possible to prevent any output spikes. These are caused by sharp changes, or transitions at the input. Finally this signal is fed into an amplifier which combines the sine wave with the computer generated ramp, which is discussed in subsection 3.3.2. The output from this circuit is fed to the laser diode driver.

### 3.3.2 Combining Ramp and Modulation

As shown in figure 3.13, the resistors scale the input signals so that the output scans the laser from 80mA to 100mA with a modulation depth of approximately half the line width.

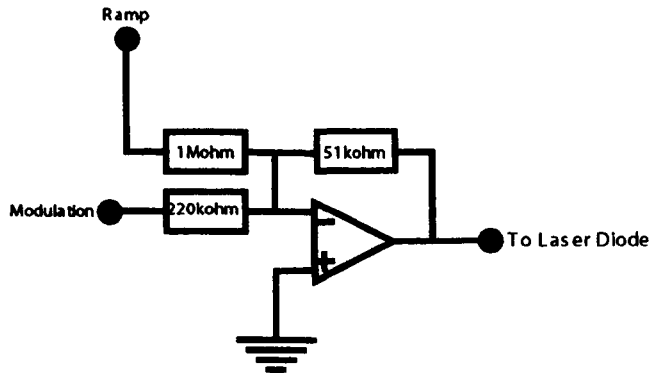


Figure 3.13: Circuit designed to combine the ramp and modulation signals

### 3.4 Functional Cost Efficient Prototype

The laser pointer could now be used by trained personnel to search for gas leaks in test conditions, but the entire system still needed to be tripod mounted and powered either by two 12V lead-acid batteries, or a laboratory power supply. The next advancements needed to reduce the weight and size of the system still further, and minimise the cost of production of this system to enable it to be commercially viable. For a product to be a secure development investment, it should not rely on components sourced from outwith the VOGUE consortium. Prominent changes planned for this instrument iteration involved:

**Phase Sensitive Detectors Design** Construct and test our own PSD based on commercially available integrated circuits.

**Partner Input** Use updated components supplied by consortium members to improve the instrument, specifically with the introduction of a laser module.

**Control Electronics** Replace the temperature controller and laser driver with smaller and more power efficient modules.

**Housing** Change the instrument layout so that the optical head and control electronics would be separately housed.

The key in-house development stage was in the design, construction and testing of phase sensitive detectors. These were based upon the Analogue Devices AD630 chip. The second harmonic phase sensitive detector is described in subsection 3.4.1, and a photograph is shown in figure 3.14.

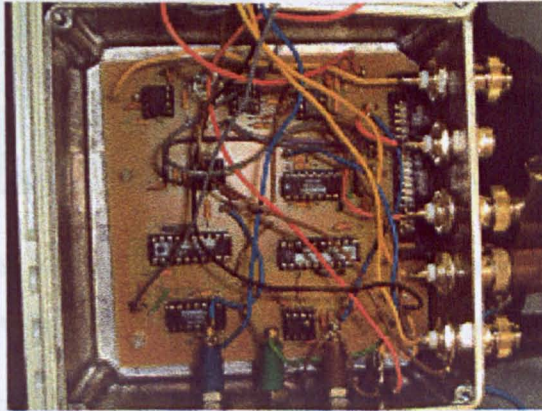


Figure 3.14: 1F and 2F in-house designed and constructed PSD's

Siemens have now housed the laser diode in a small hermetically sealed enclosure, with a 5mm focal length collimating lens mounted in front of the diode. The diode was seated onto a TEC element, with two temperature dependant resistors (2.2k thermistor and a Pt Resistor) also housed in the enclosure. The rear facet of the laser diode was directed at a small InGaAs detector. This detector which is at the rear of the package is individually sealed within a standard T05 enclosure, containing methane gas (see figure 3.15). This gas/detector package forms the basis for ensuring the system is operating at the correct wavelength, and provides the mechanism for frequency locking the laser diode. It is this new component that gives our instrument an advantage over competitors. The incorpo-

ration of a reference methane cell ensures absolute wavelength stability at exactly the correct wavelength; no amount of temperature and current adjustment can provide this level of lifetime stability, since the laser's characteristics can change over time.

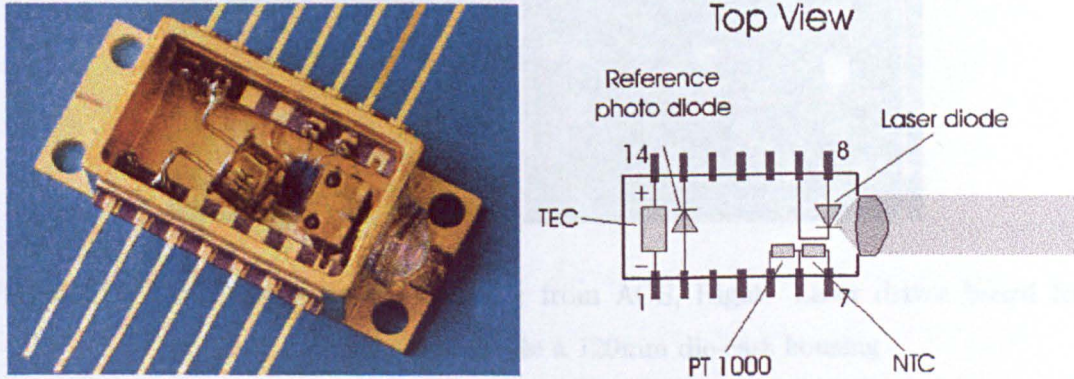


Figure 3.15: Left: laser diode module with top section removed, Right: Schematic diagram showing connection points of internal components

The combined temperature controller and laser driver was replaced by separate units. These units were more compact, and required less drive current, making them ideal for a small battery powered device. The temperature controller (see figure 3.16) was designed and supplied by a consortium partner (AOS Technology Ltd), who were also in the process of developing a laser driver specifically for our application. A suitable temporary laser driver was sourced (LD2000 from Thorlabs) and can be seen in figure 3.16.

Previously the generated reference signal for both of the PSD's was provided by a National Instruments DAQ card. These reference signals and associated phase shifters are now generated using a modulator and a digital phase shifter, also designed and supplied by AOS Technology Ltd, as shown in figure 3.17. This circuit utilised a high frequency modulator, and used a digital processor to return the required frequencies. Initially the first derivative signal was intended to be used to provide an error voltage (since it is

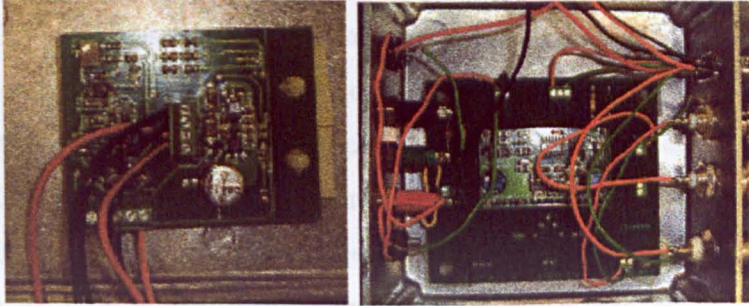


Figure 3.16: Left: Temperature controller from AOS, Right: Laser driver board from Thorlabs, both mounted inside a 120mm die-cast housing

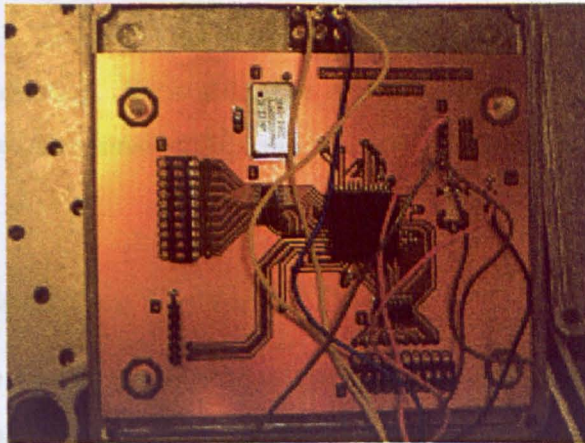


Figure 3.17: Modulator and digital phase shifter

anti-symmetric) for feedback to the laser driver, providing a mechanism to be wavelength locked to the methane absorption. For the likely signal levels that are to be detected, the zero offset of the 1f trace is significant compared to the peak-to-peak height of the signal. The magnitude of the offset varies, depending on laser characteristics and returned light levels. It is not possible, therefore, to simply add a constant to ensure a zero offset to the 1f trace. The 3f trace is also anti-symmetric about the methane absorption line, and has zero offset; this trace is suitable to provide an error voltage for feedback.

A new feature has been added to the software whereby the laser initially ramps through the methane transition (as before). Once the transition line from the methane in the reference cell has been identified, the laser fixes at the peak absorption wavelength, and can maintain this position by making small adjustments corresponding to the 3f signal. This addition to the program is discussed in more detail in subsection 3.4.2.

The entire electronics assembly was housed in a shoulder-mountable sealed plastic enclosure, connected to the optical head by a shielded multi-way cable. The two sections can be seen in figure 3.18. This enabled the unit to be operated by a single user without the need for a tripod mounting. Separating the optical head from the electronics reduced the arm fatigue of the user considerably and was considered important by the gas utility representatives.

### 3.4.1 Phase Sensitive Detector Design

The signal from the transimpedance amplifier (see section 3.4.3) is fed into an active filter chip from Texas Instruments (UAF42). The external resistor configuration on this chip determines the filter parameters. For the resistor combination shown in figure 3.19, the filter was designed to have a bandwidth of 11kHz; because this let sufficient 12kHz component through while minimising the overall bandwidth of signal passed to the phase

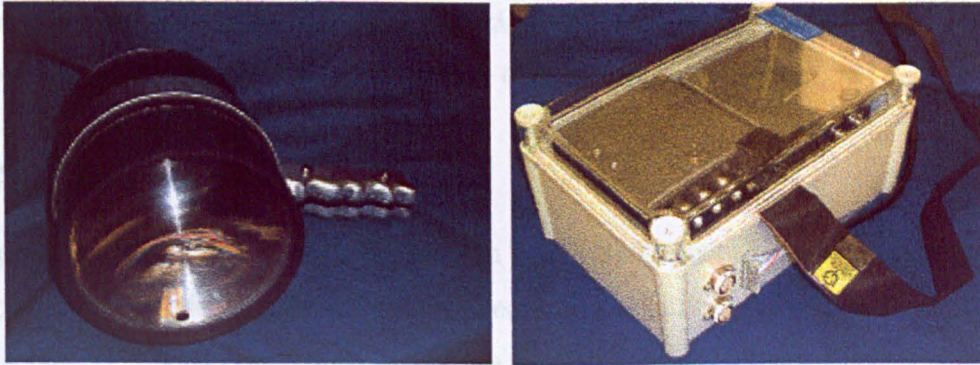


Figure 3.18: Left: 6" diameter optical head unit, Right: Shoulder mounted box containing signal processing electronics and batteries

sensitive detector. The filtered signal is fed into an Analogue Devices AD630 chip. This

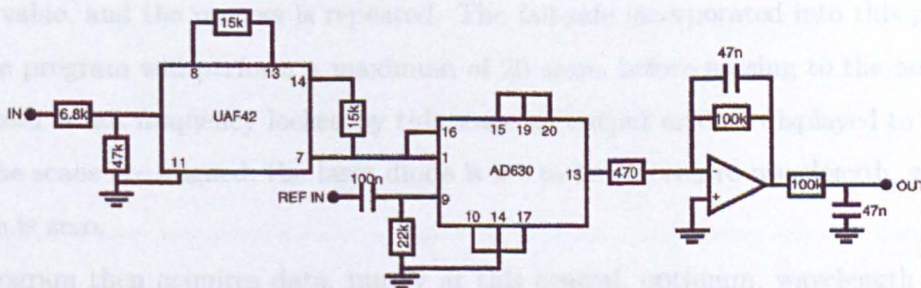


Figure 3.19: Circuit diagram of PSD designed to detect the 2nd harmonic

chip is a high precision balanced modulator/demodulator. The chip acts as a detector and narrow band filter combined. As stated on the data sheet "It can detect very small signals in the presence of large amounts of uncorrelated noise, when the frequency and phase of the desired signal are known. The precision input performance of the AD630 provides more than 100dB of signal range and its dynamic response permits it to be used with carrier frequencies of over 50kHz" [42]. As is shown in figure 3.19, a further low pass

---

output filter has been added to aid in rejecting wider bandwidth interference. This final low pass filter determines the time constant of the output readings.

### 3.4.2 Line Locking

The program starts up as before (subsection 3.1.1), and scans the laser wavelength. The  $3f$  signal from the reference detector is cross-correlated against a previously recorded spectrum - "X-FIT". This pre-recorded spectrum was taken while the laser diode was carefully temperature and current controlled under laboratory conditions. Provided the laser characteristics have not changed then the present spectrum should match the pre-recorded spectrum - for the same temperature and current. The cross-correlation provides a measure of how well the two spectra are aligned. The centre of the scan is adjusted according to this value, and the process is repeated. The fail-safe incorporated into this process is that the program will perform a maximum of 20 scans before passing to the next stage. If the laser is not frequency locked by this stage an output error is displayed to the user. Once the scans are aligned, the laser diode is set to be the centre wavelength, where the  $3f$  value is zero.

The program then acquires data, purely at this central, optimum, wavelength while simultaneously monitoring the signal at the  $3f$  output. A multiple of the signal at the  $3f$  output is added to the laser driver. In this way, the laser output wavelength is maintained at precisely the wavelength of the centre of the methane absorption line.

### 3.4.3 Transimpedance Amplifier

The bench-top system used a bare InGaAs PIN photodiode. This was connected to a laboratory amplifier and electronic filter, before the signal was fed into the phase sensitive detector. This was efficient in the laboratory, where sophisticated shielded wires were

used. The small photodiodes (approximately  $100 \text{ pA}$ ) which were powered by the photodiode were easily swamped by any noise sources which could be picked up by the cables. To overcome this problem, an amplifier was built into the front of the photodiode, reducing the potential for pickup (before the amplifier) as much as possible. The gain stage was simply an inverting operational amplifier as shown in Figure 3.20. Because such a large gain was needed, the dc signal was high-passed. This prevents saturation of the inputs of the phase sensitive detectors.

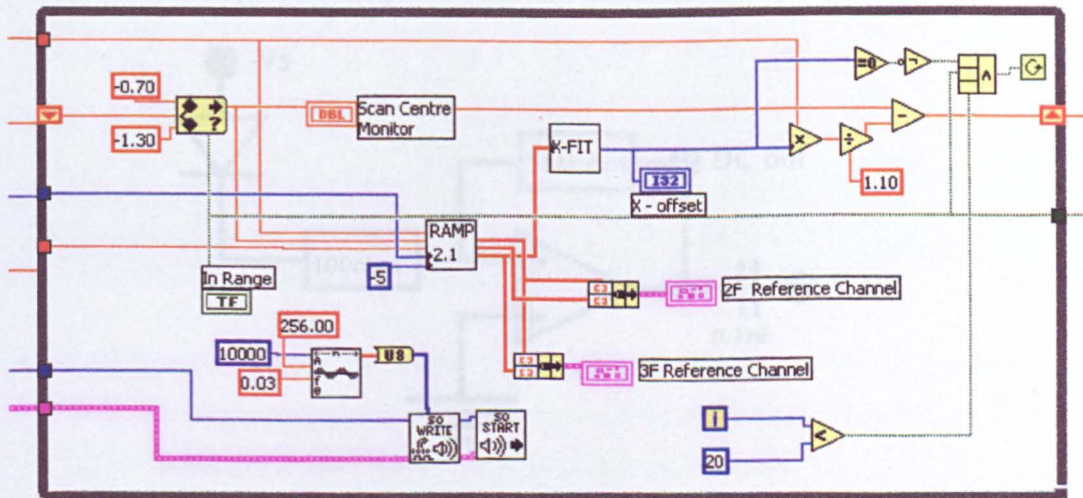


Figure 3.21: The in-house designed transimpedance amplifier using a TL071 operational

Figure 3.20: LabVIEW code which frequency locks the laser diode onto the methane absorption line

### 3.5 Technology Demonstrator

All prototypes thus far had used a PC (usually a laptop) to control the system via the interfacing software LabVIEW. The PC gave feedback on the performance of the instrument, and enabled the user to control parameters such as laser diode current and scan width. To use these functions reliably required knowledge of the system design. The final

used. The small photocurrents (approximately tens of nanoamps) which were produced by the photodiode were easily swamped by any noise sources which could be picked up by the cables. To overcome this problem, an amplifier was built onto the rear of the photodiode, reducing the potential for pickup (before the amplifier) as much as possible. The gain stage was simply an inverting operational amplifier as shown in figure 3.21. Because such a large gain was needed, the dc signal was high-passed. This prevented saturation of the inputs of the phase sensitive detectors.

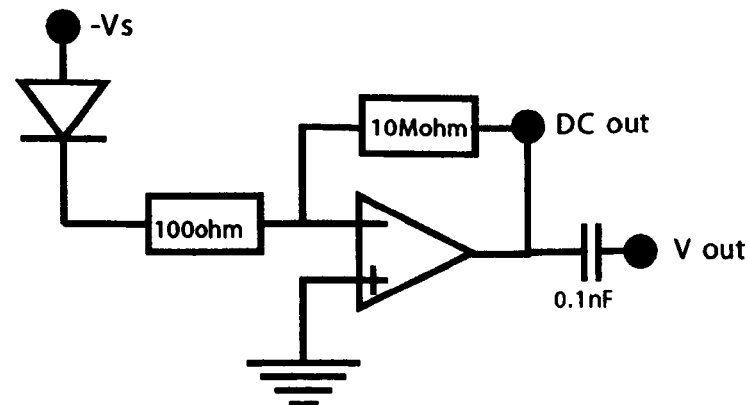


Figure 3.21: The in-house designed transimpedance amplifier using a TL071 operational amplifier

### 3.5 Technology Demonstrator

All prototypes thus far had used a PC (usually a laptop) to control the system via the interfacing software LabVIEW. The PC gave feedback on the performance of the instrument, and enabled the user to control parameters such as laser diode current and scan width. To use these functions reliably required knowledge of the system design. The final

modifications to be addressed enabled the entire system to be operated by a single user without any training (but with an instruction manual). It was also necessary to integrate the PC control into the system so that the prototype was fully self-contained and required no knowledge of computers to operate. This increased the current drain to  $\sim 1.5\text{A}$  on the batteries, and so a battery belt was sourced to provide ample power for 8 hours continuous use.

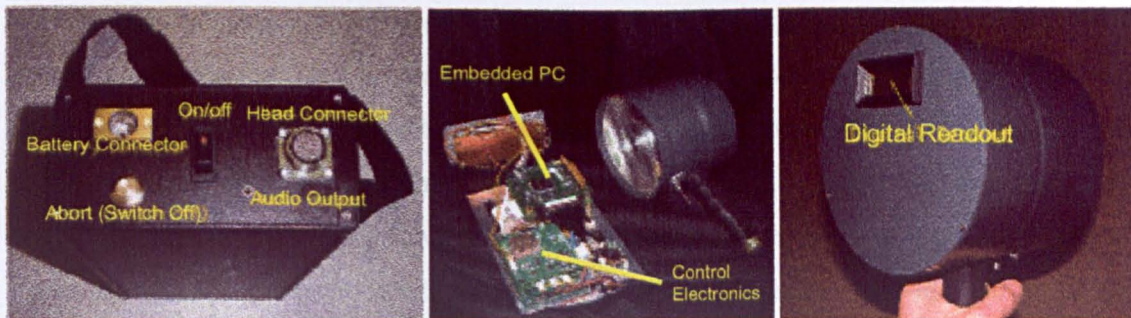


Figure 3.22: Left: connection panel of control box, Middle: inside of the control box showing the embedded computer and control electronics, Right: the digital readout on the rear of the hand-held optical head

An embedded PC (TP400 system based on the National Semiconductor Geode processor, in a PC-104 form factor) running Windows XP was incorporated into the control box as shown in figure 3.22. This was programmed to load the control software on startup, and perform a system check before running automatically. The user interface comes in two forms. Firstly a digital readout on the rear of the optical head gives the user a direct indication of the gas levels (mm thickness of gas cloud) in the line-of-sight of the instrument; secondly an optional audio signal gives out continuous beeps, the pitch of which corresponds to the gas signal.

The control software has been completely redeveloped. On Windows startup, a command

line control automatically loads the self-contained LabVIEW program which then undertakes system diagnostics. Once these have been completed, and everything is performing as required, the system then begins to lock to the methane absorption line and record gas levels. This program is discussed in more detail in subsection 3.5.1. A flow diagram showing the signal path through the software is shown in figure 3.23.

While the instrument is measuring gas levels it is also performing system checks; to ensure the laser is operating and is operating in the correct wavelength range, to ensure the system is receiving enough returned laser light to make a correct reading and to ensure the detector is not being saturated by an external light source (e.g. the Sun). Should the instrument detect it is not operating correctly it will either report an error and await user correction or shut itself down to prevent damage, depending on the fault. Should the system shut itself down, it will be for one of three reasons (or any combination of the three) and the fault code it displays will indicate where the problem lies:

User Display	Laser Fail	Lost Lock	Lock Out Of Range
-1	X	-	-
-2	-	X	-
-3	X	X	-
-4	-	-	X
-5	X	-	X
-6	-	X	X
-7	X	X	X

Should the system receive too little laser light it will display "-8", and if the detector becomes saturated it will display "-9". In both of these cases the system will continue to run, expecting the user to point the optical head in a different direction.

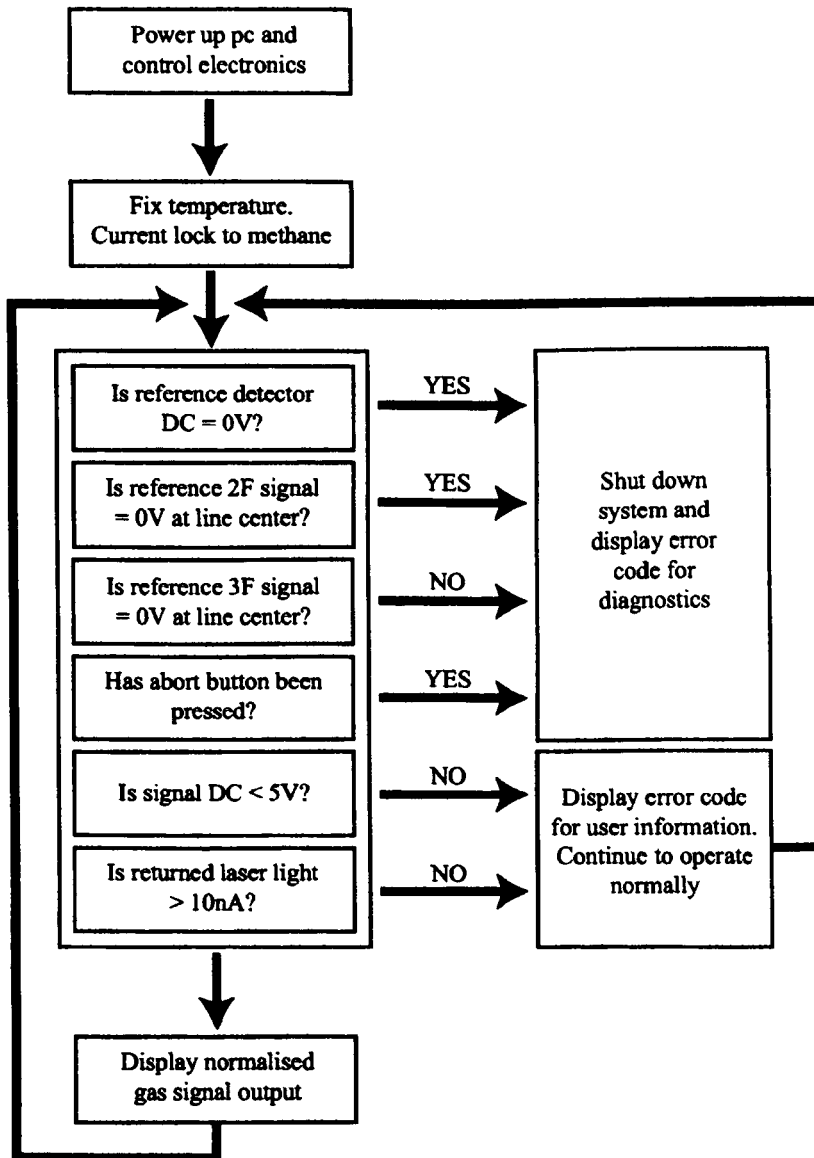


Figure 3.23: Flow diagram showing pathways through control software

The full system can be packaged into an aluminum flight case (550x420x200mm) for security and transportation and is shown in figure 3.24.

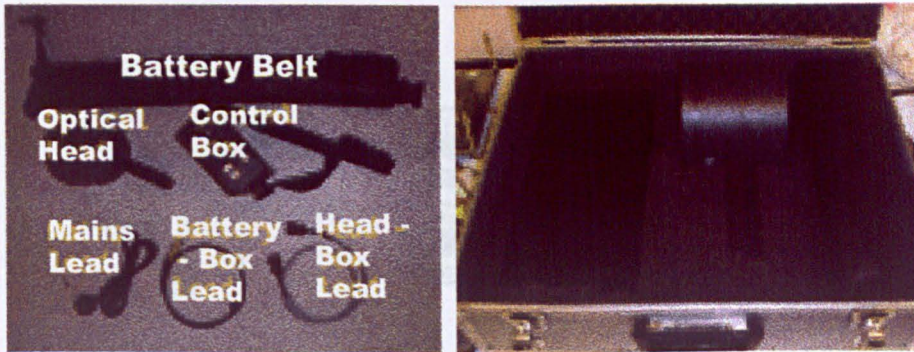


Figure 3.24: Left: system components, Right: all the component packaged into an aluminum flight case

### 3.5.1 Self Executing Program

The program is split into two main sections. The first control section is a sequence of eleven commands which execute one after the other. Initially the system ensures the laser is off. Secondly, there is a pause to allow time for all of the electronics to settle. Thirdly the outputs from the PSD's are recorded, with the laser off, to set their zero reading as shown in figure 3.25. Next the laser diode is switched on. The dc signal on the reference channel is then read to ensure the laser is operational. An output to the user (both audio and on the digital output) confirms operation. The seventh stage is the stage which contains the second section of controls.

This second sequence loop initially scans the laser diode, and locks to the absorption line as discussed in subsection 3.4.2. Once locked the program calculates and displays gas concentration data, either until a fault is discovered or until a user intervenes as shown

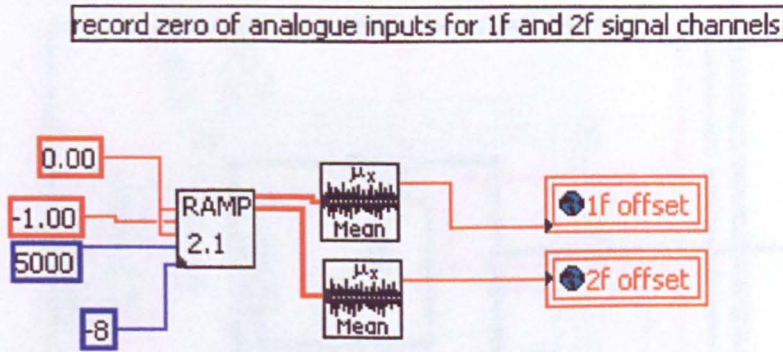


Figure 3.25: Obtaining PSD outputs before laser is switched on

in figure 3.26. Once the user has chosen to shut down the instrument, or a fault has been identified, the laser is immediately switched off to prevent any possible damage. The instrument displays a negative reading to indicate why the instrument has been shut down. A reading of -0.5 on the display indicates that the instrument was shut down properly by the user. A fault code is calculated as shown in figure 3.27 in all other cases. The program will hold the fault code on the display for 5 seconds, and then quit execution and close down. The command line code which called the LabVIEW program (on Windows startup) detects that the program has closed, and initiates a Windows shutdown.

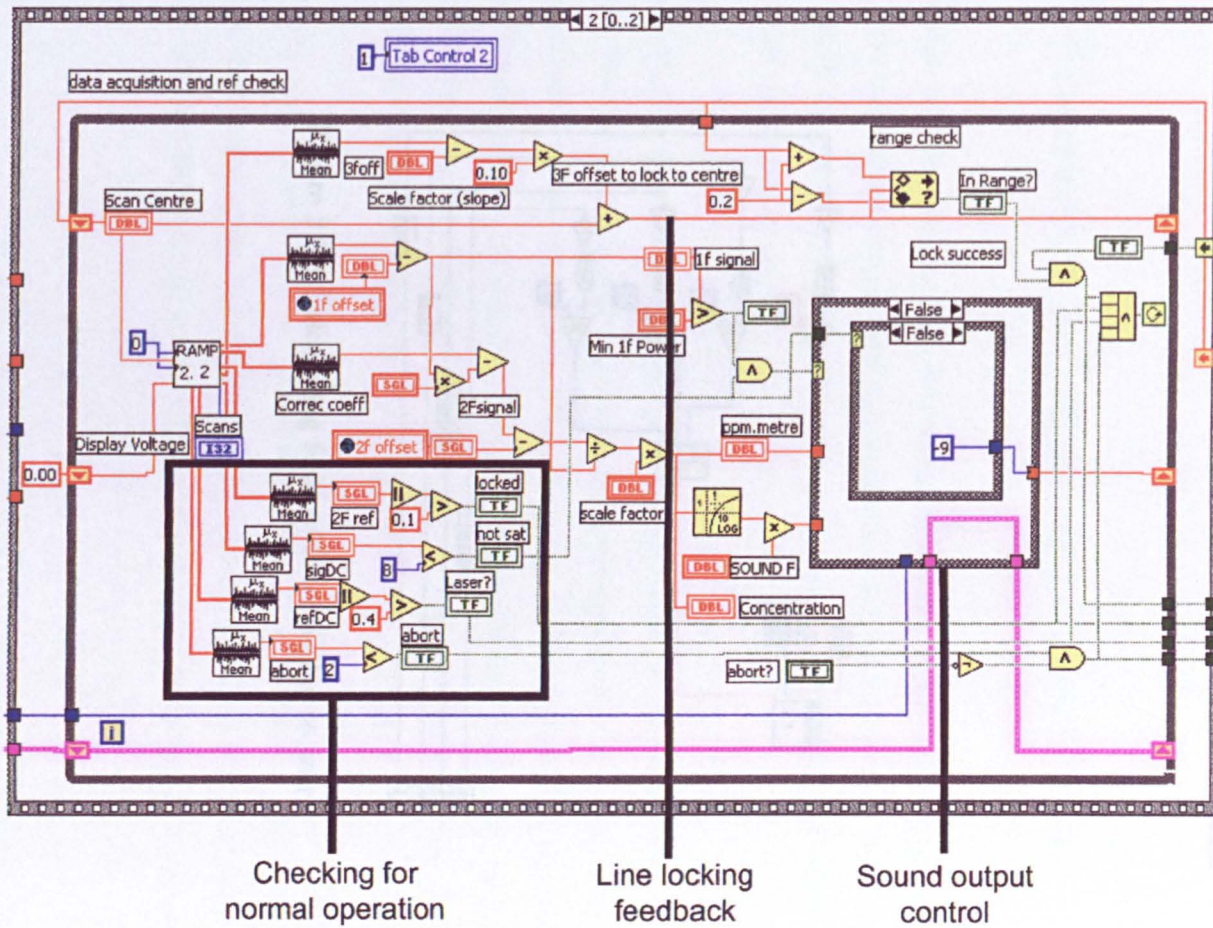


Figure 3.26: Main data acquisition loop

## 4. Laboratory Characterisation

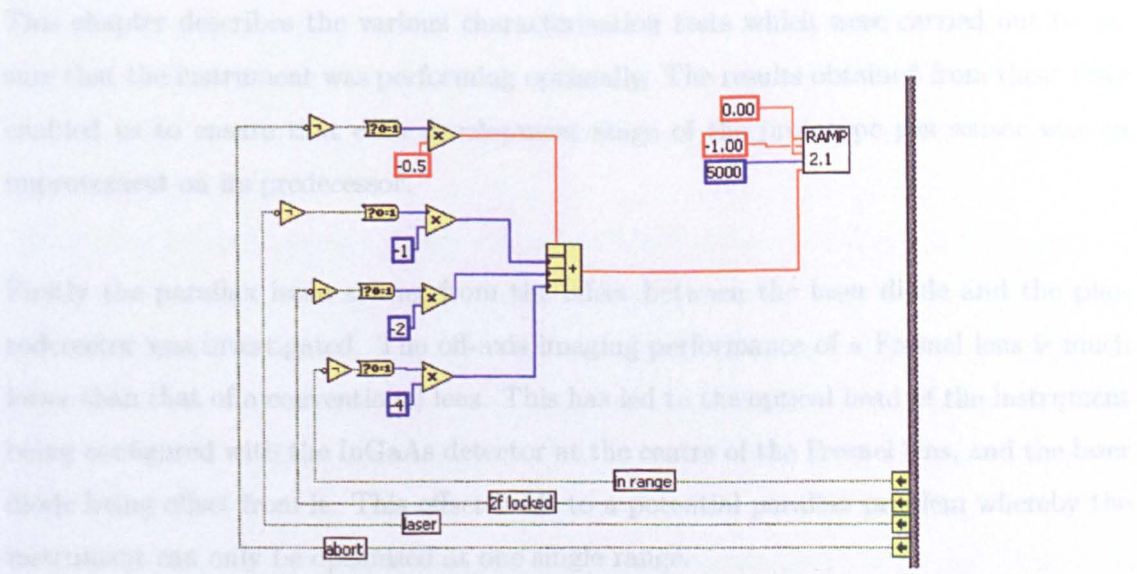


Figure 3.27: Calculating fault code to display to user

## 4. Laboratory Characterisation

This chapter describes the various characterisation tests which were carried out to ensure that the instrument was performing optimally. The results obtained from these tests enabled us to ensure that each development stage of the prototype gas sensor was an improvement on its predecessor.

Firstly the parallax issue arising from the offset between the laser diode and the photodetector was investigated. The off-axis imaging performance of a Fresnel lens is much lower than that of a conventional lens. This has led to the optical head of the instrument being configured with the InGaAs detector at the centre of the Fresnel lens, and the laser diode being offset from it. This offset leads to a potential parallax problem whereby the instrument can only be optimised at one single range.

Secondly the noise performance of the detector was characterised. The overall sensitivity of the instrument should ultimately be dependant on the sensitivity of the detector. A suitable detector has to be sourced, configured and tested to ensure it is performing as specified.

Thirdly, the instrument has to be calibrated so that for a known level of returned laser light, the sensitivity of the instrument is known. The minimum detectable level of methane

depends on the amount of laser light interacting with the gas cloud. The system has been characterised for a range of photocurrents incident on the detector, and this characterisation graph is used as a benchmark to ensure the system is configured correctly.

## 4.1 Parallax Optimisation

An ideal setup of laser diode module and InGaAs detector would be to have them collinear. This would ensure that the optical head would not be sensitive to changes in range. Furthermore, the optical head would work at all ranges, provided sufficient backscattered light could be collected.

The plastic Fresnel lens is a cheap and robust method for collecting a large amount of back-scattered light. The off-axis performance of the lens is, however, very poor. This increases the importance of ensuring that the light incident on the centre of the lens is also incident on the detector. In other words, the detector is best positioned such that normally incident light is refracted by the lens and comes to a focus on the detector surface.

Preliminary laboratory testing, with the laser diode mounted next to (within 30mm) the InGaAs detector, showed that at ranges of 8-10m the returned signal could be satisfactory to make measurements with a sensitivity of 10ppm.m (normal reflectance off of a sheet of white cardboard). Maintaining the component orientation, and moving the optical head closer to the target showed that the light level incident on the detector increased. If the outgoing laser light beam was of a sufficiently large diameter, and was incident on a truly diffuse reflector with the Fresnel lens and detector optimally positioned, it would be expected that the collected light would vary with the square of the distance. However because the optics were optimised at 10m, the instrument was not collecting light as

efficiently at shorter ranges; consequently the collected light was lower than expected at ranges other than 10m. The instrument was envisaged as having a quoted maximum operating distance of 10m, but clearly this value depends heavily on the backscatter material. To overcome any signal reduction arising from parallax, the instrument would initially be optimised at the longest required range.

With the instrument working optimally at 10m, it is still possible to saturate the transimpedance amplifier on the InGaAs detector when the optical head is moved to within 2m of the target. This could be prevented by reducing the output gain of the amplifier, but would in turn reduce instrument sensitivity. Alternatively, by increasing the offset between the laser diode and the detector, the decrease in collection efficiency of the lens could be made to negate some of the effects of increased signal due to shorter operating ranges. This in turn would mean decreased methane sensitivity at intermediate distances, but would give the instrument a larger range of operating distances.

The distance between the laser diode and detector was increased to 60mm so that the outgoing laser beam still originated from within the radius of the (150mm diameter) Fresnel lens. This ensures that at ranges approaching 0m, backscattered light will still be incident on the collection lens. This increase in separation ensured that with the instrument optimised at 10m, when operating at shorter ranges the optical head would be far from optimal. This would compete with the inverse square law to ensure that the variation in collected light levels was within the dynamic range of the detector and amplifier.

The light collected by the Fresnel lens could be due to either background light, or light from the laser diode. A program was written in LabVIEW to turn the laser diode on and off quickly, as discussed in subsection 4.1.1. The respective returned levels would then be due to either all sources, or just background light. Subtracting the background value from the signal received when the laser was switched on would yield the amount of light

incident on the detector from the laser. This value is critical to the instrument sensitivity; the more light that passes through a methane escape and is picked up by the detector, the greater the sensitivity and accuracy of the gas reading.

An experiment was conducted to measure how the returned laser light levels change with distance, for a given laser diode and detector orientation. The instrument was aimed towards a standard reflectivity card target (7% reflectance) and the detector signal level was recorded. The instrument was optimised (maximum returned signal) at one distance, e.g. 10m. The target distance was then varied. This was repeated for 3 different optimisations.

As can be seen in figure 4.1, with the instrument optimised at 10m, the signal level due to laser light varies from 0.036V to 0.158V which is smaller than a factor of five. When the instrument is optimised at 5m, the largest signal is still only eight times the smallest. This changes the perception of how best to set up the instrument; previously the instrument was optimised at the longest distance possible, and worked well at shorter ranges. However, the trade off between the instrument working, and instrument sensitivity means that it is important to have the maximum sensitivity possible within the dynamic range of the detector/amplifier package. It is envisaged that although potentially useful to have the instrument capable of working over long (>10m) ranges, it is increasingly difficult to accurately aim the instrument at a distant target. The majority of leak location work would take place by aiming the optical head a few metres forward of the operators feet. For this reason the instrument was optimised to work at a distance of 5m, and would provide more accurate readings off a larger diversity of topographic targets.

This graph is used to ensure that the instrument has not become misaligned over time, or after being in transit.

### 4.1.1 Laser On/Off

The LabVIEW program designed to rapidly toggle the laser output between on and off states is based around the "Ramp 2.1.vi" subroutine. This subroutine is placed within a while loop; the program will execute continuously until a stop command is given. Half of the time the laser is in the off state. The second half of the time the laser is in the on state designated by the user. All the time the program is running, the signal voltage on the InGaAs detector is measured and displayed as a graph every time the

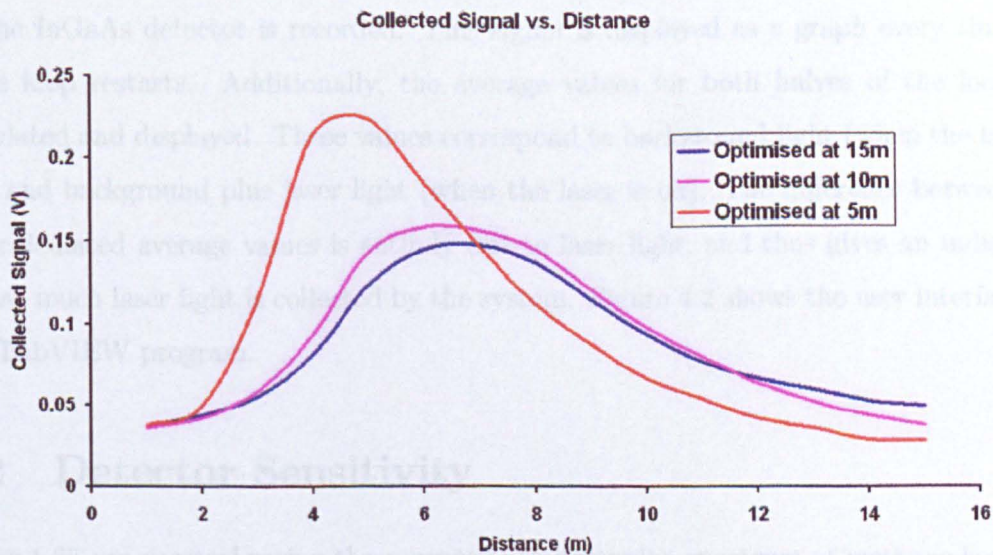


Figure 4.1: Trade off between operating distance and parallax to achieve a suitable dynamic range

In the 1.65  $\mu\text{m}$  spectral region the complex absorption spectrum of methane is shown in Figure 4.2. The spectral line that we have used at 1651nm. From this we can see that Methane at its peak absorption, at 1651nm will produce a fractional change in signal of  $4.4 \times 10^{-3}$ . Thus, a change in the received power by a factor of  $4.4 \times 10^{-3}$  will indicate the presence of 100ppm methane. A different way to present this information is that it would expect a signal level equivalent to 237 times the noise floor of the system to detect the presence of 100ppm methane.

The noise on the photodiode detector provides a fundamental sensitivity limit for the entire system which cannot be bettered. The InGaAs photodiode and amplifier package

### 4.1.1 Laser On/Off

The LabVIEW program designed to rapidly toggle the laser output between on and off states is based around the “Ramp 2.1.vi” subroutine. This subroutine is placed within a while loop; the program will execute continuously until a stop command is given. Half of the time the laser is in the off state. The second half of the time the laser is in a state designated by the user. All the time the program is running, the signal voltage on the InGaAs detector is recorded. This signal is displayed as a graph every time the while loop restarts. Additionally, the average values for both halves of the loop are calculated and displayed. These values correspond to background light (when the laser is off), and background plus laser light (when the laser is on). The difference between the two calculated average values is entirely due to laser light, and thus gives an indication of how much laser light is collected by the system. Figure 4.2 shows the user interface for this LabVIEW program.

## 4.2 Detector Sensitivity

In the 1.65  $\mu\text{m}$  spectral region the composite transmission spectrum of methane is shown in figure 4.3. The individual laser diode that we have works at 1651nm. From this we can see that 100ppm.m, at peak absorption, at 1651nm will produce a fractional change in signal of  $4.4 \times 10^{-3}$ . Thus, a change in the received power by a factor of  $4.4 \times 10^{-3}$  will indicate the presence of 100ppm.m methane. A different way to present this information is that it would expect a signal level equivalent to 227 times the noise floor of the system to detect the presence of 100ppm.m methane.

The noise on the photodiode detector provides a fundamental sensitivity limit for the entire system which cannot be bettered. The InGaAs photodetector and amplifier package

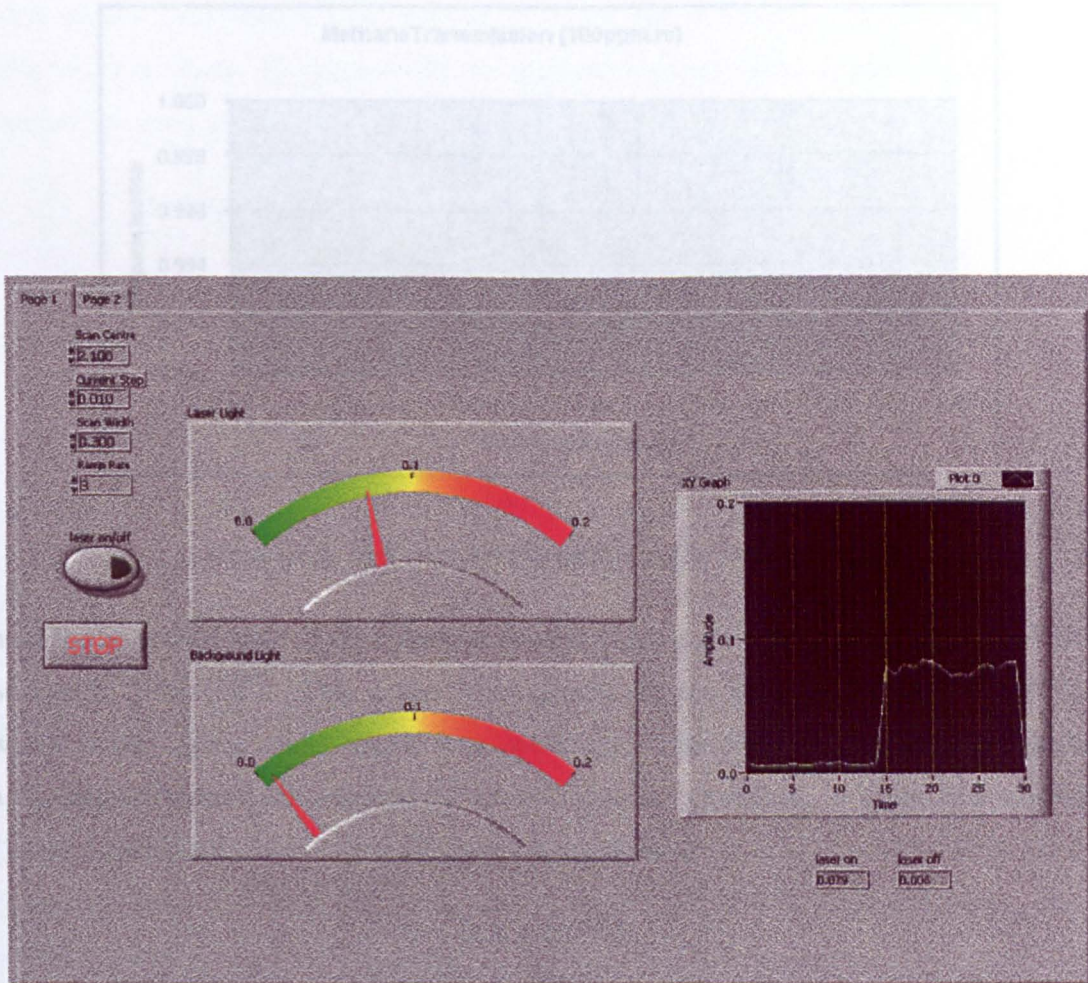


Figure 4.2: User interface of software designed to switch laser on and off

$$2.9 \times 10^{-11} \text{ W} \times 0.25 \text{ A/W} = 7.25 \times 10^{-12} \text{ A}$$

The current noise in the detector is given  $2.4 \times 10^{-11} \text{ A}$ , and a signal to noise ratio of 227 is needed to resolve 100 p.p.m. methane. Thus:

$$(2.4 \times 10^{-11}) \times 227 = 5.4 \text{ nA}$$

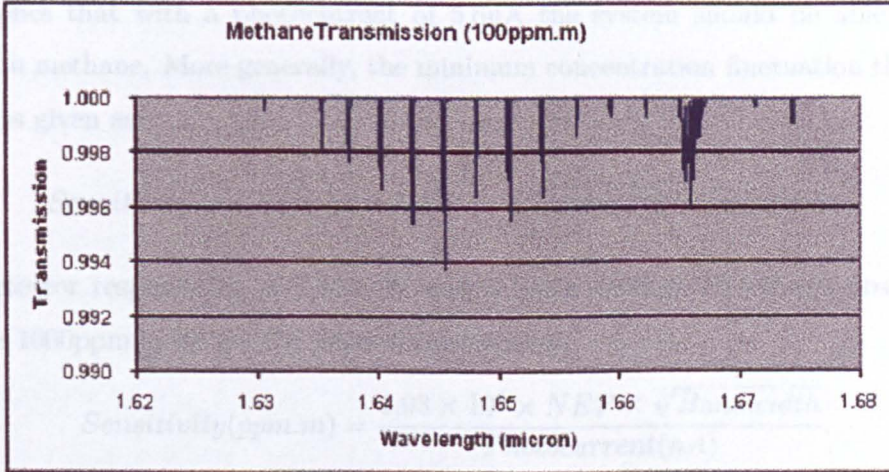


Figure 4.3: Methane transmission in the  $1.65\mu\text{m}$  region

used in the optical head of the system is quoted as having a noise equivalent power (NEP) of  $2.9 \times 10^{-12} \text{W}/\sqrt{\text{Hz}}$ . This is the NEP quoted for the gain setting of  $1.5 \times 10^6 \text{ V/A}$ , which is the regime under which it is operating. This NEP can be used to calculate a theoretical signal level required to detect 1ppm.m. Operating at 10ms time constant (100Hz bandwidth, see Chapter 5) gives a noise floor of

$$2.9 \times 10^{-11} \text{W}.$$

Using the given responsivity of the InGaAs detector at 1651nm gives

$$2.9 \times 10^{-11} \text{W} \times 0.85 \text{A/W} = 2.465 \times 10^{-11} \text{A}.$$

The current noise in the detector is then  $2.465 \times 10^{-11} \text{A}$ , and a signal to noise ratio of 227 is needed to resolve 100ppm.m methane. Thus:

$$(2.465 \times 10^{-11}) \times 227 = 5.6 \text{nA}.$$

This implies that with a photocurrent of 5.6nA the system should be able to detect 100ppm.m methane. More generally, the minimum concentration fluctuation that can be resolved is given as

$$\textit{Sensitivity} = \textit{Constant} \times \textit{NEP} \times \sqrt{\textit{Bandwidth}} \times \textit{Responsivity}.$$

For a detector responsivity of 0.85A/W and a linear methane fractional absorption of 4.4% per 1000ppm.m we get the general relationship:

$$\textit{Sensitivity}(\textit{ppm.m}) = \frac{1.93 \times 10^4 \times \textit{NEP} \times \sqrt{\textit{Bandwidth}}}{\textit{Photocurrent}(\textit{nA})}. \quad (4.1)$$

Relating this information back to figure 2.14, we see that for the given parameters (3% surface reflectivity) the instrument should generate enough photocurrent to resolve 100ppm.m at ranges up to 5.5m.

### 4.2.1 Backscatter From Surface

The sensitivity of the instrument is dependant on the photocurrent generated in the In-GaAs detector. The amount of laser light incident on the detector changes not only with distance (figure 2.14) but also with varying topographic backscatter targets, as can be seen in table 4.1.

The error in the measured angle is estimated to be 0.1°, and the estimated reading error in the reflectivity is 0.1%. Clearly a replacement surface of the same material would not exhibit the same reflectivity to this accuracy, so a more realistic error to consider here is of the order of 1%. These results are all given relative to the measured reflectivity from the Spectralon sample. This sample provides better than 99% diffuse reflections, with negligible specular characteristics. This removes the need for any polarisation considerations. A result of 50% at an angle of incidence of 75° means that the spectrometer measured

MATERIAL	15° to normal	45° to normal	75° to normal
Spectralon Reference	100%	100%	100%
White Melamine	69.3%	69.4%	50.6%
Red Brick	59.1%	70.3%	112.3%
Damp Red Brick	44.0%	45.3%	81.5%
White Road Marking	58.5%	66.3%	59.1%
Grass	45.1%	34.1%	32.1%
Wood (Old Rough Pine)	40.0%	42.6%	70.8%
Damp Wood	19.0%	20.4%	23.6%
Wet Wood	9.0%	14.8%	8.6%
Soil (Clay Type)	36.9%	50.0%	131.9%
Damp Soil	16.4%	18.6%	56.4%
Concrete Slab	26.8%	32.4%	53.1%
Damp Concrete Slab	9.7%	8.1%	8.6%
Wet Concrete Slab	5.8%	5.0%	3.1%
Steel Bench	22.5%	6.8%	47.9%
Grey Painted Lab Floor	13.7%	9.6%	11.8%
Paving Bricks	13.1%	20.5%	39.3%
Old Tarmac on Road	10.9%	13.1%	31.0%
New Tarmac (3 Months Old)	6.5%	6.9%	18.1%
Wet New Tarmac	3.4%	2.6%	3.3%
Bitumen	5.3%	9.4%	15.7%
Damp Bitumen	2.8%	-	-
Wet Bitumen	0.6%	-	-
Black PVC	3.6%	1.3%	1.3%

Table 4.1: Comparison of the reflectivity of different surfaces with a reference, in the 1.65 $\mu$ m wavelength range of interest for methane detection

half as much light from the test surface at  $75^\circ$  as from the Spectralon, also at  $75^\circ$ . So, for example, a measurement made at  $75^\circ$  might show a higher relative reflectivity than one made at  $45^\circ$ , even though the absolute amount of light collected may be much higher at  $45^\circ$ . Over five times as much light was collected from the Spectralon at an angle of incidence of  $15^\circ$  than at an angle of incidence of  $75^\circ$ .

The value of a high surface reflectivity ensures the availability of sufficient light to provide an accurate reading. The reflectivities of a variety of real-world surfaces have been measured relative to a reflectivity standard. The results have been compared with the design reflectivity figure of 5% that was used to model potential instrument performance. This was considered a likely worst-case reflectivity - a judgement that has been vindicated by these experiments.

There are few materials that would exhibit a lower reflectivity than this figure, and even fewer that occur over large areas of ground. These problem surfaces include wet concrete and wet new tarmac, where the level of water was sufficient to give a glossy surface. In many cases the level of diffuse reflectivity at glancing angles of incidence was higher than might be expected, presumably because of inherent surface roughness and/or surface dirt. In all cases, the presence of water reduces the diffuse reflectivity.

To compare the results obtained with the portable spectrometer to those which would be interpreted by the methane detector, an early prototype instrument was used with a 10mm gas sample cell to determine the minimum detectable gas concentration from a given topographic target. This experiment is discussed in more detail in subsection 6.2.2; the results are shown in figure 4.4.

As is clearly shown in figure 4.4, there are few surfaces where the returned light level is sufficiently low to prevent the instrument resolving a gas signal equivalent to a 1mm (1000ppm.m) methane cloud. In wet conditions, when a surface is effectively sealed by

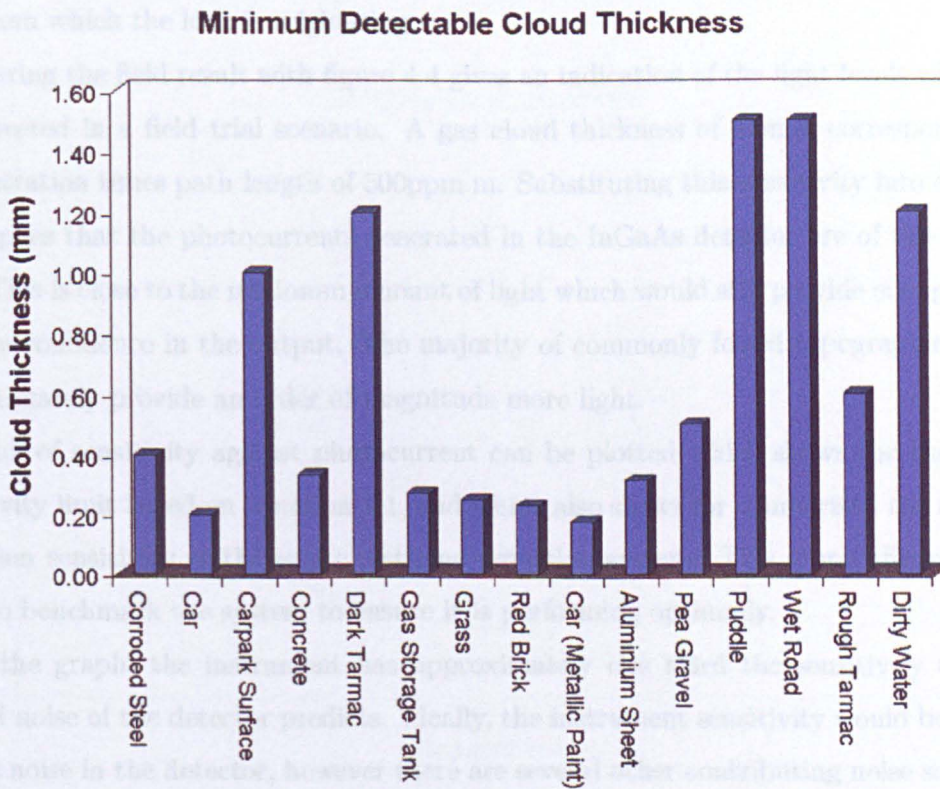


Figure 4.4: Comparing real-world reflectivities with an early prototype pointer (1mm gas cloud thickness is equivalent to 1000ppm.m)

a thin coating of water, a gas leak will not permeate through this water barrier and no gas leak will be evident to any surface optical gas detection tool. In this case, gas utility engineers will bore holes into the ground at various intervals to enable the gas to escape. By measuring the gas concentrations in these holes it is possible to identify a probable area from which the leak is originating.

Comparing the field result with figure 4.4 gives an indication of the light levels which can be expected in a field trial scenario. A gas cloud thickness of 0.5mm corresponds to a concentration times path length of 500ppm.m. Substituting this sensitivity into equation 4.1 implies that the photocurrents generated in the InGaAs detector are of the order of 1nA. This is close to the minimum amount of light which would still provide enough signal to have confidence in the output. The majority of commonly found topographic targets approximately provide an order of magnitude more light.

A graph of sensitivity against photocurrent can be plotted which shows the theoretical sensitivity limit based on equation 4.1, and which also shows for comparison the achieved detection sensitivity of the entire methane detection system. This graph (figure 4.5) is used to benchmark the system to ensure it is performing optimally.

From the graph, the instrument has approximately one third the sensitivity that the quoted noise of the detector predicts. Ideally, the instrument sensitivity would be limited by the noise in the detector, however there are several other contributing noise sources in our system, such as the in-house electronics. Given the nature of all possible noise sources within this prototype instrument, the sensitivity achieved is commendable.

## 5. Scanning

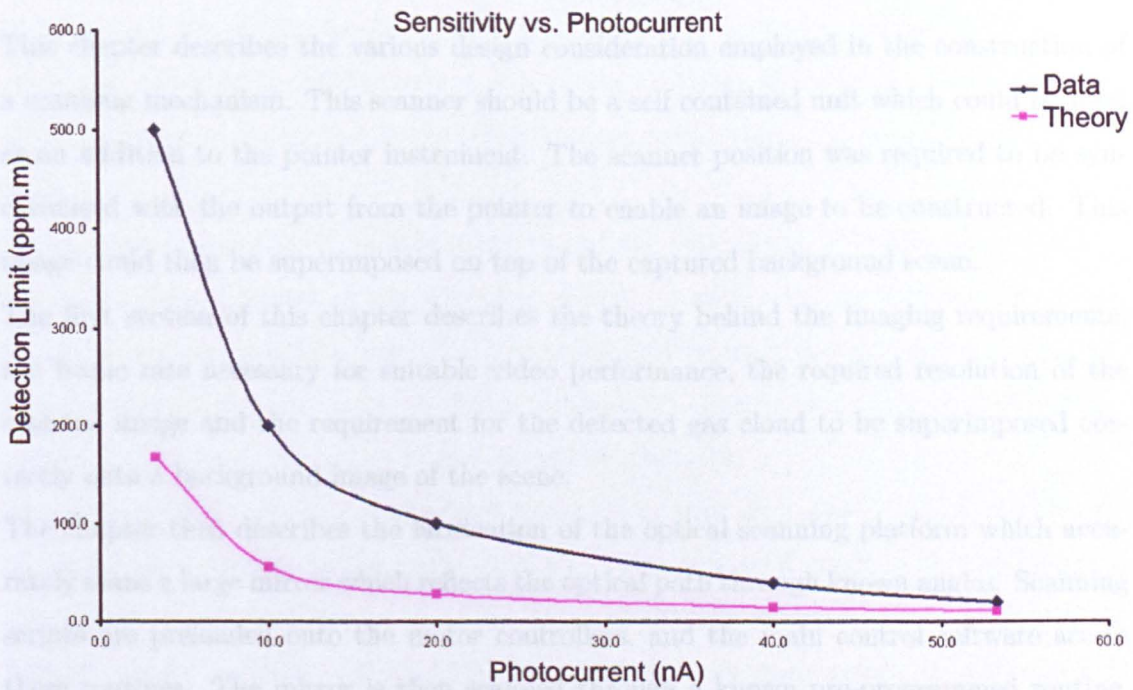


Figure 4.5: Theoretical sensitivity based on quoted detector performance compared with sensitivity achieved

## 5. Scanning

This chapter describes the various design considerations employed in the construction of a scanning mechanism. This scanner should be a self-contained unit which could be used as an addition to the pointer instrument. The scanner position was required to be synchronised with the output from the pointer to enable an image to be constructed. This image could then be superimposed on top of the captured background scene.

The first section of this chapter describes the theory behind the imaging requirements; the frame rate necessary for suitable video performance, the required resolution of the scanned image and the requirement for the detected gas cloud to be superimposed correctly onto a background image of the scene.

The chapter then describes the fabrication of the optical scanning platform which accurately scans a large mirror which reflects the optical path through known angles. Scanning scripts are preloaded onto the motor controllers, and the main control software accesses these routines. The mirror is then scanned through a known pre-programmed routine, gathering gas information. At the same time, a picture is taken of the background scene. Finally the real time image processing outputs a picture of the background scene with the gas cloud superimposed; this output is updated at the necessary frame rate.

## 5.1 Imaging Requirements

Preliminary work, performed to identify the minimum acceptable scanning frame rate, used a thermal imaging camera system to detect gas escaping against a heated background. These video clips were high resolution ( $300 \times 300$  pixels) and had a frame rate of 10Hz. The video clips could be viewed at an artificially reduced frame rate and resolution to determine the minimum rate needed to still identify a moving gas image. If the gas cloud had distorted to such an extent that it was no longer identifiable as being a simple distortion from the previous frame, then the generated video clip would appear overly jerky.

Systematically reducing the frame rate reduced the smoothness of frame transition, but also lowered the demand on any scanning system. In all but the most demanding (wind swept) conditions, a frame rate of 1Hz was sufficient to track the movement of any particular aspect of the gas cloud, as shown in figure 5.1. Furthermore, during still ambient conditions, a frame rate of less than 1Hz will be sufficient.

Having identified that sampling a fixed region of interest once every second will provide adequate video footage of the scene, it is also important to determine how many pixels this region should be sampled in. This has a direct influence on the sensitivity of the instrument, for example a  $30 \times 30$  grid has nine times as many points as a  $10 \times 10$  grid causing the finer grid to have a third of the sensitivity as the coarser one, for a fixed scan rate of 1Hz. This is because the instrument dwell time per pixel is inversely proportional to the number of pixels, and the instrument sensitivity is proportional to the square root of this pixel dwell time (time constant).

The thermal video footage was used as a basis for modelling work, designed to investigate the minimum pixel resolution necessary to visualise a gas leak. The raw footage was  $300 \times 300$  pixels. A LabVIEW program was written to average neighbouring pixels

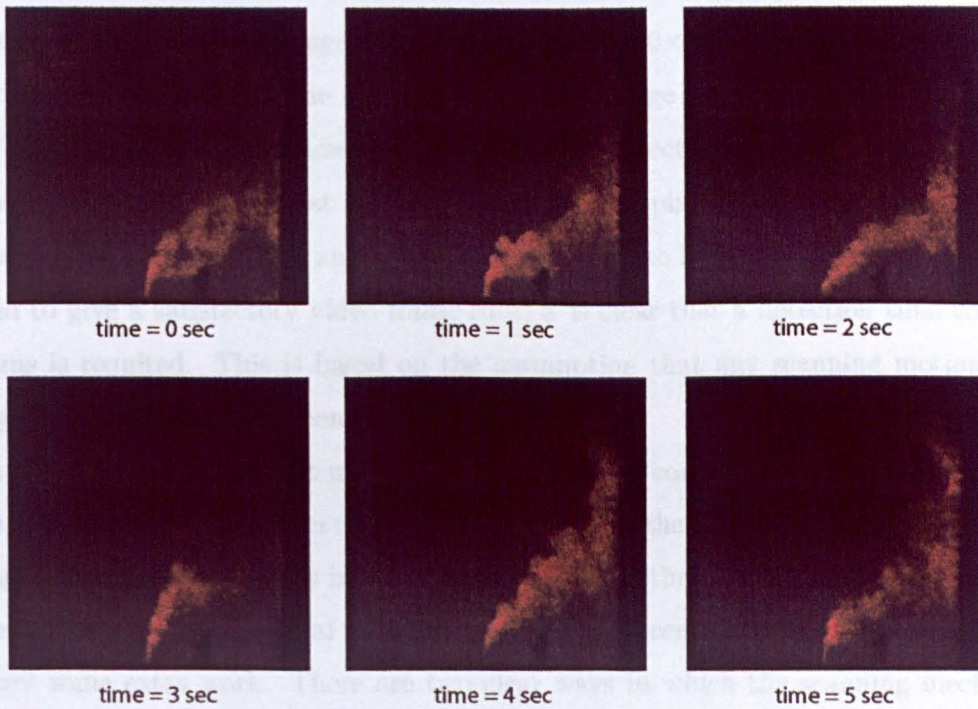


Figure 5.1: Snapshots at one second intervals of a gas leak, taken with a thermal camera, with colour enhancement as described in subsection 2.4

to produce an "equivalent" image, at a given reduced resolution. This smaller image at, say,  $10 \times 10$  pixels was then resampled at the original resolution. Finally this image could be "smoothed". This process applies a simple algorithm to each pixel such that the new value is a fraction of its original value, plus a small fraction of its neighbours, plus a smaller fraction of the next neighbours and so on. The resulting effect is that it is shown, for example, that a  $10 \times 10$  image can be resampled at  $300 \times 300$  and smoothed to produce an image not dissimilar to the original full-quality image as shown in figure 5.2. This LabVIEW program was discussed in more detail in subsection 2.4.2.

Having successfully shown that a  $10 \times 10$  image (i.e 100 pixels) can be processed to look representative of the gas leak, and that this image needs to be updated at least once every second to give a satisfactory video frame rate, it is clear that a detection time constant of 10ms is required. This is based on the assumption that any scanning motion takes negligible time to move between pixels.

For a one dimensional scan, it may be sufficient to scan continuously, at a constant rate, while acquiring data. The data can then be divided into the relevant number of pixels and averaged. Scanning ten pixels in one dimension reveals that this assumption holds true. However, for a two dimensional scan the transition between successive rows (or columns) requires some extra work. There are two clear ways in which the scanning mechanism could move, as shown in figure 5.3. The optimum scan path will be the path which requires the minimum amount of mirror movement, while the instrument is not gathering data. This clearly favours the path shown on the right in figure 5.3.

Reversing the scan direction for every second row minimises the scanner movement, but adds further complexity when processing the acquired data to display an image. As is discussed in section 5.2, the additional LabVIEW code is minimal.

The modelling of gas video clips has improved our understanding of the nature of gas

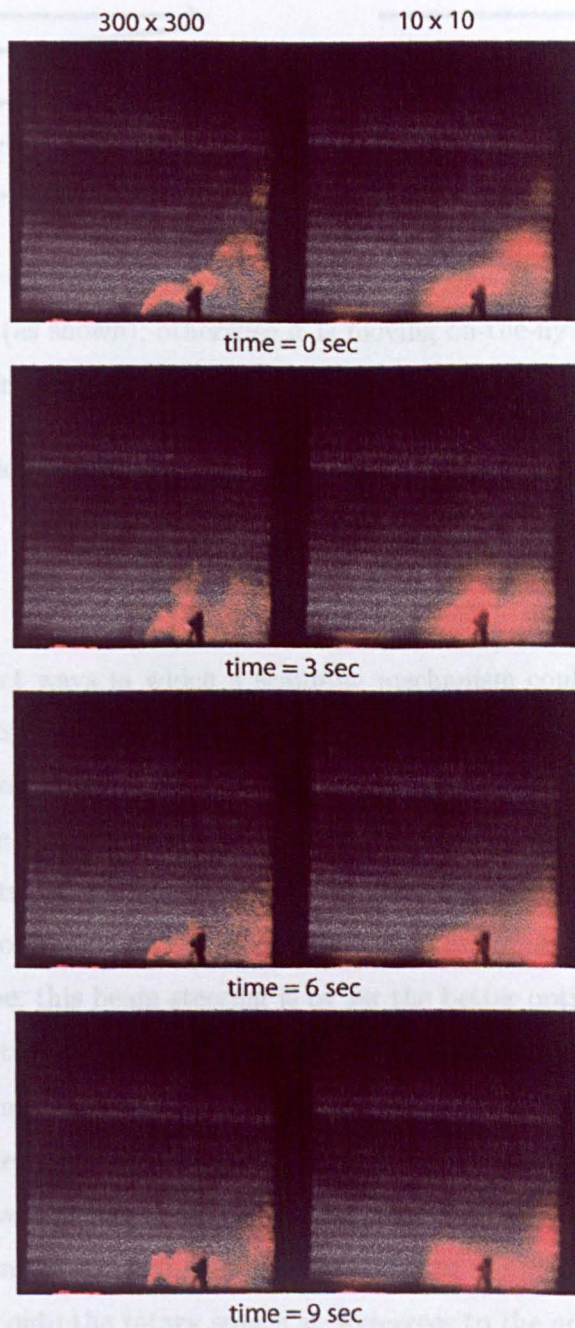


Figure 5.2: Comparing original image quality with resampled, and then smoothed image. On the left are the original images, on the right are the images which have been reduced to  $10 \times 10$  and then processed

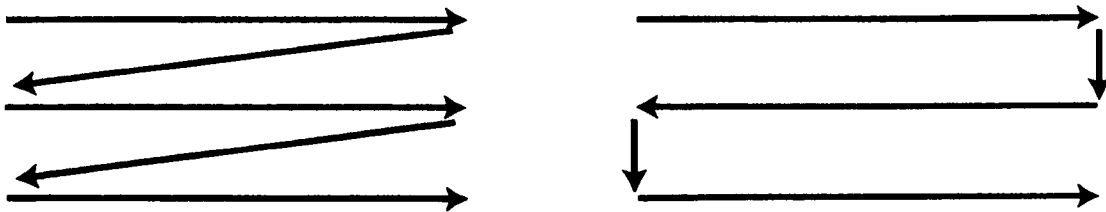


Figure 5.3: Scanning options. The instrument will be acquiring data while scanning horizontally (as shown); otherwise it is moving on-the-fly to reach a data acquisition start point

leaks, and has provided specification for an effective scanning mechanism.

## 5.2 Optical Scanner

There are two distinct ways in which a scanning mechanism could accurately steer the pointer over a range of predefined angles. Firstly, the optical head of the instrument could be mounted upon motorised translation stages, and aimed. Working with a frame rate of 1Hz, over an angle of approximately 15degrees, the forces exerted would be too large for the prototype instrument. The alternative arrangement is to scan the optical beam of the instrument by mounting a large mirror onto the scanning platform. For our in-house constructed prototype, this beam steering is by far the better option.

A suitably powerful two dimensional scanning mechanism was sourced, and supplied by Micromech. The scanner comprised many parts: the rotary stages, the d.c. motors, the motor controllers, the motor encoders and a power supply. Assembled, the motors (and attached encoders) were bolted on to the rotary stages and tripod mounted. The power supply and motor controllers were housed in a ventilated metal enclosure. A rectangular mirror was mounted onto the rotary stages at 45degrees to the optical head. This setup

can be seen in figures 5.4 and 5.5.

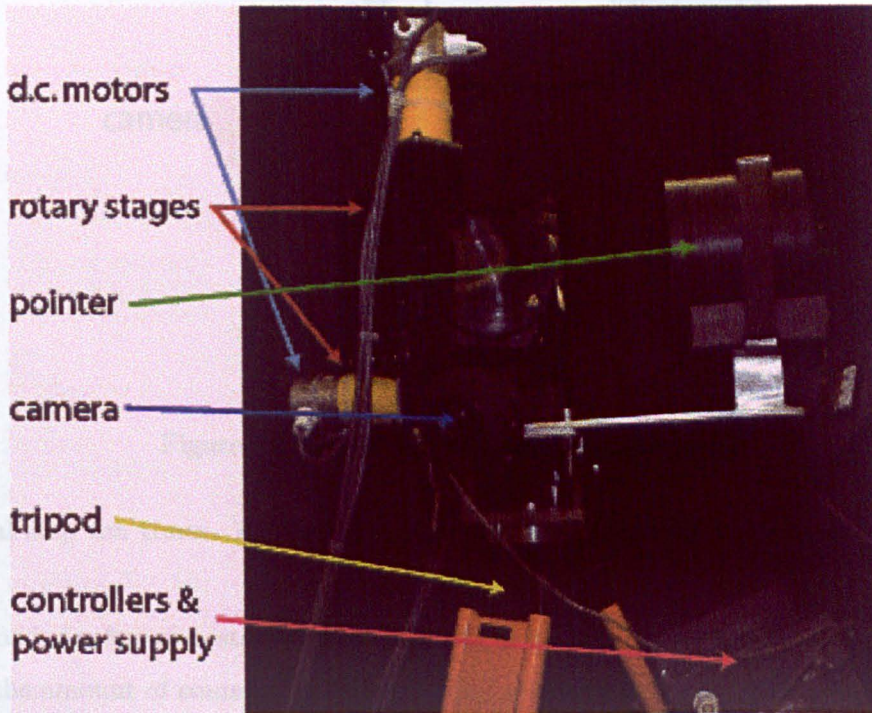


Figure 5.4: Tripod mounted scanning mechanism

To operate, predetermined routines are written and uploaded to the motor controllers. These can then be called at any time from the LabVIEW control software. Two routines are stored in the memory of the motor controllers. Firstly, an alignment program, which when called enables the user to “nudge” the start position of the scan so that it aligns with the video camera. The second routine defines the scanning parameters for the line and pan movement of the mirror, and is shown in figure 5.6. This routine has three commands: HSCAN, HSTEP and VLINE. Respectively they define a horizontal scan, a horizontal step and a vertical line. A horizontal scan consists of doing a vertical line and

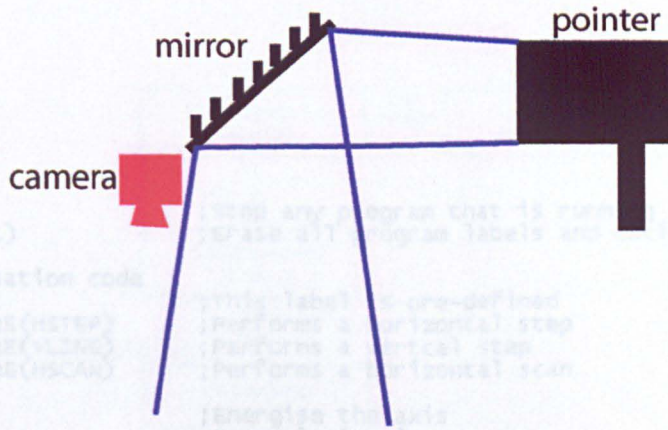


Figure 5.5: Schematic of scanning mechanism

horizontal step ten times. A schematic showing the scanner software is shown in figure 5.7.

The preloaded software is stored in the memory of the motor controllers until called. This reduces the amount of communication traffic between the controlling PC and the scanner system. At the beginning and end of each scanned line, the controller sends a trigger pulse. Firstly, this allows for timing between the two axes. The scanner will perform 10 steps before the second axis moves. Secondly this enables synchronisation between the scan position, and the gas cloud information.

The LabVIEW program which brings all aspects of the scanner control into a single environment is used predominantly to read gas information from the pointer, and synchronise this with the position information gained from the scanner. The resulting compiled gas image is superimposed onto a colour image of the background scene, taken with a webcam.

```

1S ;Stop any program that is running
1CLEAR(ALL) ;Erase all program labels and declarations

;Initialisation code
1START: ;This label is pre-defined
  1DECLARE(HSTEP) ;Performs a horizontal step
  1DECLARE(VLINE) ;Performs a vertical step
  1DECLARE(HSCAN) ;Performs a horizontal scan

  1ON ;Energise the axis
  1V30 ;Set velocity in rps
  1AA100 ;Set acceleration rate in rps/s
  1AD100 ;Set deceleration rate in rps/s
  1D3100 ;Set distance to index
  1GOSUB(HSCAN)
1END ;End of START sequence

1HSCAN:
  1LOOP(HSTEP,10) ;Do HSTEP label 10 times
  1O(XOX) ;Turn off output 2
1END

1HSTEP:
  1O(XOX) ;Turn off output 2 - we're busy!
  1GOSUB(VLINE) ;Do VLINE
  1O(XIX) ;Turn on output 2 - triggers a horizontal step
  1H ;Change direction
  1T0.1 ;wait 0.05 seconds
1END

1VLINE: ;Define VLINE label sequence
  1O(XOX) ;Turn off output 3 - triggers data acquisition
  1G ;Execute move
  1TR(IP,=,1) ;wait till in position
  1O(XOX) ;Turn on output 3
1END ;End of label sequence definition

```

Figure 5.6: Routine which defines scan parameters

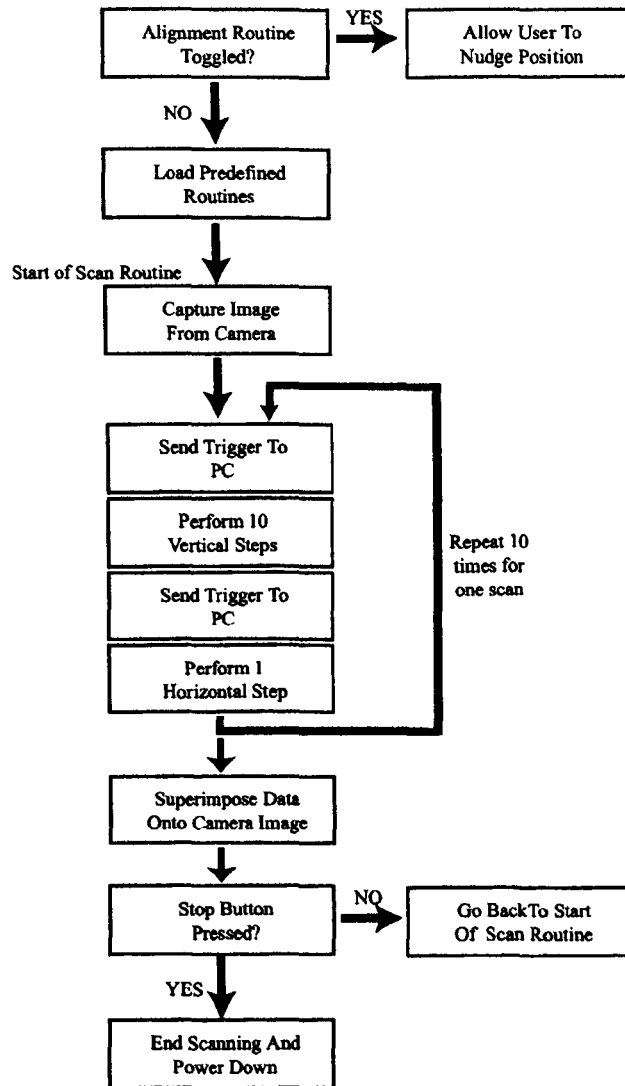


Figure 5.7: Schematic signal path through scanner software

## 5.3 Real Time Gas Imaging

### 5.3.1 Acquiring Gas Data

Combining work which has been described throughout this chapter takes place predominantly in one main scanner control LabVIEW program, and as such, is detailed here.

The program starts by creating storage space (PC virtual memory) for generated images. All communication hardware is then initialised and cleared of any prior settings; the USB digital web-cam is activated and prepared to acquire images. Once these stages have completed, the program starts the scanner hardware.

The data acquisition is continuous, receiving gas data from the pointer. This is held in vectors, as shown in figure 5.8. The timing is predetermined and is such that the instru-

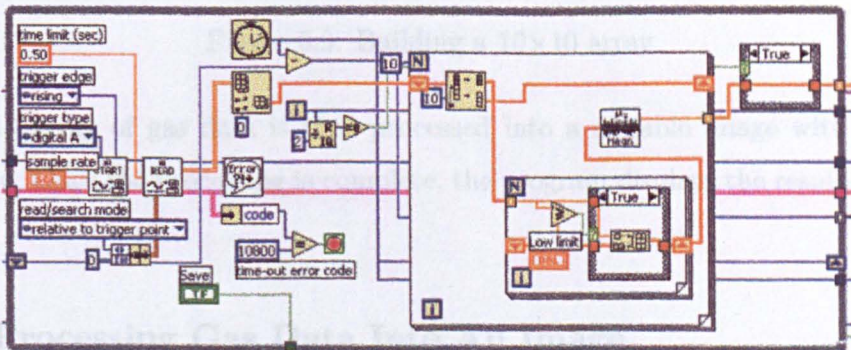


Figure 5.8: Trigger from scanning mechanism defines scan pattern

ment will acquire between ten and twelve data points in the time between the scan start and scan finish triggers. The first ten data points are selected, and checked to remove any negative values. Negative values can occur if the gas reading is smaller than the random error in the system. After receiving 10 data points (a column), the program first checks to see if the column should be reversed (because of the scan pattern), and then outputs

this data into a  $10 \times 10$  array, as shown in figure 5.9.

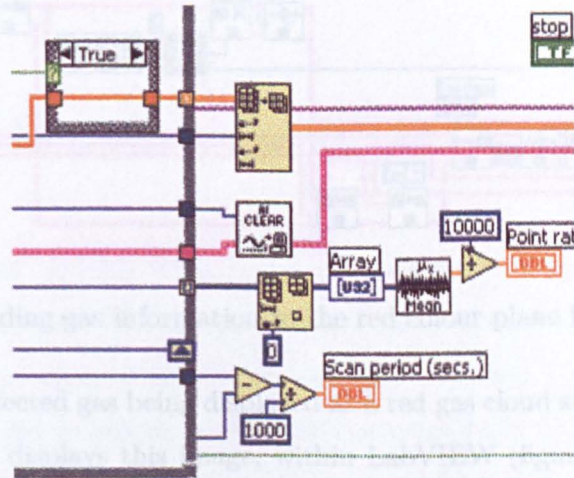


Figure 5.9: Building a  $10 \times 10$  array

This  $10 \times 10$  array of gas data is then processed into a suitable image with a separate sub-routine. Once the processing is complete, the program displays the results and starts over.

### 5.3.2 Processing Gas Data Into An Image

The acquired gas data is passed into the program, together with the camera image, taken of the background scene. The background image is rotated, since the camera is mounted on its side for convenience. The gas data is orientated and checked to make sure the pixel size is the same as for the background image. The gas data is then smoothed, with scaling, before being added to the red colour plane from the image, as shown in figure 5.10. This is the same process that is used to colour enhance the monochrome thermal video camera footage. The resulting image looks identical to the image acquired by the

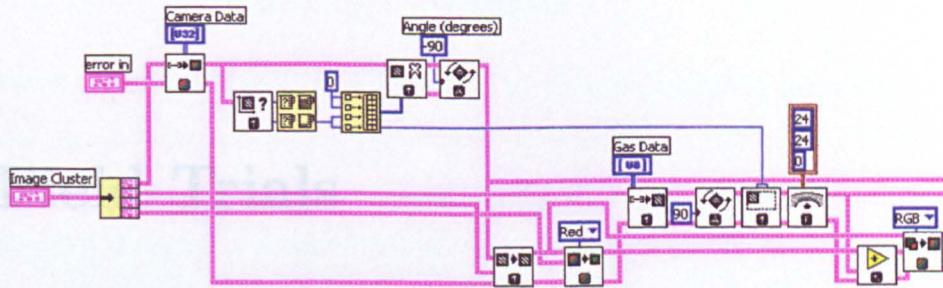


Figure 5.10: Adding gas information to the red colour plane from the web-cam camera, with any detected gas being displayed as a red gas cloud superimposed onto this. Finally the program displays this image, within LabVIEW (figure 5.11), before closing down and returning to the start of the gas data acquisition. Results from the scanned

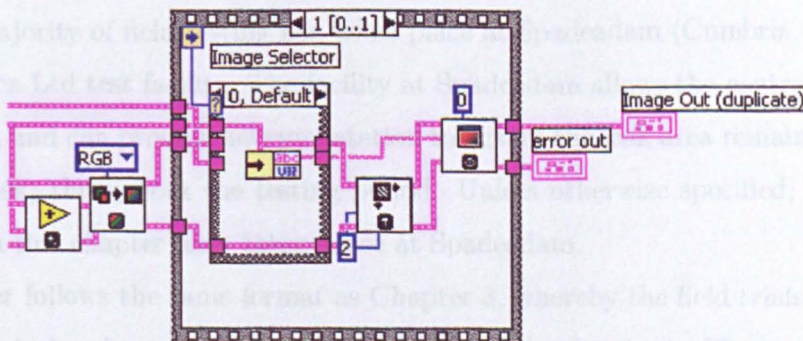


Figure 5.11: Displaying resulting image

pointer are discussed in section 6.5.

## 6. Field Trials

This chapter describes the field trials that were carried out in order to test the various demonstration instruments. The results obtained from various trials on simulated leaks helped to steer the progress of the instrument over necessary hurdles, and were useful in marking development progress. It was also necessary to demonstrate the instrument working outwith a laboratory environment to gain confidence from other consortium partners about the future of a potential product.

The vast majority of field testing has taken place at Spadeadam (Cumbria, UK) which is an Advantica Ltd test facility. The facility at Spadeadam allows the controlled release of natural gas, and can provide instrumentation to ensure the leak area remains safe (not an explosion risk) throughout the testing period. Unless otherwise specified, all field trials discussed in this chapter have taken place at Spadeadam.

This chapter follows the same format as Chapter 3, whereby the field trials are discussed in chronological order to coincide with instrument development. The section headings are named to provide easy cross referencing with Chapter 3. The subsections split each development stage into the relevant distinct experiments, where necessary.

## 6.1 Proof of Concept System

This system consisted of an optical head and bench-top electronics (see section 3.2). The recovered signal was recorded and displayed on a desktop computer. The optical head consisted of a metal enclosure which held a large, 150mm diameter, Fresnel lens in position. situated at the focal point of this lens was a bare InGaAs detector; the current signal from the detector was amplified by a transimpedance amplifier with a current to voltage gain of  $1 \times 10^6$  V/A. The bench-top control electronics (which consisted of a temperature controller, laser diode driver, phase sensitive detector, amplifier/filter unit and a power supply) were all housed within a flight case to provide them with some protection, as shown in figure 3.9.

The preliminary laboratory tests had provided sufficient backscattered light levels to identify methane by direct absorption. Reducing the concentration  $\times$  path length of methane to 10,000ppm.metre (100% methane over a 1cm path) increased the detection difficulty, but was more representative of a real-life scenario. Wavelength modulation spectroscopy (WMS) was employed as a signal recovery technique, to help reduce the effect of signal level changes caused by fluctuations in background reflectivity. The proof of concept system was temperature tuned to the wavelength region of interest. A current ramp combined with a fine modulation was applied to the laser diode. The second harmonic recovered signal was studied for identifying signs of methane.

A pipe connected to a methane supply was initially vented in a clear area. The tripod mounted optical head was directed onto the known location of the leak, and an initial attempt was made to detect the presence of methane. No significant signal levels were recorded. This was attributed to the turbulent and blustery nature of the weather. The vented gas was immediately swept away by the wind, and didn't remain in any position long enough to be detected by the instrument (working with a response time of 100ms per

reading). A signal flare was released in the vicinity of the earlier leak to give an indication of the wind conditions, and is shown in figure 6.1.



Figure 6.1: Signal flare released to show turbulent nature of wind conditions

The free end of the gas pipe was buried in a half-barrel, which was then covered in a coarse stone aggregate, and topped with some dry sand. This had the effect of reducing the vertical velocity of the escaping methane gas, which now slowly seeped out from the sand, and is more representative of a real leak. The half-barrel was partially shielded from the wind by the front bucket of an industrial earth moving vehicle, as shown in figure 6.1. With the instrument optical head downwind of the gas leak, a further attempt was made to detect the presence of methane. This time, with reduced wind, the instrument detected the methane as it escaped the sand, before the wind carried it away.

Various leak rates were used, between 1l/min and 10l/min, and all were detected by the instrument at a range of 4m. Longer ranges were desired, but the instrument was not easily re-optimised at longer ranges in the field. A screen grab from the control pc is shown in figure 6.2, where the white line is the real-time data, and the red line is a trace which was recorded in the laboratory for comparison. As can be seen, the levels of gas detected were comparable, but the noise in the field is significantly increased. This is due to the reduction in backscattered light collected by the instrument.

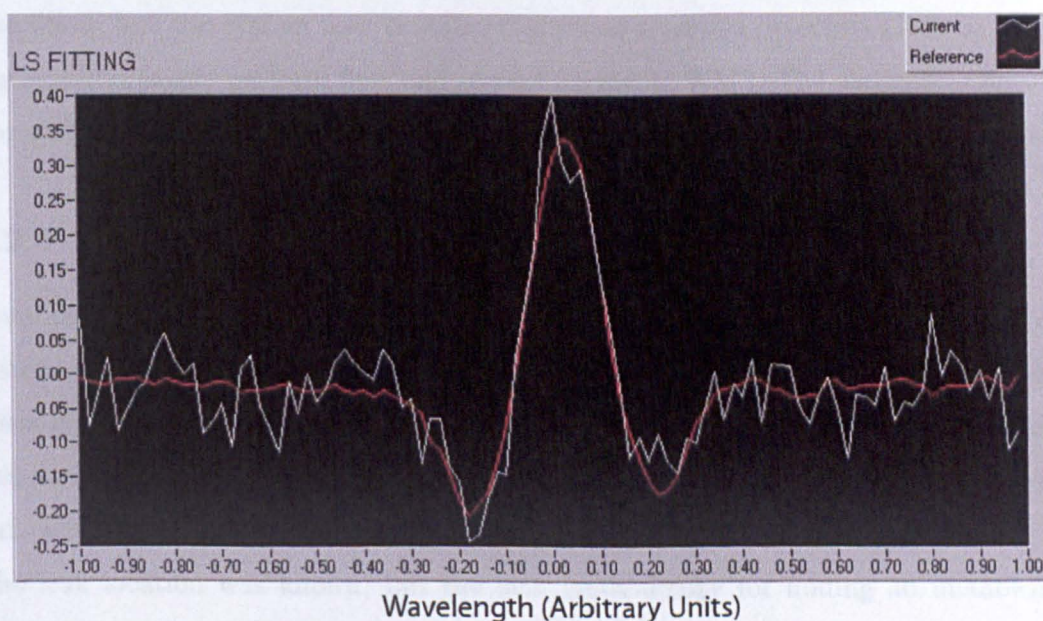


Figure 6.2: Second harmonic trace from 4m looking at 1l/min leak

## 6.2 Portable System

This system initially comprised of two metal boxes hinged together. The first box, was a modified version of the optical head from section 6.1; the support electronics had been replaced by smaller commercially available units, and mounted in the second metal container, as shown in figure 3.10. This instrument was controlled by a laptop pc.

This system still applies a current ramp to the laser diode, to scan through the methane transition, but the system now contains two phase sensitive detectors (PSD's) and thus can simultaneously perform first and second harmonic WMS. The electronics have been changed accordingly to accommodate this, with two waveforms now being generated.

### 6.2.1 User Methods

Consortium partners in Malmö, Sweden have constructed a test site on which gas detection instruments can be evaluated. The site consists of several pits, each with several buried open pipes in them. The pipes are at various depths, and the pits have various fill and surface components, as shown in figure 6.3. Each methane pipe is connected to an individual meter which controls the flow rate of the escaping gas.

The leak location was known, but the best methodology for finding an unknown leak source has not been established for a line of sight instrument. The pointer was equipped with a red laser pointer in addition and running parallel to the infrared laser diode. This was used to aid with aiming the instrument. The pointer was aimed around the known location of the methane escape as shown in figure 6.4, and the results graphed. Intuitively one would imagine that by pointing directly at the leak location, the highest gas signal would be recorded. This is only true when very close to the leak source. Further away (with the pointer situated downwind) as the gas cloud expands, the largest gas signal is



Figure 6.3: Various surfaces at Malmö test site

received when the pointer is aimed behind the leak, as shown in figure 6.5; these values were recorded from a distance of 5m.

The values plotted on figure 6.5 are the normalised 2nd harmonic peak values, which are recorded over time. The recorded signal fluctuates heavily; we believe that these are real fluctuations in the gas cloud as it moves around, and is not noise fluctuations, as revealed by thermal images. The peak value occurring at 2300ppm.metre is the maximum value that this instrument can display, any greater value saturates the instrument and so it still displays 2300ppm.metre.

This result changes the way an operator could use the instrument. Remaining stationary, and pointing in all directions, the highest value does not necessarily correspond to the leak location. However, by following the direction given by the greatest gas reading, the user will eventually end up at the leak location.

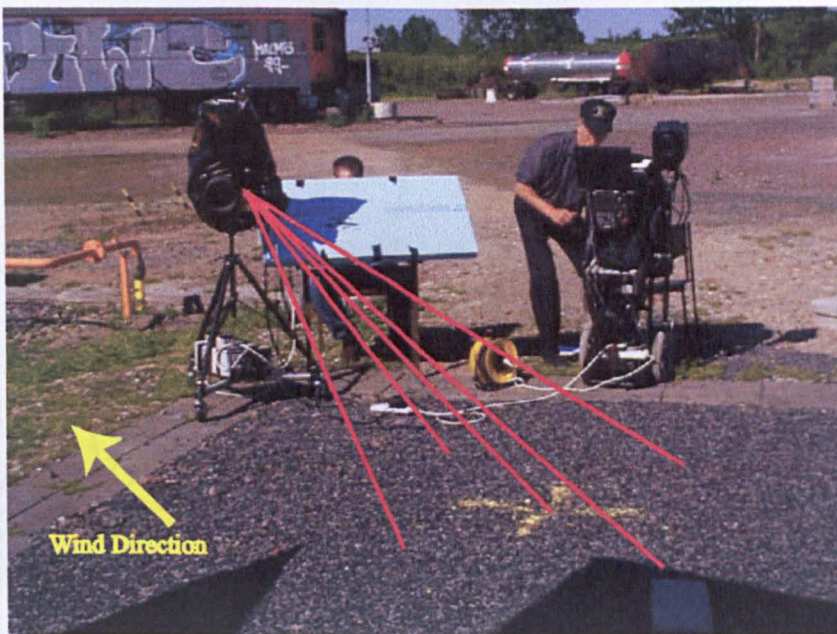


Figure 6.4: Aiming the pointer around the leak location

### 6.2.2 Real World Reflectivity

The information gained from the very first field trial showed that more information was needed on the required light levels. Information from table 4.1 indicated that the low level signal was sufficient but that the light level was not accurate enough to make. However, this had to be verified by the portable system.

Signal Fluctuations (20litre/minute flow rate)

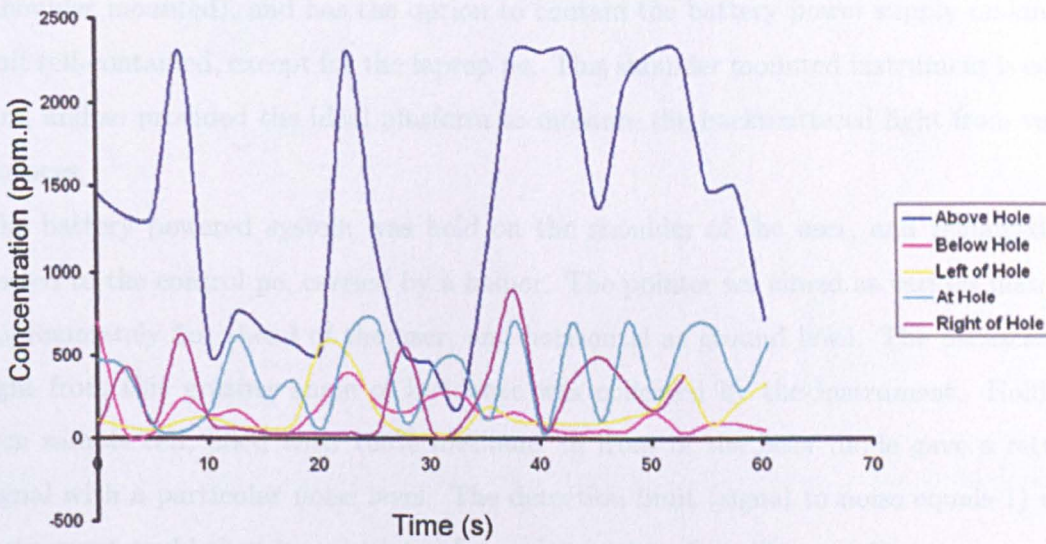


Figure 6.5: Signal levels varying with pointer direction

## 6.2.2 Real World Reflectivity

The information gained from the very first field trial showed that more information was needed on the returned light levels. Information from table 4.1 indicated that most surfaces should provide sufficient backscattered light to enable an accurate reading to be made. However, this had to be verified by the portable system.

The metal boxes have been replaced by a grey cylindrical tube, which is more portable (shoulder mounted), and has the option to contain the battery power supply making the unit self-contained, except for the laptop pc. This shoulder mounted instrument is easy to aim, and so provided the ideal platform to measure the backscattered light from various surfaces.

The battery powered system was held on the shoulder of the user, and remained connected to the control pc, carried by a helper. The pointer was aimed at various materials, approximately 5m ahead of the user, and horizontal at ground level. The backscattered light from this grazing angle of incidence was collected by the instrument. Holding a 1cm sample cell, filled with 100% methane, in front of the laser diode gave a returned signal with a particular noise level. The detection limit (signal to noise equals 1) of the instrument could then be calculated for each target surface (figure 4.4).

## 6.2.3 Scanning Through A Gas Cloud

The pointer instrument was tripod mounted, 5m away from a known leak source. The objective of this experiment was to try to identify the leak location, and to investigate the effect wind direction had on the signal levels.

The pointer was initially situated downwind from the leak, assuming that having the pointer in the gas cloud, the signal levels would be largest and thus would provide the

easiest detection scenario. The pointer was then positioned perpendicular to the wind direction, and scanned both upwind and downwind from the leak to try to identify the magnitude and location of the detectable gas cloud (figure 6.6 right).

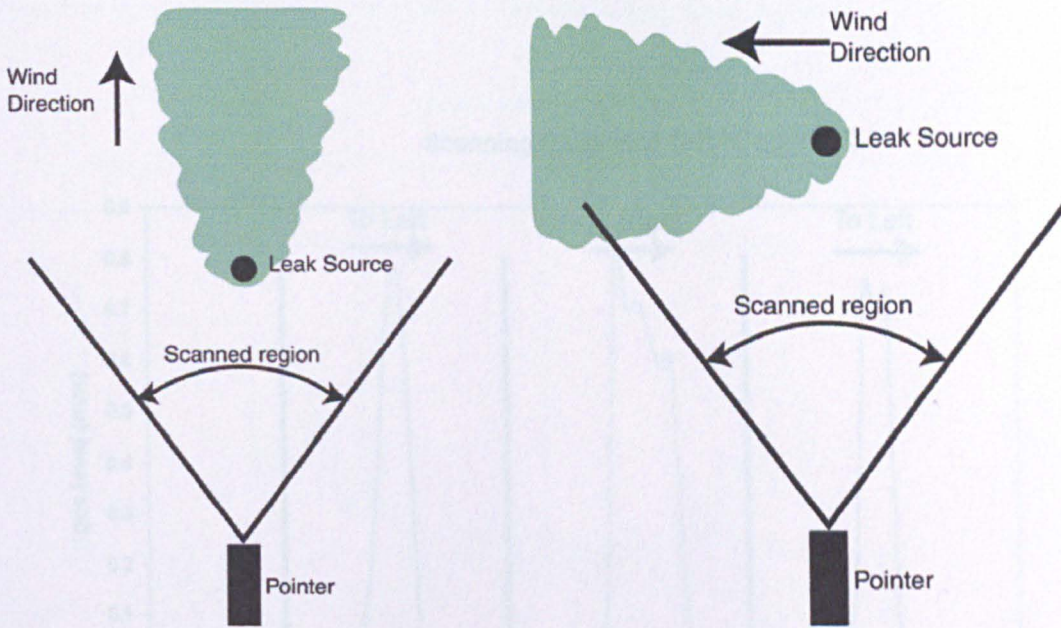


Figure 6.6: (Left) Scanning parallel and then (right) perpendicular to the wind direction

When scanning head on to the wind, the gas cloud appears very thin; the strong (approximately 8m/s) wind conditions disperse the gas very strongly in one direction. This makes locating the leak difficult. By scanning the pointer through the known location, the rise in gas signal level is clear (figure 6.7). The transition between no gas detected, and gas being detected is very sharp, and is characteristic of the strong wind conditions. After moving the pointer to be perpendicular to the wind direction, the instrument was slowly scanned through the leak location. As can be seen from figure 6.8, upwind of the leak there is a very distinct cut-off, where no methane can be detected. Downwind from

the back location, the gas level slowly reduces as it is dispersed by the wind. The fluctuations shown in figure 6.5 are due to variation in the levels of methane present within the line of sight of the instrument. The fluctuations are not indicative of noise within the system but are an artefact of the turbulent wind nature.

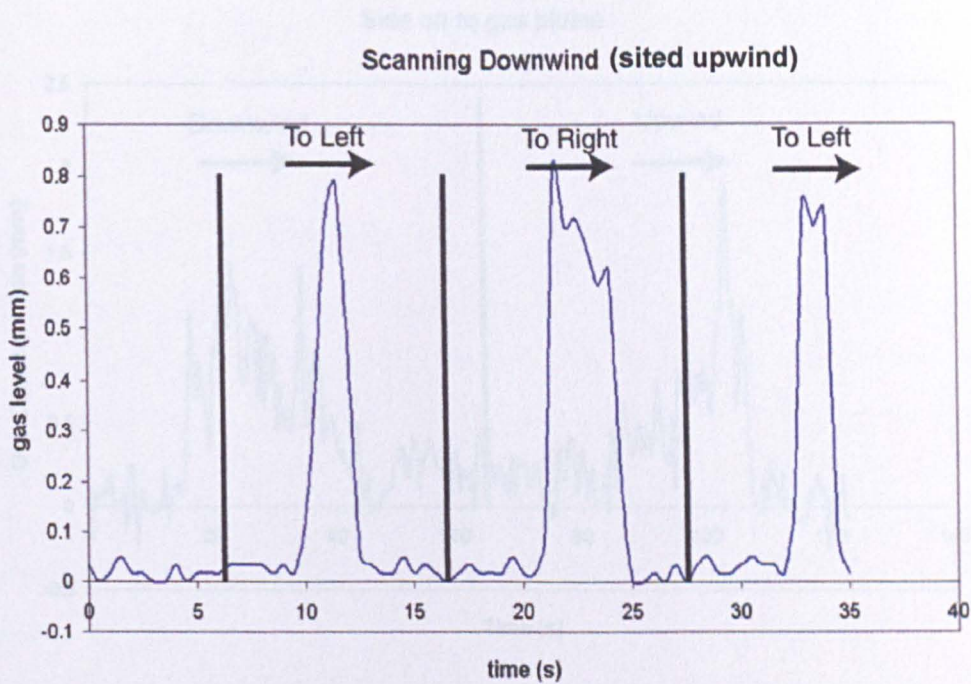


Figure 6.7: Results when positioned parallel to the wind direction (1mm gas cloud is equivalent to 1000ppm.m)

### 6.3 Functional Cost Efficient Prototype

The prototype system was adjusted by incorporating a custom designed electronics, greatly reducing the overall cost of the instrument. Furthermore, the optical head and signal processing electronics were separated into two enclosures. The optical head was

the leak location, the gas level slowly reduces as it is dispersed by the wind.

The fluctuations shown in figure 6.8 are fluctuations in the levels of methane present within the line of sight of the instrument. The fluctuations are not indicative of noise within the system but are an artefact of the turbulent wind nature.

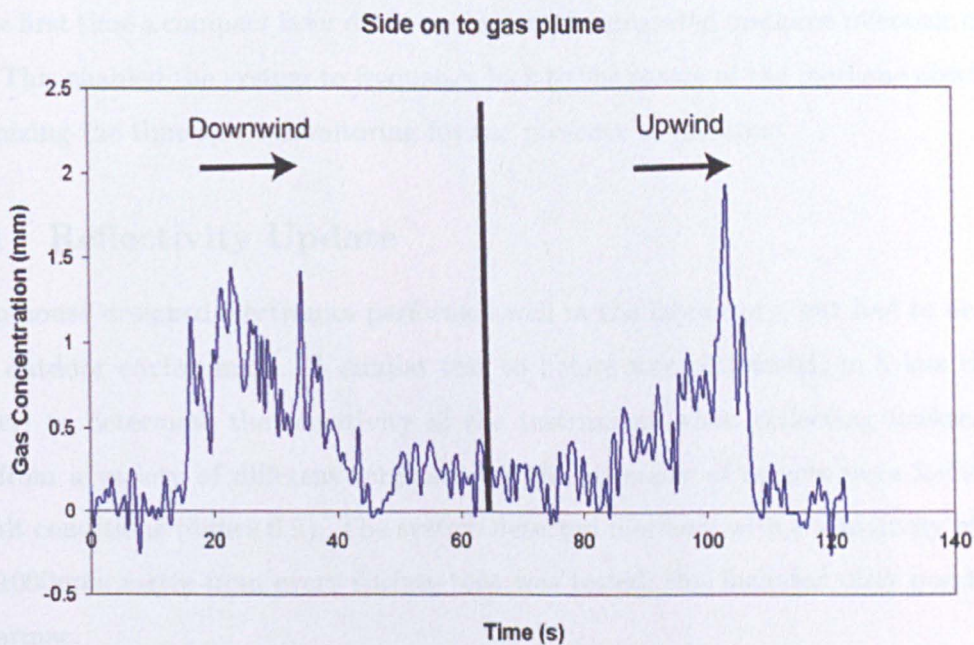


Figure 6.8: Results when positioned perpendicular to the wind direction

### 6.3 Functional Cost Efficient Prototype

This prototype system was advanced by incorporating in-house designed electronics, greatly reducing the overall cost of the instrument. Furthermore, the optical head and signal processing electronics were separated into two containers. The optical head was

made as light as possible, capable of being operated in one hand for a prolonged period of time. The support electronics were shoulder mounted and connected to the optical head via a multi-way shielded cable. There was still a laptop pc used to interface between the user and instrument.

For the first time a compact laser diode package with integrated methane reference cell was used. This enabled the system to frequency lock to the centre of the methane absorption, maximizing the time spent monitoring for the presence of methane.

### 6.3.1 Reflectivity Update

The in-house designed electronics performed well in the laboratory, but had to be tested in an outdoor environment. A similar test to before was performed, in a less rigorous manner, to determine the sensitivity of the instrument when collecting backscattered light from a variety of different targets. A wider diversity of targets were found, with difficult conditions (figure 6.9). The system detected methane with a sensitivity of better than 1000ppm.metre from every surface that was tested; this included dirty puddles and wet tarmac.

### 6.3.2 Comparison with Flame Ionisation Detector

There was enough confidence in the instrument performance to compare its detection ability with that of the industry standard flame ionisation detector (FID). The FID is a point measurement device and so a direct comparison of signal levels, and hence performance, is not possible. Furthermore, strong wind conditions would favour the FID as it operates at ground level, and could detect gas as it escapes, before the wind disperses the gas cloud.

The experiment to compare the two instruments involved performing a sweep of the gas



Figure 6.9: Carbon coated storage tank used to test the sensitivity of the instrument under low backscattered-light conditions

leak area with the FID. The pointer was tripod mounted and, while stationary, was aimed at the FID (figure 6.10). As the FID user walked around the leak site, the pointer user remained by the pointer instrument and aimed at the FID.

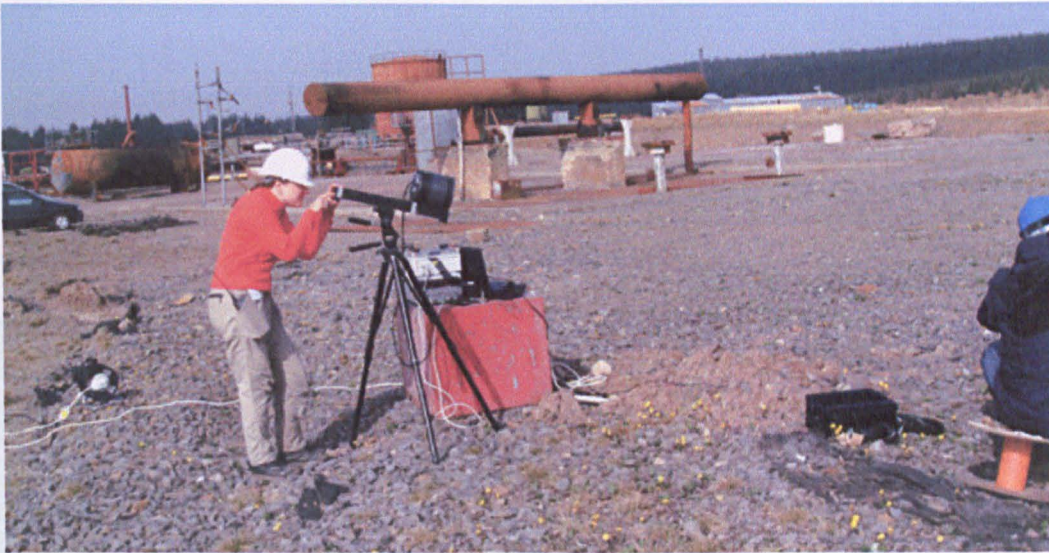


Figure 6.10: Aiming the pointer instrument at the flame ionisation detector

The time stamped output from each instrument was saved, so they can be plotted on the same graph (figure 6.11). As expected, the absolute recorded values cannot be compared since the instrument measure a different variable. However, the shape of each signal (over time) is similar, indicating that when the FID detected methane, so also did the pointer. Furthermore, there were no instances where one instrument detected methane and the other did not. Confidence is placed in the FID by the gas utilities to reliably detect a methane escape. This same reliability has been demonstrated by the pointer.

The apparent larger noise in the signal from the pointer is again due to the fluctuating signal levels, and not random noise fluctuations. This would also be apparent in the FID output if it had a faster response time, and the output wasn't time averaged over a 1

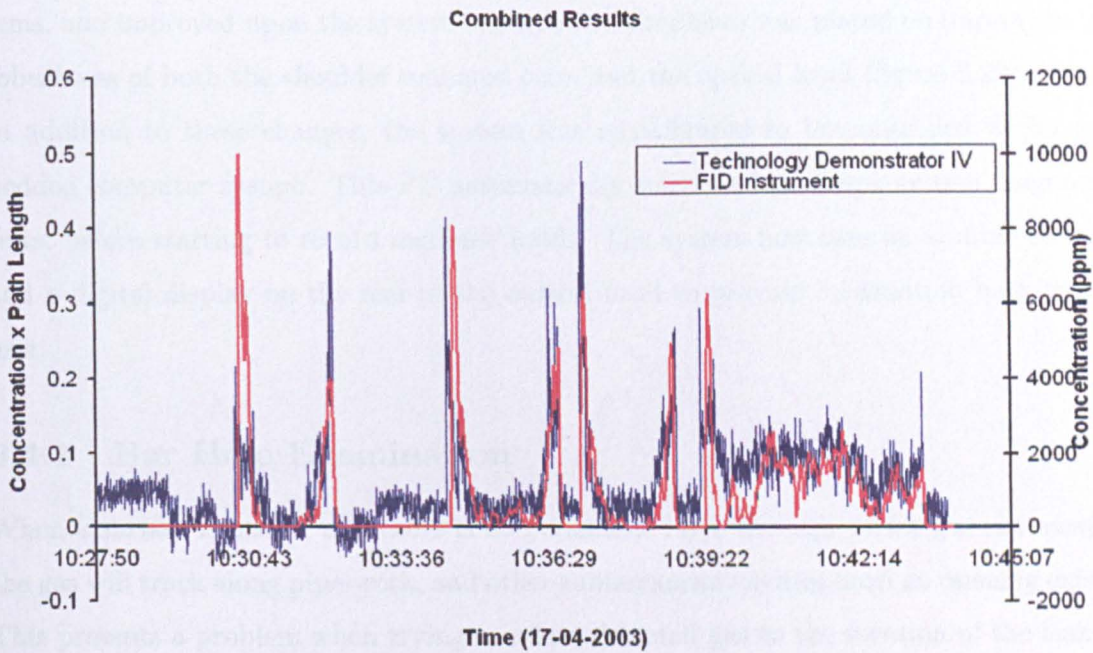


Figure 6.11: Comparing the FID output with the results from the pointer instrument (note similar performance but the pointer is operating remotely)

second interval.

## 6.4 Technology Demonstrator

The final in-house designed and built prototype contained the previous electronic systems, and improved upon the system ergonomics. Emphasis was placed on improving the robustness of both the shoulder mounted case, and the optical head (figure 3.22).

In addition to these changes, the system was reconfigured to be controlled by an embedded computer system. This PC automatically starts and performs system diagnostic tests, before starting to record methane levels. The system now uses an audible output, and a digital display on the rear of the optical head to provide information back to the user.

### 6.4.1 Bar Hole Examination

When a surface is intact, and there is no permeable layer through which gas can escape, the gas will track along pipe-work, and other subterranean cavities until an opening exists. This presents a problem when trying to relate detected gas to the location of the leak in the gas pipe. For non-permeable surfaces, such as roads, the current technique is to bore several holes through this layer (bar-holing) and measure the gas concentration in each.

At the Transco depot office in Leicester, there is a small test site facility, where instruments can be examined. One area of this site consists of a tarmac pathway, with buried pipes underneath. The pipes can simulate leaks from several different locations along the length of the path. The surface of the path has been bar-holed.

The instrument was carried around the location of the bar-holes, and an attempt was made to measure the relative amount of methane escaping from each hole, and hence find

the leak location (figure 6.12). The returned light levels from this damp tarmac surface



Figure 6.12: Detecting gas escaping from bar-holes

were very low, and so the sensitivity of the instrument was also low. The measured signal levels were all comparable, and so no conclusion could be made about the location of the gas leak.

#### 6.4.2 Blind Leak Search

At the Transco Leicester depot, there is a pipe line with leak locations buried under 80cm of coarse aggregate gravel. The leak location was known to the safety officer present, but

not to the instrument users.

The pointer instrument was given the task of searching the area and finding any potential number of separate leaks. The area in question was approximately 7m × 13m in size and was without any distinguishing features. The area was scanned while the operator remained stationary at the downwind side of the area. Three points of interest were noted, and marked by placing markers in the approximate areas. The operator then moved position, until he was perpendicular to the wind direction, and examined the area again. Two of the marked positions were adjusted slightly, while the third marker was removed completely.

Further movement and examination of the area gained no further information. Seeking clarification from the safety officer revealed that one leak was directly below the first marker, but the second marker appeared to be somewhat from the second leak location (there were only two leaks) as shown in figure 6.13. The area was swept with an FID to show the actual leak locations; the FID agreed with the pointer instrument.

Further explanation revealed that the gas from the second leak was most probably tracking back along the pipe because the ground was saturated by heavy rain. The pointer had indeed spotted the correct location of the above-ground gas, but as with other techniques this does not always correspond to the location of the leak.

### 6.4.3 Saturation Test

The sensitivity of the pointer instrument depends on the amount of backscattered light that can be collected by the Fresnel lens. By increasing amplifier gain, electronically, it is possible to improve the signal to noise performance of the instrument. The electronics have a threshold, above which they saturate and output their maximum value. It is important that this will not happen during normal use, but also that the operator is aware

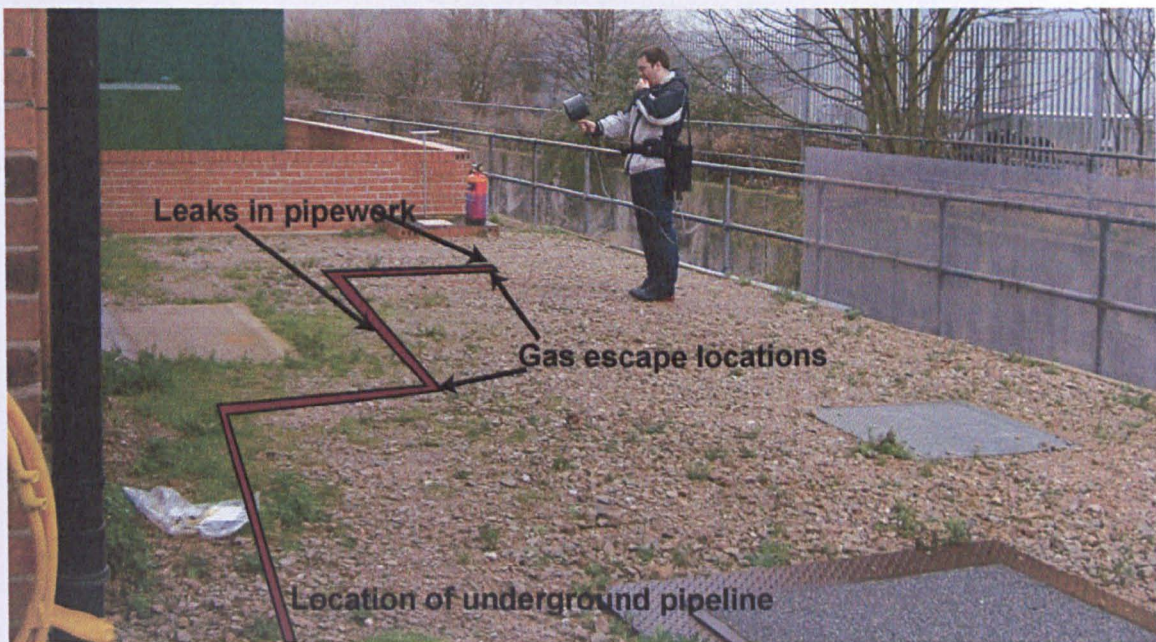


Figure 6.13: Layout of Leicester depot training area

of this potential issue. Laboratory testing gave information about the possible maximum returned light levels. This information was used to set the amplifier dc gain on the In-GaAs detector.

The potential also exists to saturate the optical path with sufficient methane such that at peak absorption no light is returned to the detector (figure 6.14). In this case, it is important that the dangerously high levels of methane do not cause the instrument to malfunction or display an erroneous reading. To aid this, the display electronics were scaled to have an upper threshold smaller than the instrument electronics. If the display was within its working range, the instrument would still be operating normally.

The digital output display, on the rear of the optical head, was configured to give a read-out in units of 1000ppm.metre (equivalent to 1mm thickness of a gas cloud). The scale had a maximum display of 19.999, so any greater gas signal would saturate the display. By examining figure 6.14 we can see that a gas signal of 19.999 would not saturate the optical path. The signal processing electronics could therefore withstand a greater level of methane in the line of sight of the instrument.

The task was to try to saturate the display of the instrument, causing a malfunction, in an outdoor environment. Any gas escaping is usually quickly dispersed, so a sheltered environment would limit the dispersion and provide greater signal levels. At the Leicester depot there is an examination pit, containing a large methane pipe. This pipe was cut, releasing a large flow of gas into the pit, and escaping into the atmosphere. The gas escape was clearly audible, and the scented additive easily smelled. The pointer was directed into the pit to record as large a signal as possible (figure 6.15). The largest signal recorded by the pointer was approximately 14000ppm.metre. At no point during the trial did it fail to return a high gas reading.

The pointer instrument could not be blinded by the largest gas leak available at the Leices-

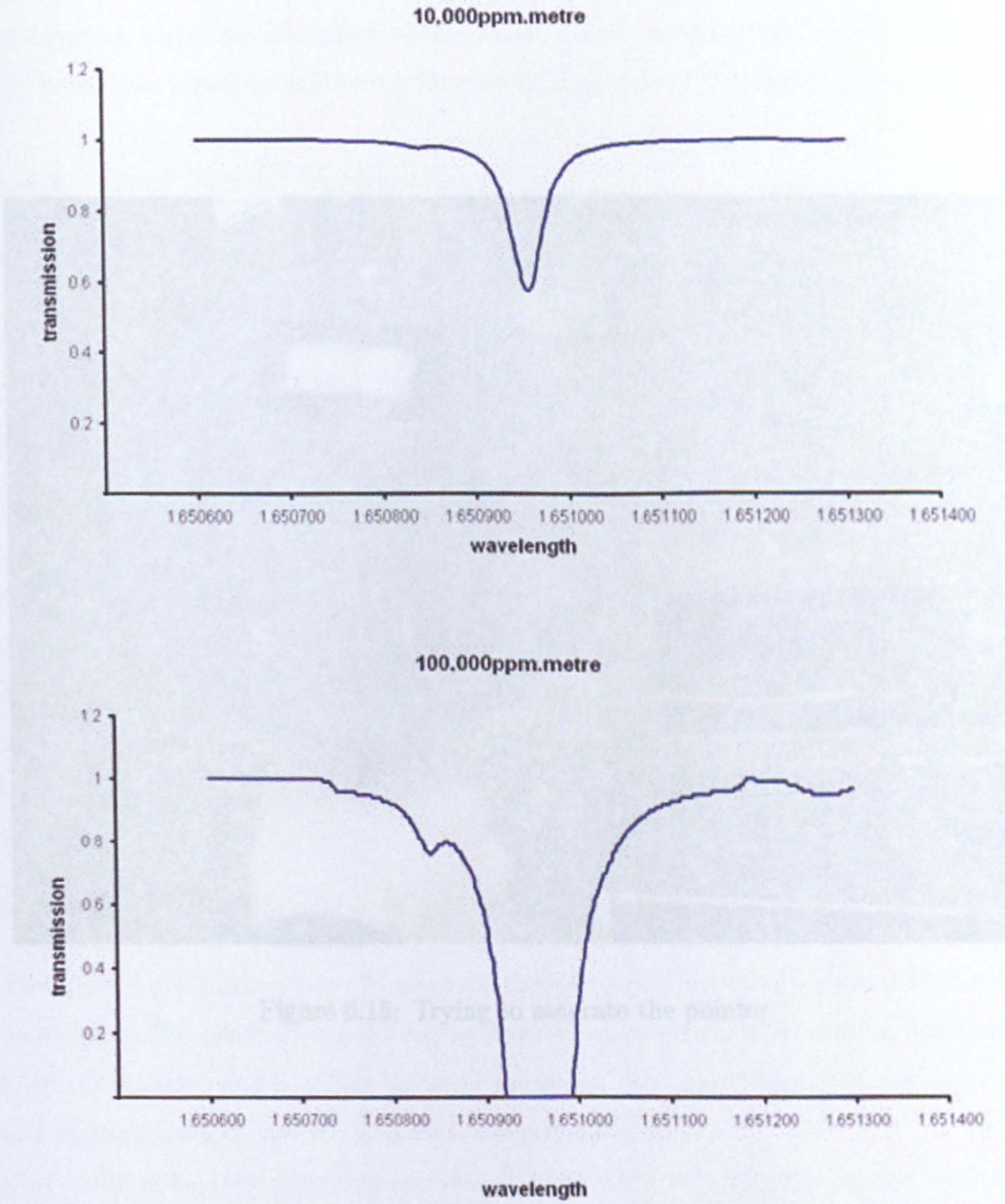


Figure 6.14: Signal saturated by large amounts of methane

ter depot. A bigger gas leak which could provide a large enough gas flow past the instrument would be sufficiently large to be detected without any assistance.

#### 6.4.4 Real World Verification



Figure 6.15: Trying to saturate the pointer

The scanner platform (chapter 5) was used to rapidly scan the optical beam of the pointer instrument. The returned signal from the pointer was correlated with position information from the scanner, and a colour image of the scene. The gas information was processed and superimposed on top of the colour background image.

The scanning hardware development was still in its infancy when the scanner was taken to the Leicester depot. Initially it was setup in a confined environment, and aligned using

ter depot. A bigger gas leak which could provide a large enough methane path to saturate the instrument would be sufficiently large to be detected without instrumentation!

#### 6.4.4 Real World Verification

The final consortium meeting took place in Brussels where the opportunity arose to take the instrument outside to try to identify a known leak. The gas company had identified the gas leak previously, but had not yet initiated the repair process. The information reported to the gas utility on the location of the leak was passed on to the users of the prototype pointer, and the pre-commercial instruments. This reduced the search area to a 30m length of pathway, about 3m wide. The instruments were used to search the given area for traces of methane as shown in figure 6.16.

It was known that the gas pipes were buried under the centre of the pathway, however, the unbroken tarmac pathway would not let any methane permeate through. Searching the area revealed that methane was escaping from the boundary between the pathway and the neighboring grass area. Both the Glasgow and Siemens instruments agreed on the location of the strongest gas signal, which was verified by independent means.

### 6.5 Scanning The Pointer

The scanner platform (chapter 5) was used to rapidly scan the optical beam of the pointer instrument. The returned signal from the pointer was correlated with position information from the scanner, and a colour image of the scene. The gas information was processed and superimposed on top of the colour background image.

The scanning hardware development was still in its infancy when the scanner was taken to the Leicester depot. Initially it was setup in a confined environment, and aligned using

transparent bags filled with methane. Once the instrument was aligned, it was placed outside in the test area, and positioned roughly in the middle of each test area. Looking at the pit in the ground, the gas was turned on so that a slow leak was created. The metal pit covers were spaced very slightly (figure 6.17), and a small amount of gas escaped. The small holes were used to measure the methane concentration in the air.



Figure 6.16: Locating a real leak location in Brussels

The images clearly show the methane which has been detected, and further indicate the source of the gas leak. The only problem with the current method is too long to gain insight into the behaviour of the leak dispersion, but this can be resolved with changes to the software. The software changes will reduce the scan time to approximately 1 second, which should be quick enough to detect changes in the gas behaviour. This in turn will allow a more intuitive approach to locating the gas leak source.

transparent bags filled with methane. Once the instrument was aligned, it was taken outside to the test area, and positioned roughly in the middle of the test area. Aiming at the pit in the ground, the gas was turned on so that a slow leak was created. Initially the metal pit covers were opened very slightly (figure 6.17), and a small amount of gas escaped. The metal lid was further opened to allow more gas to escape, to see the effect this had on the gas image (figure 6.18).



Figure 6.17: Narrow opening in metal pit lid

The images clearly show the methane which has been detected, and further indicate the source of the gas leak. The cycle time of the scanning platform is too long to gain insight into the behaviour of the leak dispersion, but this can be reduced with changes to the software. The software changes will reduce the scan time to approximately 1 second, which should be quick enough to detect changes in the gas behaviour. This in turn will allow a more intuitive approach to locating the gas leak source.



Figure 6.18: Pit lid completely open allowing gas to escape freely

## 7. Commercialisation

This chapter will discuss the commercialisation potential of the laser pointer. Every stage of development of the instrument was discussed with various consortium partners so that a route to market could be developed and then exploited. The scientific detail of the instrument was passed on to Siemens AG (Munich, Germany) at every development stage so that a pre-production prototype could be developed in tandem with the work discussed in this thesis.

This chapter will primarily outline the development of the Siemens instrument, where direct parallels are clearly visible with the development discussed in Chapter 3. The instrument designed by Siemens was fabricated predominantly in-house, which may provide the simplest route to market.

Secondly this chapter will outline the work performed by various consortium partners to promote the instrument to a wider audience. Such activities include the production of a brochure and the development of a web-site.

Finally this chapter will cover the options available to the consortium members to develop the instrument into a saleable item, and the potential producers of such an item.

## 7.1 Pre-production Prototype

At the outset of the project, the work performed by Rainer Strzoda at Siemens AG used a different technique for methane detection. After several technical discussions, the consortium consensus was that the WMS technique used at Glasgow was the better approach. A different strategy was employed so that I, at Glasgow University, would continue with the development of the instrument; Siemens AG would concentrate their efforts into taking my design developments, and integrating them into a pre-production prototype. For example, I had used a fully operational PC to control the system, so that changes could be made to the software throughout testing; Siemens took this resulting information and programmed a microprocessor for system control.

The effect of these changes on the resulting system ensured that it was smaller, lighter and more power efficient than the instrument developed in Glasgow (see figure 7.1). As can be seen in figure 7.1, the user interface is provided by a palm-top device. This is connected to the internal micro-processors by way of a serial connection. The palm top gives a graphical readout of gas concentration with time, as well as an audible signal. As is also visible in figure 7.1, the laser diode module has been positioned closer to the optical axis of the system. This is possible within this instrument configuration since the Siemens units employed a variable gain detector amplifier. The usable dynamic range is thereby significantly increased. In addition, further work had been done to characterise the power consumption and temperature performance of the instrument as shown in table 7.1.

Laser Operating Wavelength	1651nm
Laser Output Power	<10mW
Beam Divergence	60mm @ 10m distance
Laser Class	1
Visible Laser wavelength	635nm
Laser Output Power	<1mW
Laser Class	2
Response Time	100ms
Methane Gas Concentration Range	Depending on reflected power, 0..>1000ppm.m. With rising reflected power the max. resolvable concentration decreases
Power Consumption	2.5..4W depending mainly on ambient temperature
Operating time with one battery charge	3.5 hours with rechargeable cells (2000mAh) depending on ambient temperature, with primary cells probably longer
Operating temperature range	-10..+40°C
Operating distance range	>10m depending on reflecting surface
Lower detection limit	10-20ppm.m depending on reflecting power

Table 7.1: Performance figures for Siemens pre-production prototype

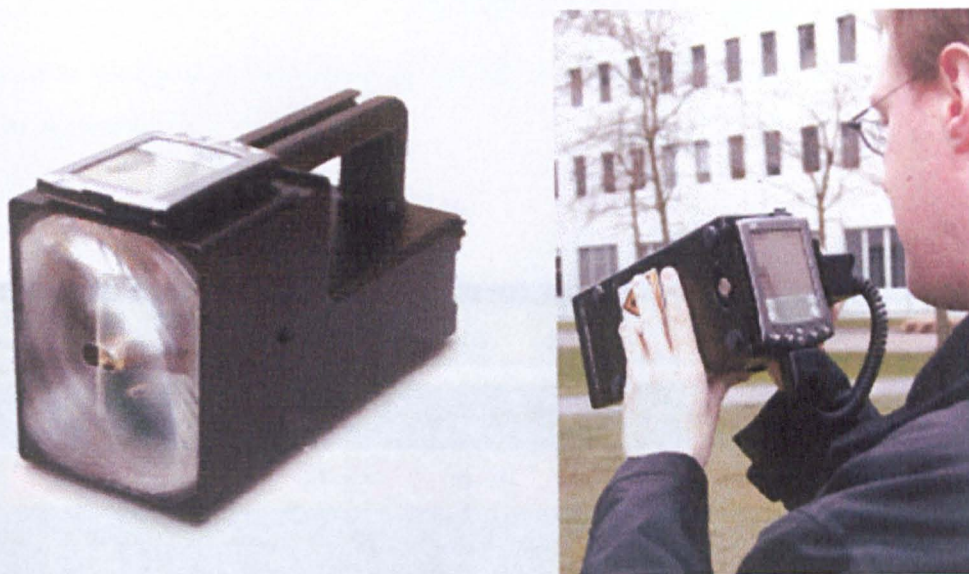


Figure 7.1: Instrument developed by Siemens, based on the Glasgow design

## 7.2 Advertising

Several avenues for advertising the project have been explored. A requirement set by the EC for funding projects is that a website must be designed and maintained, which satisfies certain criteria. I designed and developed a website, hosted on the Optics group web-space (at Glasgow University). This website is very simple in architecture, but gives broad information on the project, the consortium partners, and the goals which we set out to achieve (see figure 7.2). A domain name (<http://vogue.no-ip.org>) was purchased, and setup to point towards the site, but this registration may now have expired.

Throughout the project various partners attended conferences aimed at gas utilities. On various occasions a presentation included mention of the work being conducted on this project. Because of the commercial sensitivity of the details, care had to be taken not to divulge too much information. To this end, and for more general advertising purposes, a

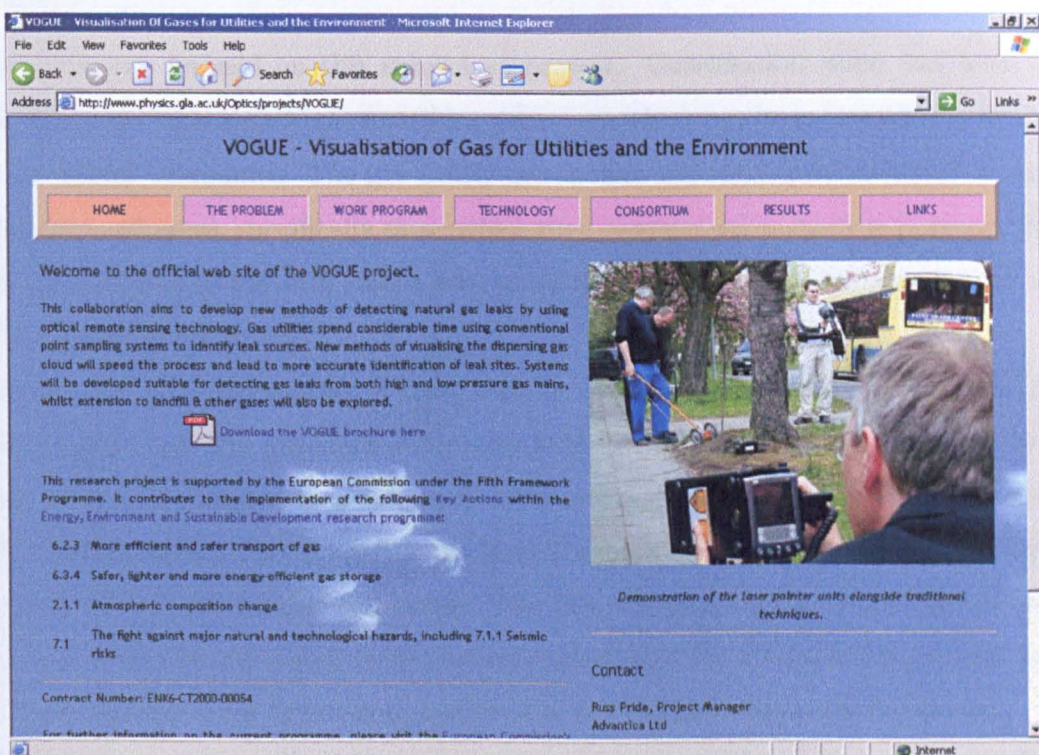


Figure 7.2: Website hosted at Glasgow University

---

brochure was designed by Advantica and made public. The six pages of the brochure are shown in Appendix A.

### **7.3 Marketing**

Very little can be said on this subject at present. Considerable effort has been spent developing the instrument into a working prototype which can be independently evaluated by gas utility companies. The gas utility consortium members have provided invaluable feedback in all areas, specifically those which they consider particularly important. Design and construction of the instrument has, at all times, taken into consideration the needs of the potential end-users.

However, the potential market of these tools is, like any business, financially constrained. The potential cost of a produced instrument is likely to be in the region of EUR10,000 and sales likely to be limited to a couple of instruments per gas utility depot. The financial risk involved with proceeding with the final development of this instrument is sufficient to deter all but the largest companies. My belief is that consortium members such as Semelab would be interested in producing components for a salable instrument, but do not have the resources to develop, market and sell the instrument on their own.

Whether the instrument will become a commercial success depends on too many factors outwith our control. One thing is certain, though, the instrument developed at Glasgow University has been a technological success.

---

# Bibliography

- [1] I. G. McWilliam. *Chromatographia*, 17:241–243, 1983.
- [2] L. S. Rothman; C. P. Rinsland; A. Goldman; S. T. Massie; D. P. Edwards; J.-M. Flaud; A. Perrin; C. Camy-Peyret; V. Dana; J. Y. Mandin; J. Schroeder; A. McCann; R. R. Gamache; R. B. Wattson; K. Yoshino; K. V. Chance; K. W. Jucks; L. R. Brown; V. Nemtchinov and P. Varanasi. The hitran molecular spectroscopic database and hawks (hitran atmospheric workstation): 1996 edition. *J. Quant. Spectrosc. Radiat.*, 60:665–710, 1998.
- [3] Health and Safety Executive. *A guide to gas safety (management) regulations*. HSE Books, 3 edition, 1996.
- [4] R. P. W. Scott. *Nature (London)*, 176:793, 1955.
- [5] I. G. McWilliam and R. A. Dewar. *Gas Chromatography (Amsterdam Symposium)*, 1958.
- [6] D. Steers; C. Gerrard; B. Hirst; W. Sibbett and M. J. Padgett. Gasoline analysis and brand identification using a static fourier-transform ultraviolet spectrometer. *Journal of Optics A: Pure and Applied Optics*, 1:680–684, 1999.

- 
- [7] J. Courtial; B. A. Patterson; W. Hirst; A. R. Harvey; A. J. Duncan; W. Sibbett and M. J. Padgett. Static fourier-transform ultraviolet spectrometer for gas detection. *Applied Optics*, 36:2813–2817, 1997.
- [8] P. Jacquinet. The luminosity of spectrometers with prisms, gratings or fabry-perot etalons. *Journal of the Optical Society of America*, 44:761–765, 1954.
- [9] P. Jacquinet. New developments in interference spectroscopy. *Rep. Prog. Phys.*, 23:267–312, 1960.
- [10] R. Harig; G. Matz; P. Rusch; J-H. Gerhard; K. Schafer; C. Jahn; P. Schwengler and A. Beil. Remote detection of methane by infrared spectroscopy for airborne pipeline surveillance: first results of ground based measurements. *Proceedings of SPIE*, 5235, 2004.
- [11] M. Murtz; B. Frech and W. Urban. High resolution cavity leak-out absorption spectroscopy in the  $10\mu\text{m}$  region. *Applied Physics B*, 68:243–249, 1999.
- [12] H. Dahnke; D. Kleine; W. Urban; P. Hering and M. Murtz. Isotopic ratio measurement of methane in ambient air using mid-infrared cavity leak-out spectroscopy. *Applied Physics B*, 72:121–125, 2001.
- [13] B. A. Paldus; C. C. Harb; T. G. Spence; B. Wilke; J. Xie; J. S. Harris and R. N. Zare. Cavity-locked ring-down spectroscopy. *Journal of Applied Optics*, 83:3991–3997, 1998.
- [14] R. Engeln; G. von Helden; G. Berden; and G. Meijer. Phase shift cavity ring down absorption spectroscopy. *Chemical Physics Letters*, 262:105–109, 1996.

- 
- [15] D. Romanini; A. A. Kachanov and F. Stoeckel. Diode laser cavity ring down spectroscopy. *Chemical Physics Letters*, 270:538–545, 1997.
- [16] J. J. Baumberg; S. A. Crooker; D. D. Awschalom; N. Samarth; H. Luo and J. K. Furdyna. Ultrafast faraday spectroscopy in magnetic semiconductor quantum structures. *Physical Review B*, 50:7693–7694, 1994.
- [17] J. M. Kikkawa; I. P. Smorchkova; N. Samarth and D. D. Awschalom. Optical studies of spin precession in magnetic two-dimensional electron gases. *Physica E*, 2:394–298, 1998.
- [18] M. M. J. W. van Herpen; I. Shaocheng; S. E. Bisson and F. J. M. Harren. Photoacoustic trace detection of ethane using a continuously tunable continuous-wave optical parametric oscillator based on periodically poled lithium niobate. *Applied Physics Letters*, 81:1157–1159, 2002.
- [19] Z. Zelinger; M. Strizik; P. Kubat and S. Civis. Quantitative analysis of trace mixtures of toluene and xylenes by CO<sub>2</sub> laser photoacoustic spectrometry. *Analytica Chimica Acta*, 422:179–185, 2000.
- [20] C. N. Banwell and E. M. McCash. *Fundamentals of Molecular Spectroscopy*, chapter 4. McGraw-Hill, 4 edition, 1997.
- [21] S. Amoruso; A. Amodeo; M. Armenante; A. Boselli; L. Mona; M. Pandolfi; G. Pappalardo; R. Velotta; N. Spinelli and X. Wang. Development of a tunable IR lidar system. *Optics and Laser in Engineering*, 37:521–532, 2002.
- [22] G. Thomson and D. Batchelder. Development of a hand-held forensic-lidar for stand-off detection of chemicals. *Review of Scientific Instruments*, 73:4326–4328, 2002.

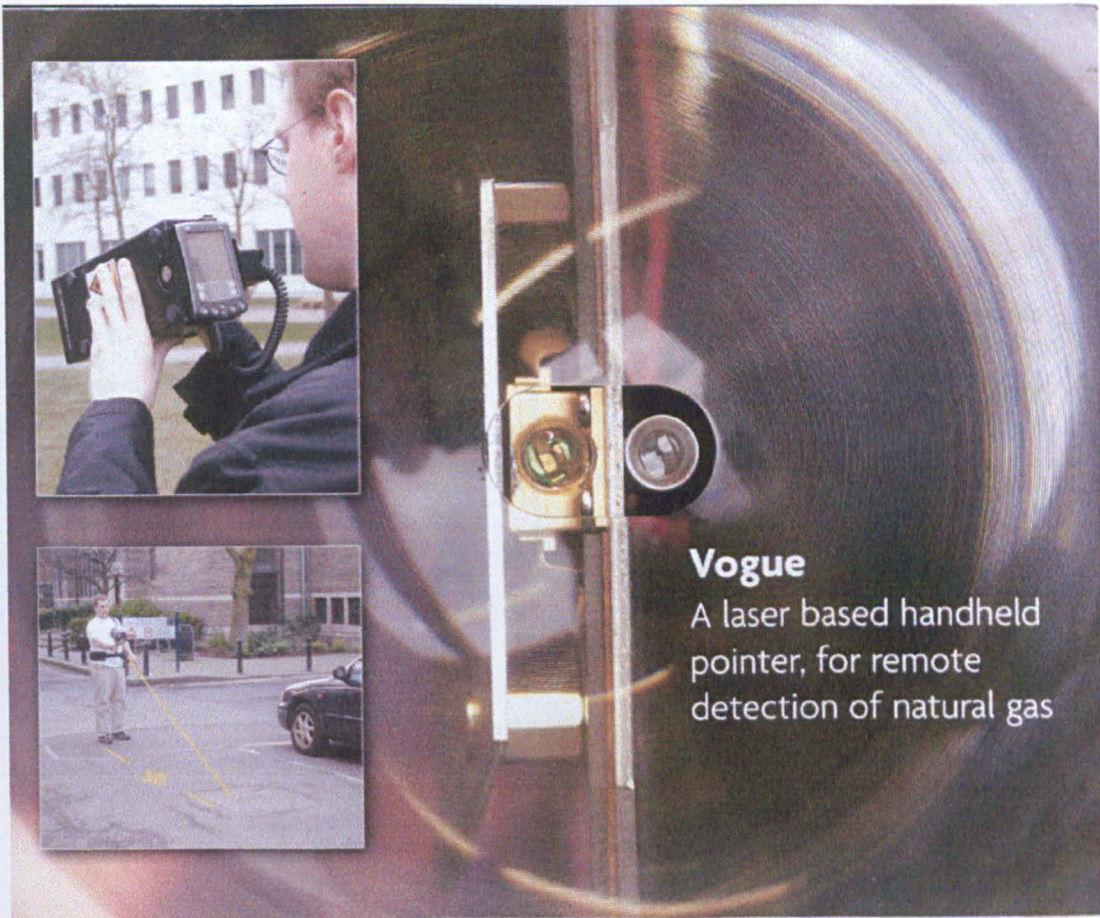
- 
- [23] P. Weibring; J. N. Smith; H. Edner and S. Svanberg. Development and testing of a frequency-agile optical parametric oscillator system for differential absorption lidar. *Review of Scientific Instruments*, 74:4478–4484, 2003.
- [24] H. L. Walmsley and S. J. O'Connor. The accuracy and sensitivity of infrared differential absorption lidar measurements of hydrocarbon emissions from process units. *Pure and Applied Optics*, 7:907–925, 1998.
- [25] K. Ikuta; N. Yoshikane; N. Vasa; Y. Oki; M. Maeda; M. Uchiumi; Y. Tsumura; J. Nakagawa and N. Kawada. Differential absorption lidar at  $1.67\mu\text{m}$  for remote sensing of methane leakage. *Japanese Journal of Applied Physics*, 38:110–114, 1999.
- [26] N. S. Prasad and A. R. Geiger. Remote sensing of propane and methane by means of a differential absorption lidar by topographic reflection. *Optical Engineering*, 35:1105–1111, 1996.
- [27] J. D. Houston; S. Sizgoric; A. Ulitsky and J. Banic. Raman lidar system for methane gas concentration measurements. *Applied Optics*, 25:2115–2121, 1986.
- [28] A. Minato; M. A. Joarder; S. Ozawa; M. Kadoya and N. Sugimoto. Development of a lidar system for measuring methane using a gas correlation method. *Japanese Journal of Applied Physics*, 38:6130–6132, 1999.
- [29] S. Schilt; L. Thevenaz and P. Robert. Wavelength modulation spectroscopy: combined frequency and intensity laser modulation. *Applied Optics*, 42:6728–6738, 2003.
- [30] D. S. Bomse; A. C. Stanton and J. A. Silver. Frequency modulation and wavelength modulation spectroscopies: comparison of experimental methods using a lead-salt diode laser. *Applied Optics*, 31:718–731, 1992.

- 
- [31] S. M. Jackson; G. H. Morgan; A. D. Morse; A. L. Butterworth and C. T. Pillinger. The use of static mass spectroscopy to determine the combined stable isotopic composition of small sample of atmospheric methane. *Rapid Communications in Mass Spectrometry*, 13:1329–1333, 1999.
- [32] D. Kleine; H. Dahnke; W. Urban; P. Hering and M. Murtz. Real-time detection of  $^{13}\text{CH}_4$  in ambient air by use of mid-infrared cavity leak-out spectroscopy. *Optics Letters*, 25:1606–1608, 2000.
- [33] M. S. Zahniser; D. D. Nelson; J. B. McManus and P. L. Keabian. Measurement of trace gas fluxes using tuneable diode laser spectroscopy. *Phil. Trans. R. Soc. Lond. A*, 351:371–382, 1995.
- [34] P. Werle and A. Popov. Application of antimonide lasers for gas sensing in the 3–4  $\mu\text{m}$  range. *Applied Optics*, 38:1494–1501, 1999.
- [35] D. Blaha; B. Mosher; R. C. Harriss; C. E. Kolb; J. B. McManus; J. H. Shorter and B. Lamb. Mapping urban sources of atmospheric methane. *Geo Info Systems*, pages 34–38, 1994.
- [36] K. P. Petrov; S. Waltman; U. Simon; R. F. Curl; F. K. Tittel and E. J. Dlugokencky. Detection of methane in air using diode-laser-pumped difference-frequency-generation near 3.2  $\mu\text{m}$ . *Applied Physics B: Lasers and Optics*, 61:553–558, 1995.
- [37] G. C. Liang; H. H. Liu; A. H. Kung; A. Mohacsi; A. Miclos and P. Hess. Photoacoustic trace detection of methane using compact solid-state lasers. *Journal of Physical Chemistry A*, 104:10179–10183, 2000.
- [38] Kiyoji Uehara and Hideo Tai. Remote detection of methane with a 1.66  $\mu\text{m}$  diode laser. *Applied Optics*, 31:809–814, 1992.

- 
- [39] P. Werle and R. Kormann. Fast chemical sensor for eddy-correlation measurements of methane emissions from rice paddy fields. *Applied Optics*, 40:846–858, 2001.
- [40] H. Tai; K. Yamamoto; M. Uchida; S. Osawa and K. Uchara. Long distance simultaneous detection of methane and acetylene by using diode-lasers coupled with optical fibers. *IEEE Photonics Technology Letters*, 4:804–807, 1992.
- [41] D. Fowler; K. J. Hargreaves; T. W. Choularton; M. W. Gallagher; T. Simpson and A. Kaye. Measurements of regional  $\text{ch}_4$  emissions in the uk using boundary layer budget methods. *Energy Conversion and Management*, 37:769–775, 1996.
- [42] Analog Devices. Ad630 - balanced modulator/demodulator. *Data Sheet*.

## A. Brochure

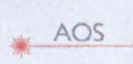
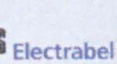
The brochure contained within this appendix has 6 A4 sized faces. Face 1 (the front page) gives an indication to the nature of the content, it introduces the product. Face 2 gives an overview of why the work is of interest to gas utilities, and goes some way to describing how the work was carried out. Face 3 gives some key results, which were obtained during testing, and explains how these should be interpreted. Face 4 is a diagram detailing the project structure, showing key development stages. Face 5 puts the work into context, describing how the work performed in this project may have influences on future EU policies. Finally face 6 (the back page) gives the performance specification of the Siemens instrument, and references the website as a source for updated future information.



**Vogue**

A laser based handheld pointer, for remote detection of natural gas

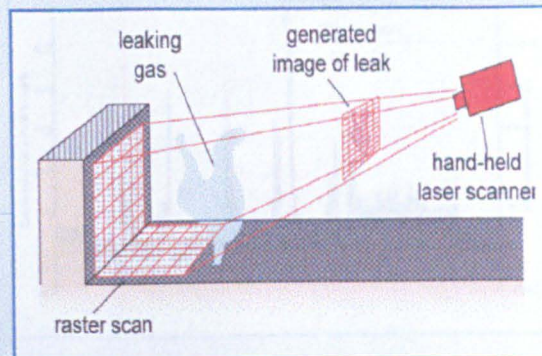
**VOGUE:** Visualisation of Gas for Utilities and the Environment



# The Vogue Project

## Objectives

The VOGUE project objectives were to provide new knowledge and instrumentation to aid the process of locating gas leaks from both high and low pressure gas mains. Gas distribution utilities have long wished for a method of visualizing gas leaks. A performance step change in gas leak detection was expected, compared with current techniques. VOGUE was targeted to provide improved understanding of gas leak behaviour through "passive" infrared (IR) imaging of gas leaks, supported by development of numerical models. The range of applicability of IR techniques in the field would be quantified, and material produced for training purposes. An "active" gas leak indicating instrument, using a remotely hand-held, distributed feedback (DFB) laser pointer was to be developed and tested in the laboratory and field. Novel methods of laser scanning to provide gas images would be developed with the aim to provide an instrument with marketable cost / benefits.



## Workplan and methodology

The programme, shown in the accompanying chart, was structured into 10 work packages (WPs), the first two encompassing project management, exploitation and dissemination strategies. The next two technical WPs provide for a design specification and from experimental and theoretical activities on the spatial and temporal characteristics of gas leak behaviour, the anticipated limits of practical system design. A separate WP deals specifically with the use of passive, infra-red thermal imaging of gas leaks, and within this activity a field test site has been established where a series of controlled gas leaks from buried pipes have been examined. From this activity, images of a wide range of gas leaks have been obtained.

A remote active laser based pointer for gas detection was the key objective of the project and the many design and safety aspects of controlling and managing the laser component have been addressed in a discrete WP. Using this knowledge, bench technology that can detect methane at low concentrations over a distance of 10m was the target of development in a further WP. Additional focus was on methods to provide a rugged, low-cost scanner to produce an interrogation beam for rapid leak location and zero gas confirmation.

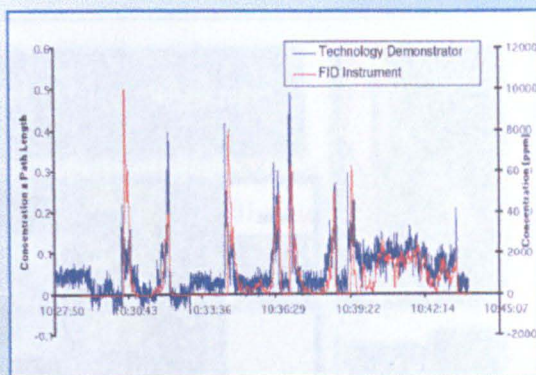
The bench-top developments have been transferred into a number of field prototypes in a further WP and these have been tested in two further WPs a) under controlled conditions in specially designed outdoor field test sites and b) finally in field evaluations with the gas utility operators.



## Key Results

The key results from the project include the following:-

- Design for a hand-held laser pointer for gas leak detection.
- Detailed understanding of gas leak behaviour through imaging.
- Limits of thermal imaging for gas leak detection
- Training material on gas leak detection
- Test site for evaluation of gas leaks from buried pipes
- Interpretation of gas concentration measurements using a laser pointer
- Six prototype units evaluated in controlled and under field conditions
- Demonstrator gas leak imaging system based on a laser pointer



Response comparison with standard flame ionisation gas leak



Optical sensor head design of laser pointer



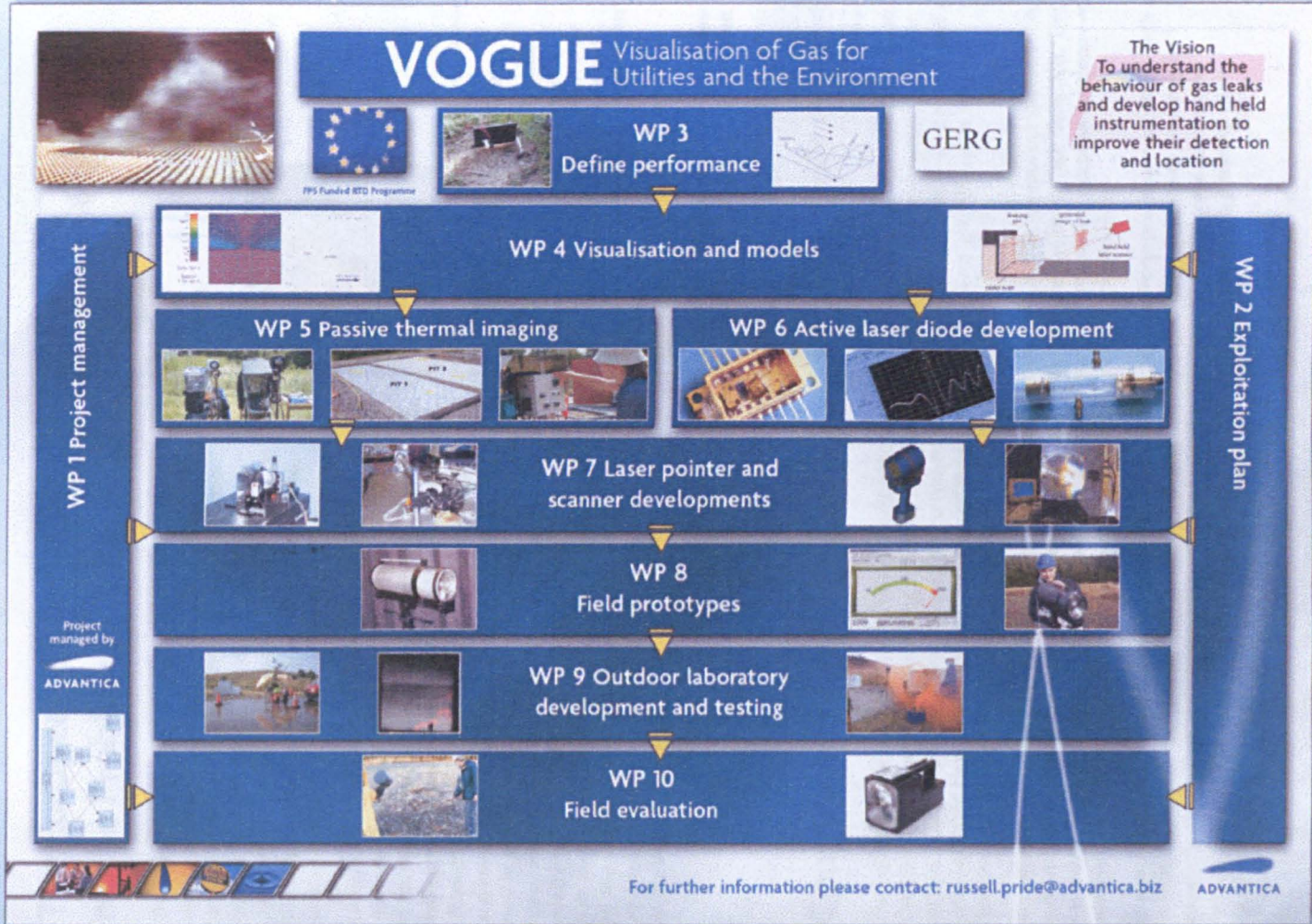
First gas cloud image from laser scanner

## Assessment of Results

The laser pointer was able to identify most leaks identified by conventional instruments. Correlation between ppm.m and ppm gas concentrations from conventional instruments still requires further interpretation. Factors that influence performance include wind speed and as with conventional instruments, the porosity of the ground. Factors that do not affect performance include sunlight and other gases. A number of additional benefits are seen from the use of a remote detector, including looking through windows, viewing gas risers or inaccessible locations, testing barholes without extracting the gas sample, remotely checking an area before entry, etc.

The project has improved understanding of gas leak dispersion in air from buried gas pipes, particularly from thermal imaging. An active laser gas pointer has been developed to remotely detect gas from distances up to 15m and has been extensively demonstrated under real world conditions. A first commercial design for use by gas field engineers has provided encouragement for its broader application within the gas industry. Conversion of the laser pointer unit into a scanner has been demonstrated in the field but further work is required to make a practical unit. The future potential of these types of unit for scanning in leak surveys and vehicle patrols is recognized and the consortium is developing an exploitation business plan.

Vogue project structure showing key developmental stages

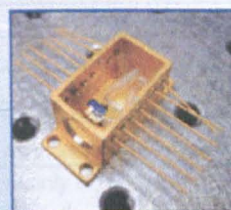


# The Bigger Picture

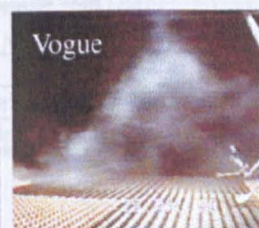
## The European Dimension of the Problem

The leakage of gas from distribution, transmission and storage systems is a problem which, to a greater or lesser degree, affects all the countries in the European Union. Leakage is conventionally associated with older distributions networks, such as may be found in the UK and Italy, but the problem is by no means confined to such systems.

Leakage from the gas mains network is an important issue that must be managed by the gas industry world-wide. It has been estimated that approximately 90% of the leakage (by volume) emanates from the low pressure distribution mains<sup>[1]</sup>. The primary focus, for safety, cost and environmental reasons, has been to detect and reduce leakage from this part of the system. A secondary focus was to detect leaks from higher pressure sections of the transmission and storage system, in which the gas may not be odourised. These objectives have been advanced by the successful development, in this project, of advanced gas detectors and an improved understanding of the behaviour of gas leaks.



Opto-electronic components developed within the project



### Gas Leaks

Training material for improved understanding of gas leak behaviour

**Including:- Information on current & new methods of leak detection & measurement**

EC Contract NO. ENK6-CT-2000-00054

Amendment No.1

Copyright 2003. ©Vogue consortium. All rights reserved

Training CD

## Contributions to EU Policies

The benefits of the project will be shared by many stakeholders, not limited to members of the consortium. The European gas network is becoming increasingly integrated, as pipelines are extended between different regions. Safety improvements will benefit gas customers and personnel working within the industry as well as others affected by explosion hazards. Quicker and more accurate leak location will also reduce levels of disruption for affected people, transport networks and industries.

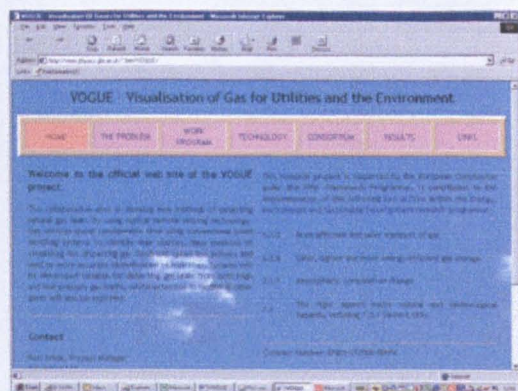
An important aspect of the research programme has been the establishment of a new product specification, test procedures and the basis for new working practices and European guidelines on gas leak detection. This has required a pan-European approach, supporting European policies on competition, industrial development, environmental legislation and freedom of movement of citizens within the community.

Economic benefits will also be felt within the EU via the reduced cost of emergency response systems, with a reduction in energy costs passed to consumers. The project has provided EU industry with fundamental knowledge that will aid the development and use of new gas detectors. The programme has fostered increased technical co-operation between European countries and required technology transfer of the specialist optical skills that rest in universities and SMEs.

[1] Methane emissions. Watt Committee report number 28, Prof Alan Williams (Editor). Report of a working group appointed by the Watt Committee on Energy (1994)

# Performance Specification

Laser operating wavelength	1651 nm
Laser output power	< 10 mW
Beam divergence	60 mm @ 10 m distance
Laser class	1
Visible laser wavelength	635 nm
laser output power	<1 mW
Laser class	2
Response time	100 ms
Methane gas concentration range	Depending on reflected power 0..>1000ppm.m. With rising reflected power the max. resolvable concentration decreases
Power consumption	2.5 .. 4 W depending mainly on ambient temperature
Operating time with one battery charge	3.5 hours with rechargeable cells (2000 mAh) depending on ambient temperature, with primary cells probably longer
Operating temperature range	-10 +40°C
Operating distance range	>10 m depending on reflecting surface
Lower detection limit	10 -20 ppm.m depending on reflecting power



<http://vogue.no-ip.org>

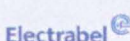
For further information on the Vogue product please contact:

**Russ Pride**  
Advantica Ltd  
Ashby Road  
Loughborough  
Leicestershire  
LE11 3GR



**ADVANTICA**

Tel: +44 (0)1509 282761  
Fax: +44 (0)1509 283119  
Email: [russell.pride@advantica.biz](mailto:russell.pride@advantica.biz)  
or [info.uk@advantica.biz](mailto:info.uk@advantica.biz)



## **B. Published Paper**

The paper contained within this appendix was published on 13th May 2005 (J. Opt. A: Pure Appl. Opt. 7 (2005) S420S424). The work was predominantly written by myself, with input from those referenced.

# An open-path, hand-held laser system for the detection of methane gas

Ben van Well<sup>1,5</sup>, Stuart Murray<sup>2</sup>, Jane Hodgkinson<sup>3</sup>, Russ Pride<sup>3</sup>,  
Rainer Strzoda<sup>4</sup>, Graham Gibson<sup>1</sup> and Miles Padgett<sup>1</sup>

<sup>1</sup> Department of Physics and Astronomy, University of Glasgow, Glasgow G12 8QQ, UK

<sup>2</sup> AOS Technology Ltd, Melton Mowbray, Leicestershire LE13 0RG, UK

<sup>3</sup> Advantica Ltd, Loughborough LE11 3GR, UK

<sup>4</sup> Siemens AG, Otto Hahn-Ring 6, CT-PS 8, D-81730, Munich, Germany

E-mail: bvanwell@physics.gla.ac.uk

Received 18 October 2004, accepted for publication 1 February 2005

Published 13 May 2005

Online at stacks.iop.org/JOptA/7/S420

## Abstract

We have developed an open-path hand-held gas detector incorporating a distributed feedback InGaAs laser diode at 1.65  $\mu\text{m}$ . Incorporated into a hand-held transceiver unit, the emitted laser beam is backscattered from nearby surfaces, collected and focused onto an amplified InGaAs detector using a 150 mm diameter plastic Fresnel lens. At ranges of 4–5 m, a typical backscattered signal is tens of nanowatts of laser light. Applying second derivative wavelength modulation spectroscopy gives a sensitivity to methane of better than 10 parts per million over a one metre path length. A number of demonstration units have been fabricated and successfully evaluated by end users.

**Keywords:** methane, wavelength modulation spectroscopy, instrumentation, infrared spectroscopy, remote detection

## 1. Background

The low-cost, sensitive detection of methane gas has wide use amongst the gas utility companies for both routine pipeline inspection and leak-report response applications [1]. The conventional approach to leak detection is based upon flame ionization detectors (FIDs) [2] but such technology measures concentration at only a single point. Using a point sensor is problematic in that the leak may be overlooked, the user may have to enter potentially explosive situations and that above-ground pipe-work could be difficult to access. This paper details the design and operational performance of an optical instrument capable of measuring methane at a range of several metres with a sensitivity close to that required for detecting the atmospheric background of 1.6 ppm.

A variety of instruments based on optical absorption of light can be configured to detect gas over the line of sight of a light beam. Sophisticated LIDAR instruments [3] have been reported using pulsed lasers, tuned to the resonant frequency of the target gas, where backscattered light from the gas in the atmosphere gives both gas concentration (from the size of

the signal) and range (from the delay time). Such instruments are usually vehicle or aircraft based, are rarely eye-safe and have a cost or complexity that limits their widespread use. Our approach has been to dispense with the need for range information and rely on the deliberate backscattered signal obtained from the ground or building over a range of only several metres, thereby giving a larger continuous signal, detectable with a lower cost/complexity instrument.

## 2. Operating principles of the optical gas detector

Methane gas has its strongest absorption in the 3  $\mu\text{m}$  spectral region, but corresponding laser sources, including cryogenically cooled laser diodes and optical parametric oscillators, exceed the cost budget for a hand-held system. Methane has an additional absorption  $\nu_3$  band at 1.6  $\mu\text{m}$  which, although over one order of magnitude weaker, does coincide with the single-mode, single-frequency emission wavelength of InGaAs distributed feedback laser diodes [4]. Furthermore, diode lasers are readily temperature-tuned to match the absorption wavelength, and subsequent control of their drive current gives fine scale tuning and the option of

<sup>5</sup> Author to whom any correspondence should be addressed.

An open-path, hand-held laser system for the detection of methane gas

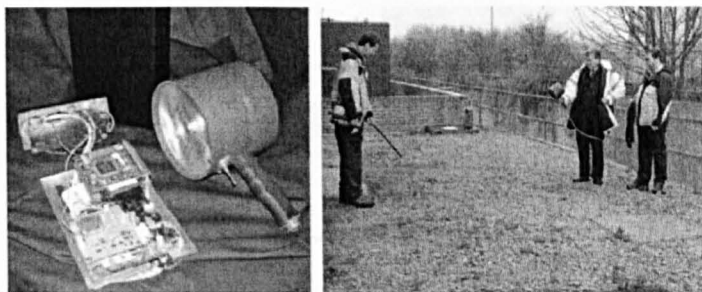


Figure 1. Left: complete instrument package. Right: field testing of prototype instrument.

wavelength modulation. InGaAs diode lasers can be readily tuned over a few per cent of their operating wavelength by changing their temperature and over several GHz by changing the drive current. However, day-to-day variation in their tuning parameters means that absolute wavelength stability is problematic—and a wide wavelength scan of a gas filled reference cell is required. Remote hand-held gas detection instruments based on a similar principle have been reported previously [5, 6]. Central to our approach has been the development of a specialized laser module where the gas reference cell and associated detector are integral to the laser module package. This means that operation of the laser at the correct wavelength is confirmed by monitoring the signal from the reference photodiode, and thus the integrity of the zero-gas signal is assured—a key requirement in all safety critical environments. Furthermore, it is this development of a reliable wavelength-referenced module that has allowed us to make field-based measurements which we present here.

Given a tuneable laser source, a number of spectroscopic techniques can be applied to the detection of gas, including photo-acoustics [7], cavity ring-down [8] and amplitude, wavelength or frequency modulation [9]. Although highly sensitive to small absorptions, photo-acoustic and cavity ring-down techniques require dedicated sample cells and are therefore not suited to open-path applications. Using a laser tuned exactly to the absorption wavelength of the gas could be used to monitor the absorption and hence gas concentration but in our configuration a change in detected power could also arise from a change in range or backscattering surface, rather than gas concentration. It is common practice in such situations to rely on a rapid modulation of the laser frequency/wavelength in the neighbourhood of the gas absorption, giving a corresponding modulation in the detected power, the magnitude of which is related to the gas concentration. When the modulation frequency is comparable to the modulation depth and large compared to the width of the gas absorption, the technique is called frequency modulation spectroscopy. When the modulation frequency is small compared to the modulation depth and width of gas absorption, the technique is called wavelength modulation spectroscopy [10]. Both techniques have been widely implemented [11] and are capable of measuring small absorptions with a sensitivity approaching that limited by the shot noise fluctuations in the power of

the laser itself. For the spectroscopy of gases at atmospheric pressure, the absorption width typically approaches 1 GHz, meaning that the modulation and demodulation required for frequency modulation spectroscopy is technologically challenging. Consequently, wavelength modulation is the natural choice as a spectroscopic technique for detection of gases at atmospheric pressure.

Current modulation of the laser wavelength over the absorption line of the gas results in a modulation of the detected laser power, the phase and amplitude of which is readily measured using a lock-in-amplifier. The amplitude of the  $n$ th harmonic of the modulated power is proportional to the  $n$ th derivative of the detected power. Within our instrument we use first, second and third harmonic demodulation to give respectively, the first, second and third derivatives of the absorption as a function of wavelength. Note that it is the second derivative of these harmonics that has a maximum value at the wavelength corresponding to the centre of the absorption feature.

### 3. Instrument design

Our instrument is configured as an optical head containing a laser diode module, temperature control electronics, collection lens and photodiode. This is coupled to a separate control box containing the microprocessor control, analogue to digital interface, laser diode driver and multiple lock-in amplifiers/phase shifters. A photograph of the complete instrument is shown in figure 1.

The laser diode module is mounted in a standard 14-pin butterfly package incorporating the 1651 nm laser diode mounted on a thermoelectric cooler, a 4.5 mm focal length aspheric lens to collimate the emission from the front facet, and a separate photodiode monitoring the rear facet emission. The commercially available monitor photodiode package (TO) is filled with methane gas, forming a reference cell from which the operating wavelength of the laser can be controlled. The 1 mm thickness of gas between the diode and package window gives an absorption of approximately 4% at 1651 nm. The optical layout and a photograph of the complete laser module are shown in figure 2. We have operated several of these modules over a period of one year and have found no problems with the methane absorption reference due to gas leakage.

The near-collimated laser beam emerges from the optical head and is backscattered from any object in the beam. The

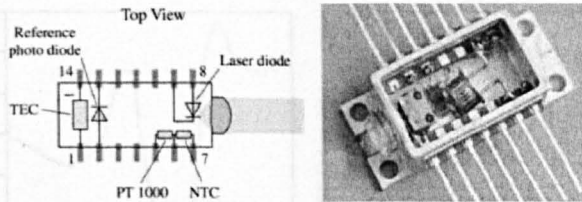
B van Well *et al*

Figure 2. Laser diode module package.

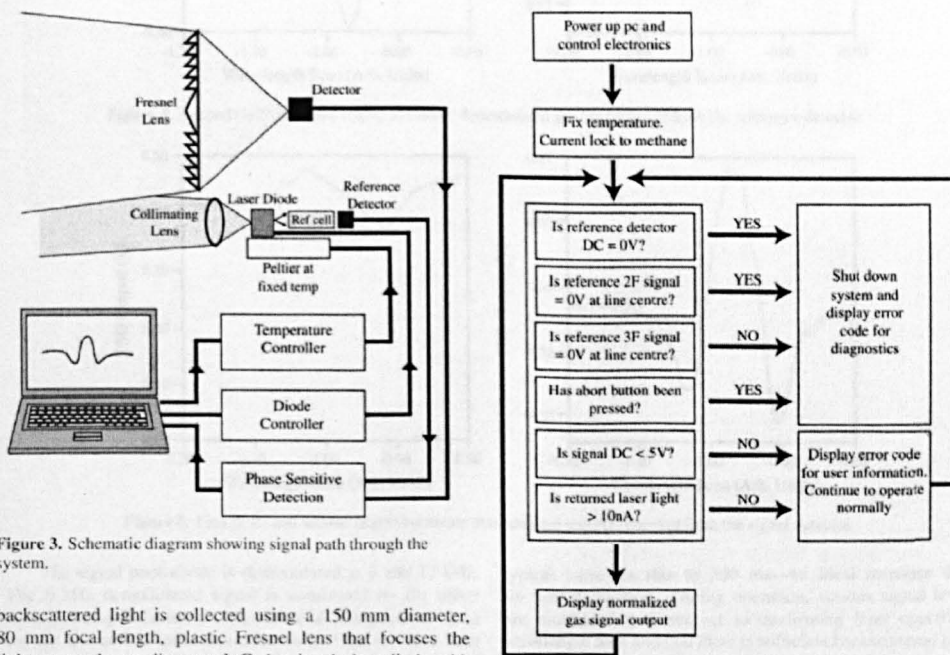


Figure 3. Schematic diagram showing signal path through the system.

backscattered light is collected using a 150 mm diameter, 80 mm focal length, plastic Fresnel lens that focuses the light onto a 1 mm diameter InGaAs signal photodiode with integral preamplifier. This detector is shielded from excess sunlight, which would otherwise saturate the amplifiers, by a 100 nm bandwidth filter centred at 1680 nm. Typically when pointed at a wall or the ground at a distance of 3–5 m the backscattered signal is of the order of 10–100 nW compared to the noise equivalent power of the detector of  $2.9 \text{ pW Hz}^{-1/2}$  ( $1.5 \times 10^6 \text{ V A}^{-1}$  gain, 3 Hz bandwidth). A schematic diagram of the system is shown in figure 3.

The laser diode driver (Wavelength Electronics) is housed within the shoulder-strapped control box and the laser current drive is fed to the optical head via a shielded multi-core cable, which also feeds the amplified signals from both monitor and signal photodiode back to the control box. The laser diode driver supplies a DC current of approximately 70 mA, giving a laser output power of around 8 mW. Superimposed upon this DC level is a 6 kHz modulation with an amplitude of 6 mA, sufficient to modulate the laser wavelength over the width of the methane absorption. This restricted range has been selected to exclude other species. This technique can be extended to detect

other species by a suitable choice of light source operating over a different spectral range.

Within the control box, the DC voltage from the monitor photodiode is read directly by the microprocessor to confirm laser operation. The photodiode signals are demodulated at various harmonic frequencies using Analogue Devices AD630 integrated circuits. The monitor photodiode signal is demodulated at both 12 and 18 kHz. The 12 kHz demodulated signal corresponds to the second derivative of the absorption, a signal which is a maximum and symmetric about the centre of the absorption feature, and is used to confirm the operating wavelength of the laser. The 18 kHz demodulated signal corresponds to the third derivative, a signal which is zero and anti-symmetric about the centre of the absorption feature, providing an error voltage enabling the software to make fine adjustments to the laser wavelength, maintaining it exactly at the absorption feature.

An open-path, hand-held laser system for the detection of methane gas

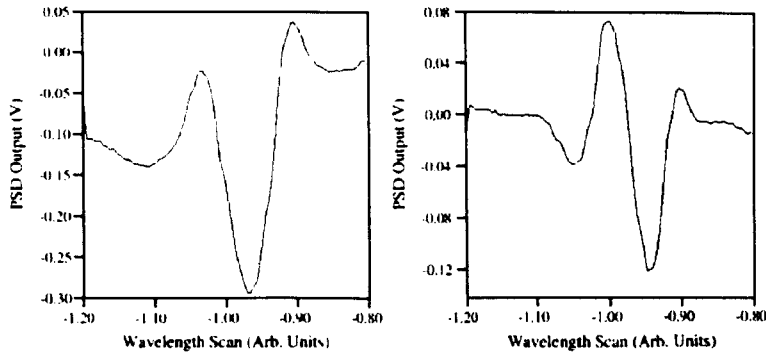


Figure 5. Second (left) and third (right) harmonic demodulated spectra recorded from the reference detector.

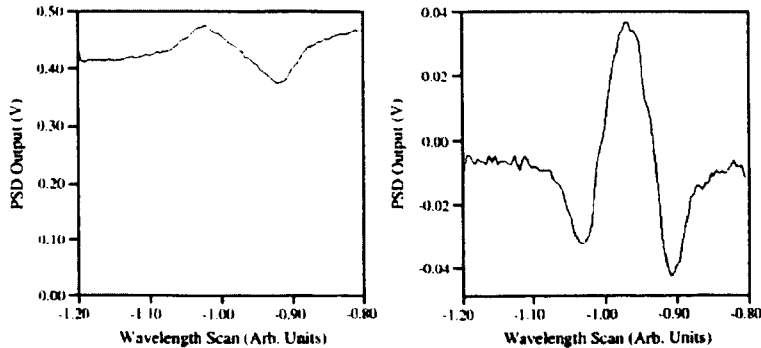


Figure 6. First (left) and second (right) harmonic demodulated spectra recorded from the signal detector.

The signal photodiode is demodulated at 6 and 12 kHz. The 6 kHz demodulated signal is dominated by the offset corresponding to the linear dependence of laser power on drive current and acts as an accurate measure of the received laser power independent of any residual sensitivity to sunlight or other thermal sources. A lower limit is set upon this detected laser power such that below a certain threshold the software gives a 'low-light' warning. The 12 kHz demodulated signal gives a measure of the methane gas within the line of sight of the instrument. The normalized gas concentration reading is obtained from the ratio of the 12 kHz to the 6 kHz signal.

The whole instrument is under microprocessor control in the form of a board level personal computer (NS Geode 300 MHz), operating under Windows XP Professional and running control software written within the LabVIEW programming environment. Upon power-up, the computer auto-boots and launches the control software. The control software maintains all aspects of instrument operation, including start-up sequence, locking the laser wavelength to the absorption feature, and calculating a gas concentration signal which is displayed on a digital readout on the back surface of the optical head. The output stage associated with all these demodulation circuits is set to a time constant of 10 ms, although additional filtering with the control software

typical increases this to 300 ms—an ideal response time for user interaction. During operation, various signal levels are monitored with respect to confirming laser operation, wavelength lock and that there is sufficient backscattered light to make an accurate reading. Failure in any of these aspects results in a specific error-code on the gas reading display. Figure 4 shows a flow diagram of the software control program.

#### 4. Laboratory characterization of the instrument performance

When operating within the laboratory, the control software is configured to scan the laser wavelength over the absorption feature and record and display the various spectral signals on an external monitor. Figure 5 shows typical traces obtained from the demodulation of the reference detector signal. Figure 6 shows typical traces obtained from the demodulation of the signal detector.

Those signals obtained from the reference photodiode are independent of gas in the atmosphere and show clearly the characteristic second and third derivative spectra. The trace from the signal photodiode is for a received power of 30 nW and a gas concentration of 1%, confined to a 100 mm length of the beam, i.e. 1000 ppm m. The key parameter in determining

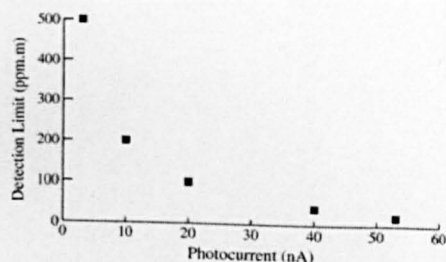
B van Well *et al*

Figure 7. Minimum detectable gas concentration for a given light level.

the smallest amount of gas that can be measured is the amount of backscattered light reaching the detector. Figure 7 shows a graph of the minimum detectable gas concentration (S:N 1:1) as a function of received power. The detection limit scales inversely with the returned light power, indicating that the system has a constant noise floor. This is approximately 2–3 times greater than that predicted by the NEP of the detector.

### 5. Field-testing and evaluation of the instrument

For outdoor use, the control software is configured to maintain the laser wavelength at exactly the absorption feature. The time constant of the demodulation is set to 300 ms, updating the gas concentration output about three times per second. A low (<10 nW) received light level triggers a negative concentration display of -9000 ppm m and a sunlight saturation of the detector as a negative display of -8000 ppm m. Most of the instrument characterization was carried out at an open air test site licensed to undertake such work.

The key comparison is to demonstrate that the optical instrument can give similar readings to a FID instrument whilst given the additional advantage of remote sensing. Using a manufactured leak buried at a realistic depth of 80 cm beneath the ground we invited a FID user to 'patrol' a defined area, looking for signs of a gas signal. At all times, standing at a distance of 4 m, we directed the beam of the laser light from the optical gas detector at the FID inlet. Figure 8 shows the readings from the two types of instrument plotted as a function of time. Although not meaningful to compare the point concentration measured by the FID with the integrated over path concentration measured by the optical instrument directly, we see that the general form of the two signals is extremely similar. For the laser pointer, a measurement of a gas cloud thickness of 1 mm is equivalent to a concentration times path-length value of 1000 ppm m. When operating over a typical range of 5 m, this corresponds to an average gas concentration, over the entire path, of 200 ppm. However, it is important to appreciate that in most 'real' leak situations the gas concentration will be strongly peaked in the vicinity of the leak itself. Prototypes have been evaluated by end users who have reported similar performance to existing technologies.

### 6. Discussion

The close equivalence of the readings from the FID and the optical instrument suggest that the optical instrument could be

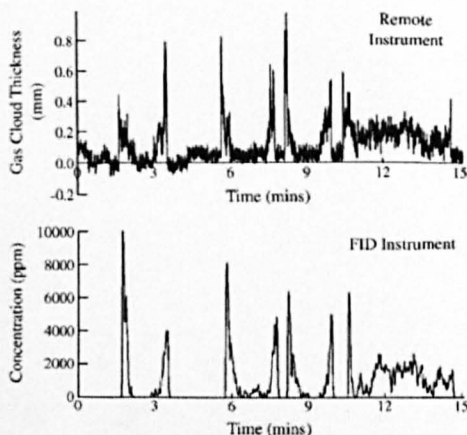


Figure 8. Comparison between a FID and the remote gas detection system.

used in the field as a direct replacement of the FID approach. Furthermore, the remote sensing capability of the optical instrument opens new modes of use such that the operator can inspect a location that is difficult to access, whether on grounds of geometry or safety.

### References

- [1] HSE Books 1996 *A Guide To Gas Safety (Management) Regulations*
- [2] Simpson C F and Gough T A 1981 Direct quantitative-analysis using flame ionization detection—the construction and performance of the fidoh detector *J. Chromatogr. Sci.* **19** 275–82
- [3] Walmsley H L and O'Connor S J 1998 The accuracy and sensitivity of infrared differential absorption lidar measurements of hydrocarbon emissions from process units *Pure Appl. Opt.* **7** 907–25
- [4] Temkin H, Tanbunek T, Logan R A, Olsson N A, Sergent M A, Wecht K W and Cebula D A 1990 InGaAs/InP distributed feedback quantum well laser *Appl. Phys. Lett.* **57** 1295–7
- [5] Iseki T, Tai H and Kimura K 2000 A portable remote methane sensor using a tunable diode laser *Meas. Sci. Technol.* **11** 594–602
- [6] Wainner R T, Green B D, Allen M G, White M A, Stafford-Evans J and Naper R 2002 Handheld, battery-powered near-IR TDL sensor for stand-off detection of gas and vapour plumes *Appl. Phys. B* **75** 249–54
- [7] Zelinger Z, Strizik M, Kubat P and Civis S 2000 Quantitative analysis of trace mixtures of toluene and xylenes by CO<sub>2</sub> laser photoacoustic spectrometry *Anal. Chim. Acta* **422** 179–85
- [8] Paldus B A, Harb C C, Spence T G, Wilke B, Xie J, Harris J S and Zare R N 1998 Cavity-locked ring-down spectroscopy *J. Appl. Phys.* **83** 3991–7
- [9] Schilt S, Thevenaz L and Robert P 2003 Wavelength modulation spectroscopy: combined frequency and intensity laser modulation *Appl. Opt.* **42** 6728–38
- [10] Supplee J M, Whittaker E A and Lenth W 1994 Theoretical description of frequency modulation and wavelength modulation spectroscopy *Appl. Opt.* **33** 6294–302
- [11] Bomse D S, Stanton A C and Silver J A 1992 Frequency modulation and wavelength modulation spectroscopies: comparison of experimental methods using a lead-salt diode laser *Appl. Opt.* **31** 718–31